

**1 Mitofusin2 cooperates with Nuage-associated proteins and involves**  
**2 mRNA translational machinery in controlling mRNA fates during**  
**3 spermatogenesis**

4

5 Xiaoli Wang<sup>1</sup>, Yujiao Wen<sup>1</sup>, Jin Zhang<sup>1</sup>, Shuangshuang Guo<sup>1</sup>, Congcong Cao<sup>1</sup>,  
 6 Stephen A Krawetz<sup>2</sup>, Zhibing Zhang<sup>2, 3</sup>, Shuiqiao Yuan<sup>1,4\*</sup>

7

8 <sup>1</sup>Institute of Reproductive Health, Tongji Medical College, Huazhong University  
 9 of Science and Technology, Wuhan, Hubei 430030, China.

10 <sup>2</sup>Department of Obstetrics & Gynecology, Wayne State University, Detroit, MI  
 11 48201, USA,

12 <sup>3</sup>Department of Physiology, Wayne State University, Detroit, MI 48201, USA,

13 <sup>4</sup>Shenzhen Huazhong University of Science and Technology Research  
 14 Institute, Shenzhen, Guangdong 518057, China.

15

16

17 \*Correspondence to Dr. Shuiqiao Yuan: [shuiqiaoyuan@hust.edu.cn](mailto:shuiqiaoyuan@hust.edu.cn)

18

19

20

21

22

23

24

25

26

27

# Abstract

Mitochondria play a critical role in spermatogenesis and regulated by several mitochondrial fusion proteins. Its interaction with other organelles forms several unique structures, including mitochondria-associated ER membrane (MAM) and a specific type of Nuage close to mitochondria. However, the importance of mitochondria functions and mitochondrial fusion proteins in its associated-structure formation and mRNA translation during spermatogenesis remain unclear. Here, we show that Mitofusin 2 (MFN2), a mitochondrial fusion GTPase protein, cooperates with Nuage-associated proteins, including MIWI, DDX4, TDRKH and GASZ and involves translational machinery to control the fates of gamete-specific mRNAs in spermatogenesis. Conditional mutation of *Mfn2* in postnatal germ cells results in male sterility due to germ cell developmental defects characterized by disruption of mitochondrial morphology, abnormal MAMs structure, aberrant mRNA translational processes, and anomalous splicing events. Moreover, MFN2 interacts with MFN1, another mitochondrial fusion protein with high-sequence similar to MFN2, in testes to facilitate spermatogenesis. Mutation of *Mfn1* and *Mfn2* simultaneously in testes causes very severe infertile phenotypes. Importantly, we further show that MFN2 is enriched in polysome fractions in testes and interacts with MSY2, a germ cell-specific DNA/RNA-binding protein, and eukaryotic elongation factor 1 alpha (eEF1A) to control gamete-specific mRNA translational delay during spermatogenesis. Collectively, our findings demonstrate that MFN2 works with Nuage-associated proteins and involves translational secession to regulate gamete-specific mRNA fates. Our data reveal a novel molecular link among Mitofusins, Nuage-associated proteins, and mRNA translational processes in controlling male germ cell development.

**Key words:** Nuage proteins, mitofusins, mRNA translation, spermatogenesis, mice

# 1 Introduction

2 Mitochondria are dynamic organelles in which maintained by a balance  
 3 between fusion and fission in mammals. They play crucial roles in multiple  
 4 biological processes, including energy generation, calcium homeostasis,  
 5 signal transduction, and apoptosis(Chen and Chan, 2004; Westermann, 2010).  
 6 In mammalian testes, the shape of germ cell mitochondria changes markedly  
 7 during spermatogenesis, of which there are three main types. It displays the  
 8 orthodox-type in Sertoli cells, spermatogonia, and preleptotene/leptotene  
 9 spermatocytes. While the intermediate-type in zygotene spermatocytes and  
 10 the condensed type in pachytene spermatocytes and early spermatids. In late  
 11 spermatids and spermatozoa, it shifts back to the intermediate-type (De  
 12 Martino et al., 1979; Ramalho-Santos et al., 2009). Emerging evidence  
 13 indicates that mitochondrial function is a critical determinant of male germ cell  
 14 development(Zhang et al., 2016; Ren et al., 2019).

15 Additionally, the mitochondria and endoplasmic reticulum (ER) form  
 16 contacts called mitochondria-associated ER membranes (MAMs), which are  
 17 important for supporting essential structural and functional inter-organelle  
 18 communication including calcium and phospholipid exchange, mitochondrial  
 19 biogenesis, autophagy, ER stress and unfolded protein response  
 20 (UPR)(Paillusson et al., 2016). Alteration of MAMs increasingly was reported in  
 21 several human diseases, highlighted by neurodegenerative  
 22 diseases(Paillusson et al., 2016). Our previous work has demonstrated an  
 23 abundance of MAMs in mouse and human testes and identified a large portion  
 24 of MAM proteins in testes (Wang et al., 2018), which suggests that MAM  
 25 proteins may have critical functions in spermatogenesis.

26 Mitofusins (MFN1/2), the homologs of Fzo in yeast and Drosophila, are  
 27 the critical regulators of mitochondrial fusion in mammalian cells and enriched  
 28 in MAMs (Hales and Fuller, 1997; Santel and Fuller, 2001; Wang et al., 2018).  
 29 Loss of either *Mfn1* or *Mfn2* in mice leads to embryonic lethality, and cultured

1 cells obtained from the mutant mouse embryos display overtly fragmented  
 2 mitochondria (Chen et al., 2003). Specific ablation of *Mfn2* in anorexigenic  
 3 pro-opiomelanocortin (POMC) neurons in the hypothalamus results in aberrant  
 4 MAMs, defective POMC processing, ER stress-induced leptin resistance,  
 5 hyperphagia, reduced energy expenditure, and obesity (Schneeberger et al.,  
 6 2013). Interestingly, the mutations in human MFN2, but not MFN1, lead to  
 7 Charcot–Marie–Tooth disease type 2A, a neurodegenerative disorder  
 8 characterized by progressive sensory and motor losses in the limbs (Zuchner  
 9 et al., 2004; Chen et al., 2007; Misko et al., 2012; Rouzier et al., 2012; Bouhy  
 10 and Timmerman, 2013). Additionally, conditional knockout *Mfn1*, but not *Mfn2*,  
 11 in growing oocytes results in female infertility (Hou et al., 2019). Although  
 12 MFN1/2 deficiency in male germ cells leads to mitochondrial defects and male  
 13 infertility (Zhang et al., 2016; Varuzhanyan et al., 2019), the underlying  
 14 mechanism of how Mitofusins regulate spermatogenesis and male germ cell  
 15 development remains largely unknown.

16 During spermatogenesis, multiple specific mitochondria-associated  
 17 germinal structures are present in the cytoplasm of male germ cells, termed  
 18 Nuage, which are electron-dense, non-membranous, close to mitochondria,  
 19 variant size yielding to different protein components, including  
 20 inter-mitochondrial cement (IMC), piP-body, and chromatoid body (CB) (Wang  
 21 et al., 2020). Several proteins have identified to localize the Nuage, such as  
 22 MIWI, DDX4, MAEL, TDRKH, and GASZ (Wang et al., 2020). Interestingly,  
 23 MIWI, DDX4, and MAEL are expressed in both IMC and CB, while TDRKH and  
 24 GASZ localize only to the IMC (Toyooka et al., 2000; Ma et al., 2009; Saxe et  
 25 al., 2013; Takebe et al., 2013). The Nuage is the proposed sites of germ cell  
 26 functions with multiple RNA processing events, including translational  
 27 regulation, RNA-mediated gene silencing, mRNA degradation, piRNA  
 28 biogenesis, and nonsense-mediated mRNA decay (Kotaja and Sassone-Corsi,  
 29 2007; Wang et al., 2020). Besides, spermatogenesis undergoes two rounds of  
 30 transcriptional secessions: one is during the meiosis, which includes the

1 synapsis and desynapsis, and the other is the histone-protamine transition  
 2 process during late spermiogenesis(Sassone-Corsi, 2002). During the  
 3 transcriptional secessions, a large number of germ cell-specific mRNAs exhibit  
 4 translational repression with a lag of up to a week between their transcription  
 5 and translation(Iguchi et al., 2006). The evidence for Nuage regulation of  
 6 mRNA processing is strongest for the chromatoid body. Translational  
 7 regulatory proteins such as MIWI, TDRD6, MAEL have been localized to the  
 8 chromatoid body and associated with mRNA translational machinery and  
 9 piRNA biogenesis(Grivna et al., 2006; Vasileva et al., 2009; Takebe et al., 2013;  
 10 Castaneda et al., 2014; Fanourgakis et al., 2016). Thus, multiple components  
 11 necessary for transcript processing physically connected to the Nuage during  
 12 spermatogenesis. Transcriptional and post-transcriptional regulation in testis is  
 13 mainly due to activation/inactivation of specific gene expression programs in  
 14 meiotic spermatocytes and post-meiotic round spermatids. However,  
 15 knowledge about the specific regulators and underlying mechanisms in such  
 16 programs during germ cell development is limited.

17 In this study, we report that MFN2, a mitochondrial fusion GTPase protein,  
 18 interacts with Nuage-associated proteins, including MIWI, DDX4, GASZ, and  
 19 TDRKH in the testes and associates with translational machinery to regulate  
 20 male germ cell development and spermatogenesis. We discovered that MFN2  
 21 provides a critical component to the translational machinery while interacting  
 22 with the Nuage-associated proteins in the male germ cells. Loss of function of  
 23 MFN2 in postnatal germ cells led to male sterility with defects in mitochondrial  
 24 formation, MAMs structure maintenance, translational processes, and mRNA  
 25 splicing events. Moreover, we found that MFN2 interoperates with MFN1,  
 26 another mitochondrial fusion protein with high sequence similarity to MFN2, in  
 27 testes to facilitate spermatogenesis. Simultaneous mutation of *Mfn1* and *Mfn2*  
 28 in testes causes severely disrupted phenotypes. Inspiringly, our data revealed  
 29 that MFN2 also cooperates with the germ cell-specific DNA/RNA binding  
 30 protein MSY2 and eukaryotic elongation factor 1 alpha (eEF1A1 and eEF1A2)

to regulate the transcription and translation of MSY2-bound gamete mRNAs in male germ cells. Our study, for the first time, presented below unveils a novel role for MFN2 in mitochondria-associated germinal structure formation and mRNA translational machinery during male germ cell development. The findings revealed a unique mechanism by which MFN2 associates with translational machinery through the Nuage-associated proteins, MSY2 and eukaryotic elongation factor 1 alpha (eEF1A1 and eEF1A2) to control male gamete-specific mRNA fates by maintaining its storage/translational delay in the germline.

## Results

### Expression and localization of MFN2 in the male germ cells during spermatogenesis

Although MFN2 is a ubiquitously expressed protein located on both the outer mitochondrial membrane (OMM) and the ER surface in mammalian cells (de Brito and Scorrano, 2008), to date, no information is available on the pattern of its expression in male germ cells during spermatogenesis. By performing RT-qPCR and Western blot assays, we found that both mRNA and protein levels of the *Mfn2* gene preferentially and highly expressed in mouse testes (Supplementary Figure.S1A-B). We then analyzed the expression of *Mfn2* in testes at various postnatal ages. The results showed that both mRNA and protein are expressed from postnatal day 0 (P0) testes to adult testes but strongly accumulate from P14 when the testes mainly consist of spermatocytes (Supplementary Figure.S1C-D). Immunofluorescence staining of MFN2 in developing testes further revealed that MFN2 mostly expressed in spermatogonia at P0 and P7, and finally highly expressed in late pachytene spermatocytes and round spermatids at P14 to P28 (Supplementary Figure.S1E).

We next determined the subcellular localization of MFN2 in adult testes during spermatogenesis by co-staining MFN2 with  $\gamma$ -H2AX (a marker of

meiotic DNA damage response). We observed the presence of MFN2 throughout most of the germ cell development, including the mitotic spermatogonia, meiotic spermatocytes (pre-leptotene to diplotene), and round spermatids (Figure.1A). Interestingly, we found that MFN2 expressed in the cytoplasm of spermatogenic cells with the highest expression level in the late-pachytene spermatocytes and round spermatid with a granular cytoplasmic localization. Modest cytoplasmic expression in meiotic metaphase spermatocytes, followed by spermatogonia, preleptotene, leptotene, and zygotene spermatocytes, was also observed (Figure.1A-B). Moreover, both mRNA and protein levels of *Mfn2* were highly expressed in pre-meiotic spermatocytes and post-meiotic round spermatids while lowly expressed in Sertoli cells (Supplementary Figure.S1F-H). Since *Mfn2* encodes a mitochondrial outer membrane protein, we confirmed its co-localization with ATP5A (an outer mitochondria membrane marker) in adult testes by co-immunofluorescence staining (Figure.1C). Together, these data indicate that MFN2 highly expressed in the cytoplasmic granules of pre-meiotic spermatocytes and post-meiotic round spermatids and may play an essential role in spermatogenesis.

## 19 **Loss of MFN2 in postnatal germ cells leads to male sterility**

To elucidate the physiological role of MFN2 in spermatogenesis, we generated germline-specific knockout mice by using *Stra8*-Cre transgenic mice in which Cre is expressed in differentiating spermatogonia (Sadate-Ngatchou et al., 2008) to delete exon 6 of *Mfn2* gene (Supplementary Figure.S2A). The efficiency of this *Mfn2* conditional knockout mouse (*Stra8*-Cre; *Mfn2*<sup>loxP/Δel</sup>, herein called *Mfn2*-cKO) was verified by determining *Mfn2* mRNA and protein levels in testes. Both *Mfn2* mRNA and protein levels dramatically reduced in *Mfn2*-cKO testes compared to that of control testes (Figure.2A-D). Thus, we successfully generated the postnatal male germ cell-specific knockout *Mfn2* mutants.

1 While *Mfn2*-cKO mice were viable and appeared to be grossly normal,  
2 they displayed complete sterility after a 5 month-period fecundity test.  
3 Consistent with this infertile phenotype, testis sizes from *Mfn2*-cKO mice were  
4 significantly smaller than their control littermates (Figure.2E). The ratio of testis  
5 weight/body weight of *Mfn2*-cKO mice was decreased substantially at various  
6 ages, starting from P35 to P120 compared with controls (Figure.2F).  
7 Histological analyses showed that as the adult *Mfn2*-cKO mice aged, the  
8 number of severely atrophic abnormal seminiferous tubules increased  
9 (Figure.2G), suggesting that spermatogenic defects are age-dependent in  
10 *Mfn2*-cKO mice. Interestingly, when the first wave of spermatogenesis  
11 culminated at P42, the late-stage spermatocytes and round spermatids  
12 continually decreased in number and appeared to vacuolize gradually  
13 (Figure.2G). In comparison, no discernible abnormality found in the *Mfn2*-cKO  
14 testes from P7 to P28 (Supplementary Figure.S2B). Consistent with these  
15 histological results, the TUNEL assay revealed that the number of apoptotic  
16 cells in *Mfn2*-cKO testes at P14 to P28 was comparable with control testes but  
17 increased significantly at P35 and P56 (Supplementary Figure.S2C-D).  
18 Moreover, the number of spermatozoa retrieved from adult *Mfn2*-cKO cauda  
19 epididymis was dramatically reduced compared to that of controls  
20 (Figure.2H-I). Only ~2% of *Mfn2*-cKO epididymal sperm showed normal  
21 morphology, compared with ~80% of the sperm in controls (Figure.2J-K).  
22 These data suggest that, upon *Mfn2* deletion in postnatal testes, germ cells  
23 gradually lost from P35 by apoptosis, leading to infertility.

## 24 **MFN2 interacts with MFN1 in testes and contributes to the male fertility**

25 Since MFN1 and MFN2 are the two Fzo homologs in humans and mice,  
26 which interact with each other in mammalian cells coordinately to regulate  
27 mitochondrial fusion (Chen et al., 2003), we next asked whether there are  
28 interaction and synergistic effects between MFN1 and MFN2 in  
29 spermatogenesis. We first examined their interaction effects in adult mouse

testes by co-immunoprecipitation (Co-IP). In the MFN2 antibody immunoprecipitants, MFN1 was detected in testes, and in the MFN1 antibody immunoprecipitants, MFN2 was detected as well (Supplementary Figure.S3A). These results confirmed that MFN1 and MFN2 are indeed bona fide interacting partners in the testes. Besides, both MAEL (a piP-body component in the piRNA biogenesis pathway (Soper et al., 2008; Takebe et al., 2013)) and GAPDH were undetectable in MFN2 antibody immunoprecipitants (Supplementary Figure.S3B), confirming the high specificity of MFN2 antibody in Co-IP assays. To determine the roles of MFN1 during spermatogenesis and male germ cell development, we then generated *Stra8*-Cre mediated *Mfn1* conditional knockout mice through the deletion of exon 4 (*Stra8*-Cre; *Mfn1*<sup>loxP/Del</sup>, herein called *Mfn1*-cKO) in postnatal germ cells (Supplementary Figure.S3C). As expected, *Mfn1*-cKO mice are also infertile due to the disruption of spermatogenesis, which showed smaller testes, decreased testis weight, and disrupted seminiferous tubule structure (Supplementary Figure.S3D-G). However, differing from the age-dependent phenotype of *Mfn2*-cKO mice, *Mfn1*-cKO testes started to exhibit vacuolization defects as early as P28. In comparison, the first wave of spermatogenesis in *Mfn2*-cKO testes proceeds until P42. This disparity between *Mfn1*-cKO and *Mfn2*-cKO mice phenotypes suggests that both MFN2 and MFN1 are essential but play distinct roles for spermatogenesis and male germ cell development.

To better understand the physiological roles of Mitofusins in spermatogenesis and male germ cell development, we next simultaneously deleted *Mfn1* and *Mfn2* in mouse testis using *Stra8*-Cre line mediated Cre-Loxp strategy to create double knockout *Mfn1/2* mice (*Stra8*-Cre; *Mfn1*<sup>loxP/Del</sup>-*Mfn2*<sup>loxP/Del</sup>, hereinafter referred to as *Mfn1/2*-cDKO). Notably, the testicular disruption in *Mfn1/2*-cDKO mice was much more severe than in either single *Mfn1* or *Mfn2*-cKO mice (Figure. 2L). Compared with the control mice, the diameters of seminiferous tubules from *Mfn1/2*-cDKO mice were much smaller as early as P14 (Supplementary Figure.S4A-B). No round

1 spermatids were observed in *Mfn1/2*-cDKO testes at P25. In comparison, both  
 2 pachytene spermatocytes and round spermatids were observed in control  
 3 testes as meiosis completed during first wave spermatogenesis (Figure.2L and  
 4 Supplementary Figure.S4A). These data suggest that *Mfn1/2*-cDKO mice  
 5 failed to complete meiosis. Consistent with the phenotypes, testis size of  
 6 *Mfn1/2*-cDKO adult mice was much smaller than that of *Mfn1* or *Mfn2* single  
 7 cKO mice (Supplementary Figure.S4C-D). Histological analyses of adult  
 8 testicular sections further revealed increased atrophic and vacuolated  
 9 seminiferous tubules in *Mfn1/2*-cDKO testes compared with single *Mfn1* or  
 10 *Mfn2*-cKO testes (Supplementary Figure.S4E). Strikingly, unlike the  
 11 distribution of mitochondria in controls, which uniformly distributed in the  
 12 cytoplasm like a donut, mitochondria were aggregated to one side of the  
 13 cytoplasm in the *Mfn1/2*-cDKO spermatocytes at P25 (Supplementary  
 14 Figure.S4F). However, this mitochondria abnormal distribution was not  
 15 observed in *Mfn1*-cKO or *Mfn2*-cKO mice (Figure.2M and Supplementary  
 16 Figure.S4F). Together, these results indicate that MFN2 could cooperate with  
 17 MFN1 to regulate the distribution of mitochondria in the testes, thereby  
 18 contributing to spermatogenesis and male germ cell development.

## 19 **Ablation of MFN2, but not MFN1 in testes disrupt the MAM and ER** 20 **structures in male germ cells**

21 Since the ablation of both MFN1 and MFN2 in postnatal germ cells  
 22 caused spermatogenesis defects and male infertility, we next asked why the  
 23 germ cells fail to full development. Using a transmission electron microscope  
 24 (TEM) analysis, we observed that mitochondria exhibit swelling and  
 25 fragmentation in germ cells from adult *Mfn2*-cKO and/or *Mfn1*-cKO mouse  
 26 testes (Figure.3A-B and Supplementary Figure.S5A). Interestingly, we  
 27 observed the IMC structure in *Mfn2*-cKO pachytene spermatocytes, but the  
 28 thickness of IMC appeared to increase (Figure.3A). We then focused on  
 29 *Mfn2*-cKO round spermatids to further examine the details of mitochondrial

defects by measurement of mitochondria length in round spermatids between control and *Mfn2*-cKO mice. The aspect ratio (AR) (AR=major axis/minor axis of mitochondria) is defined to calculate the length of mitochondria. Although the AR of all mitochondria was not significantly decreased in *Mfn2*-cKO round spermatids (Figure.3C), the AR distribution displayed an increased percentage of short mitochondria with  $AR \leq 1.5$  compared to that of controls (Figure.3D). These data indicate that developmental defects of male germ cells in both *Mfn1*- and *Mfn2*-cKO mice are mainly due to the fragmentation and swelling of mitochondria in germ cells.

Given that MFN2 supports structural and functional communication between mitochondria and ER, we next investigated whether the deletion of *Mfn2* in postnatal male germ cells disrupts MAM and ER homeostasis. In control testes, the majority of the mitochondria displayed close interactions with ER. However, the distance between mitochondria and ER increased by about 16%, and the percentage of mitochondria-ER contacts was significantly reduced by nearly 50% in *Mfn2*-cKO testes compared to that of controls (Figure.3E-F). Additionally, the ER-mitochondria contact coefficient (ERMICC) was also reduced by more than 30% in *Mfn2*-cKO testes compared with that of controls (Figure.3G). Notably, the ER displays tube-like cisternae structures in control spermatids, whereas it exhibits fragmentation in *Mfn2*-cKO spermatids (Figure.3B in yellow frame), implying that the ER structure disrupted upon MFN2 deletion in male germ cells. To further confirm these observations, calreticulin (a MAM and ER marker protein) immunostaining was employed to examine the MAM structure in P18 and P60 testes. Calreticulin displayed a diffused granular pattern in the cytoplasm of *Mfn2*-cKO spermatocytes at P18 instead of continuous perinuclear tubular localization exhibited in the controls (Figure.3H). Moreover, in P60 testes, the calreticulin signals in *Mfn2*-cKO germ cells appeared to be reduced and displayed diffused granular distribution compared to that of controls (Figure.3I). Of note, unlike the observation in *Mfn2*-cKO spermatocytes, calreticulin does not exhibit any diffused signal

pattern in *Mfn1*-cKO spermatocytes (Supplementary Figure.S5B). Together, these data suggest MFN2 but not MFN1 may have a function in the regulation of the formation of MAM and ER structures.

Since dynamic mitochondrial fusion and fission are known processes of regulating mtDNA stability and energy production (Westermann, 2010; Palmer et al., 2011), we determined mtDNA copy number in *Mfn1*-cKO and/or *Mfn2*-cKO adult testes by RT-qPCR. Unexpectedly, we found that the mtDNA copy number appeared to increase in both *Mfn1*-cKO and *Mfn2*-cKO adult testes (Figure.3J), which is inconsistent with previous reports showing that conditional a single knockout of either *Mfn1* or *Mfn2* in skeletal muscle did not alter mtDNA copy number (Chen et al., 2010). The discrepancy and the heterogeneity of mitofusins imply a possible additional mechanism of MFN1/2 in regulating mtDNA stability between somatic and germ cells. Given that the physiological and ultrastructural evidence for mitochondrial dysfunction in *Mfn1*-cKO and/or *Mfn2*-cKO germ cells, we carried out the histochemical staining of cytochrome c oxidase (COX, complex IV, brown stain, encoded by mitochondrial DNA) and succinate dehydrogenase (SDH, complex II, blue stain, encoded by nuclear DNA) activity in adult testes to directly assess whether the function of respiratory complexes was affected. In line with the increased mtDNA copy number, COX activity increased in both *Mfn1*-cKO and *Mfn2*-cKO testis sections, whereas the SDH activity appeared unaltered (Figure.3K). These results show that the deletion of *Mfn1/2* in male germ cells leads to increased mitochondrial fission and dysregulated mitochondrial metabolism. Taken together, these data reveal that both MFN1 and MFN2 are essential for the maintenance of mitochondrial morphology in male germ cells, but MFN2, not MFN1 plays a critical role in maintaining MAM and ER structure integrity during male germ cell development.

**MFN2 interacts with Nuage-associated proteins and affects their expressions and piRNA production in testes**

1 Since MFN2 displays a granular cytoplasmic localization in the cytoplasm  
2 of male germ cells (Figure.1), we assumed MFN2 maybe involve in  
3 mitochondria-associated germinal structure formation. To test this hypothesis,  
4 we selected four mitochondrial-associated germinal granule proteins (also  
5 terms of Nuage-associated proteins), including MIWI, DDX4, TDRKH, and  
6 GASZ, to perform the reciprocal immunoprecipitation (Co-IP) using MFN2  
7 specific antibody in testis and cell line. We found that, in MFN2 antibody  
8 immunoprecipitants, MIWI, DDX4, GASZ, and TDRKH strongly detected in WT  
9 testes (Figure.4A). Likewise, in MIWI, DDX4, TDRKH, and GASZ antibody  
10 immunoprecipitants, MFN2 was detected in testes as well (Figure.4B-E).  
11 These results suggest that MFN2 interacts with MIWI, DDX4, TDRKH, and  
12 GASZ in testes. We also examined their interaction *in vitro* in the cell line.  
13 When the full length of MFN2 was ectopically co-expressed with MIWI, TDRKH,  
14 and DDX4 in HEK293T cells, MFN2 was pulled down by MIWI, TDRKH, and  
15 DDX4, indicating MFN2's ability to interact with MIWI, TDRKH and DDX4  
16 proteins (Figure.4F-G). Importantly, our previous studies have shown that all of  
17 these interacting proteins are within the MAM structures of mouse and human  
18 testes (Wang et al., 2018), suggesting MFN2 may function with the  
19 Nuage-associated proteins in maintaining MAM structure integrity.

20 We next examined whether the expression levels of MIWI, DDX4, GASZ,  
21 and TDRKH interacting proteins were affected upon deletion of MFN2 in testes.  
22 Co-immunostaining of *Mfn2*-cKO and control testes revealed ectopic  
23 expression of MIWI, DDX4, and GASZ in *Mfn2*-cKO testes in IMC and CB  
24 structures while TDRKH displayed no apparent changes (Figure.4H and  
25 Supplementary Figure. S5C-E). In *Mfn2*-cKO testes, both MIWI and DDX4  
26 showed weaker staining in the IMC of pachytene spermatocytes and barely  
27 detected in the CB of round spermatids (Figure.4H and Supplementary  
28 Figure.S5C-D). Of note, unlike the perinuclear granular mitochondrial  
29 localization showed in the control spermatocytes, DDX4 displayed a diffuse  
30 cytoplasmic expression pattern in *Mfn2*-cKO spermatocytes (Supplementary

Figure.S5D). GASZ also showed a decreased signal in both pachytene spermatocytes and round spermatids within *Mfn2*-cKO testicular sections (Figure.4H and Supplementary Figure.S5E). Since MFN1 was reported to interact with GASZ and is essential for spermatogenesis(Zhang et al., 2016), we also compared the expression and localization of DDX4, GASZ, and TDRKH in *Mfn1*-cKO adult testes. However, unlike *Mfn2*-cKO testes, we found no obvious changes in expression or localization in *Mfn1*-cKO testes (Supplementary Figure.S5F-H).

Given the Nuage-associated proteins are documented in regulating the piRNA biogenesis pathway, which prompts us to determine whether MFN2 participates in the piRNA pathway. Due to the morphology and the cell populations are comparable at P25 between WT and *Mfn2*-cKO testes, we chose the P25 testes to examine the abundance and size of piRNA distributions through small RNA sequencing. The results showed about a 50% decrease of the whole piRNA populations after normalized with miRNA counts (Supplementary Figure.S6A and Table S1), suggesting that MFN2 might take part in piRNA biogenesis through its interaction with the Nuage proteins. We next tried to ask whether the retrotransposons were affected in *Mfn2*-cKO testes because the Nuage-associated proteins have reported repressing retrotransposons for maintaining the genome integrity of male germline. By RT-qPCR assays, we analyzed the mRNA expression levels of retrotransposons, including LINE1 and IAP, and found that there are no significant changes between WT and *Mfn2*-cKO testes (Supplementary Figure.S6B). Consistent with the mRNA level of LINE1, the LINE1 ORF1 protein expression showed no activation both in P25 (data not shown) and P60 *Mfn2*-cKO testes (Supplementary Figure.S6C). Taken together, these results indicate that MFN2 plays a crucial role in the formation and/or maintenance of the network of RNA processing proteins and piRNA pathways in the Nuage during spermatogenesis.

30

## RNA-seq reveals differential expression genes involved in mRNA processing in spermatogenic cells

To understand the underlying molecular mechanism of MFN2 in regulating spermatogenic cell development, we performed whole-transcriptome sequencing to assess the differential expression genes in purified pachytene spermatocytes (PS) and round spermatids (RS) from WT and *Mfn2*-cKO adult testes. After RNA deep sequencing, we performed pairwise differential gene expression comparisons to define the genes whose expression changed by at least 2-fold ( $P \leq 0.05$ ) when WT and *Mfn2*-cKO groups were compared. Hierarchical clustering of differentially expressed genes (DEG) showed that, in pachytene spermatocytes, a total of 4046 genes up-regulated and 5324 genes were down-regulated in *Mfn2*-cKO mice compared to that of WT mice. In round spermatids, a total of 3756 genes up-regulated and 3186 genes were down-regulated in *Mfn2*-cKO mice compared to that of WT mice (Figure.5A-B, Supplementary Fig.7SA-B and Table S2-3). Principal component analysis (PCA) separated the data into four sub-groups clustering each separately as WT control and *Mfn2*-cKO pachytene spermatocytes and round spermatids, showing the gross changes of the transcriptome between WT and *Mfn2*-cKO transcriptome (Supplementary Figure.S7C).

Gene Ontology (GO) was then applied to assess what molecular functions and biological processes altered upon a lack of *Mfn2* in testes. In pachytene spermatocytes, the most up-regulated genes in *Mfn2*-cKO mice mainly involved regulation of biological quality and localization (Supplementary Figure.S7D). The down-regulated genes were primarily associated with the metabolic process (Supplementary Figure.S7E). Similarly, in round spermatids, the up-regulated genes in *Mfn2*-cKO mice were mostly distributed in vesicle fraction and associated with those that regulate phosphorus metabolic processes, and the down-regulated genes were distributed in cell and intracellular part and enriched in the cellular and metabolic processes

(Supplementary Figure.S7F-G). Importantly, when the top 20 GO terms analyzed by organized *P*-value and rich factor, we found that the most up-regulated genes in *Mfn2*-cKO pachytene spermatocytes were mainly involved in glutathione binding, oligopeptide binding, glutathione transferase activity, cytosolic large ribosomal subunit and cytosolic ribosome, which run the top 5 enrichment sorted by rich factor. Besides, sperm flagellum, spermatogenesis and motile cilium were included in the top 20 GO terms (Figure.5C). While for the down-regulated genes, mRNA processing, nucleoplasm part, RNA processing, transferase complex and chromosome organization harbored the higher rich factor (Figure.5D). By contrast, in *Mfn2*-cKO round spermatids, the top 5 enrichment sorted by rich factor for the up-regulated genes were involved in protein phosphatase type 1 complex, glutathione binding, oligopeptide binding, antigen processing and platelet aggregation (Figure.5E), and for down-regulated genes with higher rich factor were involved in nuclear chromosome segregation, chromosome segregation, nuclear division, organelle fission and chromosome organization (Figure.5F).

KEGG pathway analysis revealed that, in pachytene spermatocytes, the top 5 pathways by *P*-value associated with up-regulated genes belonged to glycolysis/glucogenesis, ribosome, HIF-1 signaling, biogenesis of amino acids and carbon metabolism, and the top 5 pathways involved in down-regulated genes were related to spliceosome, RNA transport, Huntington's disease, ribosome biogenesis in eukaryotes and cell cycle (Supplementary Figure.S7H-I). In round spermatids, the KEGG pathways associated with up- and down-regulated genes were similar to that of in pachytene spermatocytes, as emphasized for the top 5 pathways (Supplementary Figure.S7J-K).

To validate the RNA-seq data, we randomly selected several genes associated with ribosome, spliceosome and mRNA transport pathways for RT-qPCR analysis. In line with the RNA-seq data, genes involved with ribosome transport pathways up-regulated, whereas genes associated with spliceosome and mRNA transport pathways were down-regulated in both

pachytene spermatocytes and round spermatids (Figure.5G-H). Taken together, these RNA-Seq analyses support the view of an association of MFN2 with cytosolic ribosomes, the spliceosome and mRNA processing pathways essential for male germ cell development act in an integral manner.

## **MFN2 ablation results in misregulated alternative splicing events**

Given that our RNA-seq data suggest MFN2 associates with mRNA processing, we next asked whether alternative splicing (AS) events were affected in spermatogenesis. To test this possibility, we performed alternative transcript splicing analyses for the RNA-seq data on several of regulated splicing events in both *Mfn2*-cKO pachytene spermatocytes and round spermatids. Indeed, a total of 1604 misregulated splicing events were identified in 1001 genes in *Mfn2*-cKO pachytene spermatocytes, and 986 misregulated splicing events in 684 genes in *Mfn2*-cKO round spermatids were found (Figure.6A-B and Supplementary Table S4-5). Interestingly, the up- and down-regulated events account for ~50% of the total changed events separately in both pachytene spermatocytes and round spermatids (Figure.6A-B).

We then further analyzed the distribution of five typical AS types for those misregulated splicing events in pachytene spermatocytes and round spermatids, including skipped exon (SE), alternative 5' splice site (A5SS), alternative 3' splice site (A3SS), mutually exclusive exons (MXE) and retained intron (RI). The percentage of the five AS events analyses showed a similar distribution ratio with the SE highest and RI lowest in both pachytene spermatocytes and round spermatids (Figure.6C-D). Strikingly, GO analyses showed that the genes with abnormal splicing events enriched in spermatogenesis and male gamete generation in both pachytene spermatocytes and round spermatids (Figure.6E-F). Importantly, in pachytene spermatocytes, the top 5 enriched GO terms were cilium, ciliary part, microtubule organizing center, motile cilium and sperm flagellum (Figure.6E).

1 In round spermatids, the top 5 enriched GO terms were spermatogenesis,  
2 male gamete generation, cilium, gamete generation and motile cilium  
3 (Figure.6F). Thereinto, among these genes with abnormal alternative splicing,  
4 ~34.67% of genes displayed up-regulated, and 45.85% genes showed  
5 down-regulated transcriptional mRNA levels in pachytene spermatocytes.  
6 Additionally, ~33.04% genes with up-regulated and 57.02% genes with  
7 down-regulated transcriptional levels observed in round spermatids  
8 (Figure.6G-H). To further verify the modulation of MFN2 in alternative splicing,  
9 we selected a mis-spliced gene, *Map2k7*, with intron retention in both  
10 *Mfn2*-cKO pachytene spermatocytes and round spermatids based on the  
11 RNA-seq analysis as a validated gene by semi-quantitative PCR with specific  
12 primers. *Map2k7* encodes a protein kinase highly expressed in testis and acts  
13 as an essential component of the MAPK signal transduction pathway to  
14 regulate mitochondrial death signaling pathway and apoptosis(Yao et al., 1997;  
15 Tournier et al., 2001). We successfully verified the aberrant splicing pattern of  
16 *Map2k7* gene in *Mfn2*-cKO testes (Figure.6I). Taken together, these data  
17 indicate that both the transcriptional levels and alternative splicing processes  
18 of genes involved in spermatogenesis were affected upon MFN2 ablation in  
19 germ cells.

## 20 **MFN2 associates with mRNA translational machinery to regulate mRNA** 21 **fates in testes**

22 Because some of the MFN2 interaction Nuage-associated proteins, like  
23 MIWI and DDX4, are associated with RNA processing and inactive  
24 translational mRNAs in spermatogenesis(Grivna et al., 2006; Nagamori et al.,  
25 2011), we wanted to determine whether MFN2 plays a role in translation. To  
26 test this relationship, we first subjected adult testicular extracts to sucrose  
27 density gradient fractionation (Figure.7A). MFN2 is co-sedimented with both  
28 monosome (80S) and polysome fractions (Figure.7A). Similar to RPS6, the  
29 addition of EDTA to dissociate the large and small ribosomal subunits shifted

1 MFN2 to the ribonucleoprotein (RNP) fractions of the gradient. Combined with  
2 the RNA-Seq data, these results suggest that MFN2 could associate with  
3 cytoplasmic monosomes and polysomes. Thus, we subsequently evaluated  
4 whether MFN2 regulates global mRNA translation in spermatogenic cells  
5 through ribosome profiling assays in control and *Mfn2*-cKO testes. Interestingly,  
6 *Mfn2*-cKO testes displayed a similar polysome proportion as the control, yet an  
7 increased ratio of polysomes to monomers (80S)(Wrobel et al., 2015)  
8 (Figure.7B-C). This result indicates the activation of global mRNA translation  
9 upon loss of MFN2 in testes.

10 Since MSY2, as a germ cell-specific DNA/RNA-binding protein,  
11 exclusively enriched in both the meiotic and post-meiotic germ cells (Gu et al.,  
12 1998), and reported to participate in both transcription and mRNA translation  
13 (Yang et al., 2005b). Considering the above, we next asked whether MFN2  
14 complexes with MSY2 to regulate mRNA translation in testes. Co-IP  
15 experiments revealed that MFN2 could interact with MSY2 both *in vivo* and *in*  
16 *vitro* (Figure.4A and G; Figure.7D). Because our unbiased RNA-seq data  
17 showed an increased *Msy2* mRNA level in both *Mfn2*-cKO pachytene  
18 spermatocytes and round spermatids, we then wanted to examine the protein  
19 level of MFN2 in adult control and *Mfn2*-cKO testes by immunofluorescence. In  
20 control testes, MSY2 was broadly expressed in nearly all types of  
21 spermatogenic cells and showed a disperse distribution in the cytoplasm and  
22 nucleus in pachytene spermatocytes and round spermatids. However, in  
23 *Mfn2*-cKO testes, the cytoplasmic signals of MSY2 increased in pachytene  
24 spermatocytes and round spermatids, and the MSY2 foci signals within the  
25 round spermatid nucleus had almost disappeared (Figure.7E). Considering  
26 that MSY2 marks specific mRNAs in the nucleus for cytoplasmic storage and  
27 links transcription and mRNA storage/translational delay in meiotic and  
28 post-meiotic male germ cells (Yang et al., 2005a), we analyzed the  
29 transcriptional levels of MSY2-bound mRNAs in our RNA-seq data. Intriguingly,  
30 most of the MSY2-bound gamete-specific mRNAs appeared to upregulate in

1 *Mfn2*-cKO pachytene spermatocytes and round spermatids, including *Msy2*  
2 itself (Figure.7F and Supplementary Table S6). To further explore the role of  
3 MFN2 in translation, we examined if any proteins mistranslated from the  
4 MSY2-bound gamete-specific mRNAs. Since SPATA19 (also known as  
5 SPERGEN1) is a mitochondrial protein previously reported to express in  
6 haploid spermatids at P28 testes(Doiguchi et al., 2002; Matsuoka et al., 2004)  
7 and germ cell-specific *Spata19* knockout mice displayed male sterility(Mi et al.,  
8 2015), we thus chose SPATA19 to examine the protein level of *Spata19* in P25  
9 testes from control and *Mfn2*-cKO mice. Notably, we found that the protein of  
10 SPATA19 can be detected in P25 *Mfn2*-cKO round spermatids by Western blot  
11 or immunofluorescence, whereas undetectable in control round spermatids  
12 (Figure.7G-H). These data show that *Spata19* was early activated and  
13 translated when a loss of MFN2 in male germ cells, suggesting MFN2 could  
14 regulate mRNA translation.

15 To determine how MFN2 regulates mRNA translation, we examined the  
16 interplay of MFN2 with the eukaryotic elongation factors (eEF1A1 and eEF1A2)  
17 in testes, which are critical regulators during translational processes  
18 (Negrutskii and El'skaya, 1998; Sasikumar et al., 2012). As expected and  
19 revealed by reciprocal Co-IP, both eEF1A1 and eEF1A2 could interact with  
20 MFN2 (Figure.7I-K). Moreover, immunofluorescence showed that the signals  
21 of eEF1A1 and eEF1A2 increased in *Mfn2*-cKO pachytene spermatocytes. Of  
22 note, we found that both eEF1A1 and eEF1A2 appeared to express in the  
23 cytoplasm of pachytene spermatocytes, and eEF1A2 co-localized with ATP5A  
24 (a mitochondria marker) but not eEF1A1 (Figure.7L). These data suggest that  
25 the early activated mRNA translation in *Mfn2*-cKO testes, especially for some  
26 gamete-specific mRNAs, is likely due to the disassociation of the interplay of  
27 MFN2 with elongation factor eEF1A1 and eEF1A2. Taken together, these  
28 results indicate that *Mfn2* is associated with mRNA translational machinery by  
29 interaction with several Nuage-associated proteins (like MIWI) and control the  
30 fates of gamete-specific genes during spermatogenesis.

# Discussion

Mitofusins, MFN1 and MFN2, are the first known mediators of mitochondrial fusion proteins in mammals (Hales and Fuller, 1997). Their functions in neuron and heart have well explored (Dietrich et al., 2013; Schneeberger et al., 2013; Hall et al., 2016; Jiang et al., 2018), yet their roles in spermatogenesis are poorly understood. In this study, we showed that the germ cell-specific deletion of *Mfn2* disrupts the mitochondria, ER and MAM structure, gamete-specific mRNA translation processes, resulting in male sterility. Importantly, the phenotype of *Mfn2*-cKO mice is age-dependent, with germ cells beginning their decline after P35. With increasing age, vacuolation of the seminiferous tubule becomes severe. In comparison, the *Mfn1*-cKO shows vacuolization as early as P28 in this study. Interestingly, *Vasa*-Cre mediated *Mfn1* knock out mice (*Vasa*-Cre; *Mfn1*<sup>flox/flox</sup>) were also infertile and displayed very severe phenotypes showing seminiferous tubule vacuolization as early as P14 (Zhang et al., 2016). The discrepancy of phenotypes between our *Mfn1*-cKO mice (*Stra8*-Cre; *Mfn1*<sup>flox/flox</sup>) and the reported mice (*Vasa*-Cre; *Mfn1*<sup>flox/flox</sup>) possibly reflects the differences in Cre recombinase expression since *Vasa*-Cre appears much earlier than *Stra8*-Cre in the male germ. Remarkably, the *Mfn1/2* double knockout testes showed a more severe phenotype of near loss of pachytene spermatocytes and round spermatids, and the accumulation of mitochondria to one side of germ cell cytoplasm. Despite some of the MFN2 interaction proteins showed abnormal expression in *Mfn2*-cKO testes, including GASZ, MIWI, and DDX4, they didn't show an apparent change in *Mfn1*-cKO testes. This data is in agreement with the previous report in which *Vasa*-Cre mediated *Mfn1* conditional knockout mice showed no apparent alteration in the localization of GASZ and DDX4 (Zhang et al., 2016). Therefore, previous *Mfn1* or *Mfn2* genetic mutation functional studies in Purkinje cells and oocytes require much careful consideration (Chen et al., 2007; Hou et al., 2019), as their interaction and role in different

mammalian cell development may differ. In this study, we found that both MFN2 and MFN1 are required for spermatogenesis and male fertility, but they may exhibit a different mechanism to control spermatogenesis during male germ cell development. Indeed, our study revealed that MFN2 might work with MFN1 coordinately in spermatogenesis by taking part in different molecular pathways.

Despite a myriad of published literature focused on the function of MAM structure in neuronal systems and metabolism with several human diseases (Paillusson et al., 2016), the role of MAM structure in spermatogenesis has not reported yet. Our previous work observed that the abundance of MAM in spermatogenic cells, and many proteins identified in mass spectroscopy data were crucial regulators of spermatogenesis (Wang et al., 2018). Unexpectedly, several MFN2 interaction proteins identified in this work, including MIWI, DDX4, GASZ, and TDRKH, were present in the MAM fraction from both mouse and human testes. The data presented in the current study showed that in *Mfn2*-cKO, pachytene spermatocytes and round spermatids, MIWI, DDX4, and GASZ expression decreased. As part of the testicular MAM structure, it is likely that MFN2 and its interacting proteins serve as MAM proteins and form a protein complex or a scaffold to regulate spermatogenesis. This complex is a dynamic partner regulated by the mitochondria fusion and fission process. Once MFN2 deleted, the morphology of mitochondria, ER and MAM structures of germ cells disrupted. Therefore, the current study, for the first time, provides a possible new role of MFN2 as the MAM component in spermatogenesis and spermatogenic cell development. Specifically, the proteins located in MAMs are possibly responsible for regulating the piRNA biogenesis and mRNA translational pathways as they are a feature of Nuage-associated proteins in germ cells. The fact that we observed the aberrant piRNA production in *Mfn2*-cKO testes, suggesting MFN2 might have a function in piRNA biogenesis. However, we could not exclude the possibility in which caused by mislocalized Nuage-associated

proteins, such as MIWI, DDX4, GASZ, and TDRKH, et al., in *Mfn2*-cKO mice. It is worth noting that although the thickness of the IMC structure appeared to increase in *Mfn2*-cKO pachytene spermatocytes, this likely reflects an increased distance between mitochondria. Therefore, it indicated that the formation of IMC might be independent of MFN2 and possibly caused by misregulated Nuage-associated proteins in *Mfn2*-cKO pachytene spermatocytes as well.

An exciting finding in our study is that MFN2 enriched in monosome and polysome fractions in spermatogenic cells and cooperates with MSY2 to mediate MSY2-bound gamete-specific mRNA translation. MSY2 showed increased cytosolic expression in both pachytene spermatocytes and round spermatids upon MFN2 depletion. This discovery raises the possibility that MFN2 partners with MSY2-bound mRNA for its function because MSY2 was enriched in RNP fraction and regulates mRNA stability, storage and translation delay in spermatogenesis (Yang et al., 2005a). Additionally, we identified, in this study, several MFN2 interaction partners, such as MIWI and DDX4, localized in the Nuage (IMC and CB) and associated with translational machinery. MIWI enriched in both RNP and polysome fractions and associates with both mRNAs and piRNAs in cytosolic ribonucleoprotein and polysomal fractions (Grivna et al., 2006), whereas DDX4 has reported stimulating translation initiation of specific mRNAs through interaction with the general translation initiation factor eIF5B (Johnstone and Lasko, 2004; Liu et al., 2009). Such partnerships might be essential for initiating spermiogenesis and gamete-specific mRNA translational delay because spermatogenesis in both *Miwi* and *Msy2* mutants are all arrested at the post-meiotic stage (Deng and Lin, 2002; Yang et al., 2005b).

In mammalian cells, most protein-coding genes are disrupted by intervening sequences (introns), which need to be precisely and effectively removed through alternative splicing in different cell types or tissues (Baralle and Giudice, 2017). Interestingly, the mammalian testis is among the tissues

1 with the highest transcriptome complexity, including alternative splicing  
 2 regulation, especially in the spermatocyte and spermatids (Ramskold et al.,  
 3 2009; Soumillon et al., 2013; Baralle and Giudice, 2017; Estill et al., 2019). In  
 4 this study, we revealed over a thousand misregulated splicing events occur in  
 5 *Mfn2*-cKO spermatogenic cells by RNA-seq analyses. Besides, most genes  
 6 identified with misregulated splicing events in this study were critical for  
 7 spermatogenesis and gamete generation. However, it is worthy to point out  
 8 that alternative splicing usually occurs in the nucleus or adjacent nuclear  
 9 envelope, but MFN2 mainly localized in the cytoplasm of germ cells. Therefore,  
 10 the misregulation of alternative splicing observed in *Mfn2*-cKO germ cells were  
 11 surmised to be secondary defects caused by *Mfn2* deletion. The possible  
 12 explanation is that disruption of an RNA binding proteins/mRNA translation  
 13 protein complex upon *Mfn2* mutated in testes, especially MSY2, which  
 14 reported to bind mRNA directly and regulate their storage and translation,  
 15 would reconcile these observations.

16 In conclusion, we report, in this study, a novel role of MFN2 in RNA  
 17 processing through interactions with Nuage-associated proteins and mRNA  
 18 translation proteins in male germ cells during spermatogenesis. We propose  
 19 that MFN2 associates with several mRNA translation associated proteins such  
 20 as MSY2, MIWI, and DDX4 at the cytoplasmic Nuage and/or MAM, and it likely  
 21 serves as a scaffold to recruit mRNA, polysomes and other RNA binding  
 22 proteins in both pachytene spermatocytes and round spermatids, which further  
 23 work together with the elongation factor1 alpha subunits (like eEF1A1 and  
 24 eEF1A2) to control gamete-specific transcripts delay during spermatogenesis  
 25 (Figure.8A-B). These are beyond its known functions in regulating  
 26 mitochondrial fusion processes. Furthermore, our research suggests that  
 27 Mitofusins (both MFN1 and MFN2) are essential for mouse spermatogenesis  
 28 and male fertility, and provide the first evidence for mitofusin proteins  
 29 associated with RNA processing and translational machinery in regulating  
 30 germ cell development during mouse spermatogenesis.

1

## 2 **Materials and methods**

### 3 **Animals and ethics statement**

4 All animal procedures were approved by the Institutional Animal Care and Use  
 5 Committee (IACUC) of Tongji Medical College, Huazhong University of  
 6 Science and Technology, and the mice housed in the specific pathogen-free  
 7 facility of Huazhong University of Science and Technology. All experiments  
 8 with mice were conducted ethically according to the Guide for the Care and  
 9 Use of Laboratory Animal guidelines. Floxed *Mfn1* or *Mfn2* mice were created  
 10 previously(Chen et al., 2007). The mice were harboring the floxed *Mfn1* or  
 11 *Mfn2* allele purchased from the Jackson Laboratory (Stock no. 026401 and  
 12 026525). *Mfn1*<sup>flox/flox</sup> and/or *Mfn2*<sup>flox/flox</sup> female mice were crossed with  
 13 *Stra8*-Cre male mice (*Stra8*-Cre mice was purchased from the Jackson  
 14 Laboratory, stock no. 008208) to obtain *Stra8*-Cre; *Mfn1*<sup>+/<sup>flox</sup></sup> and/or *Mfn2*<sup>+/<sup>flox</sup></sup>  
 15 males, then the *Stra8*-Cre; *Mfn1*<sup>+/<sup>flox</sup></sup> and/or *Mfn2*<sup>+/<sup>flox</sup></sup> male mice were further  
 16 bred with *Mfn1*<sup>flox/flox</sup> and/or *Mfn2*<sup>flox/flox</sup> to obtain *Stra8*-Cre; *Mfn1*<sup>flox/del</sup> and/or  
 17 *Mfn2*<sup>flox/del</sup> (designated as *Mfn1*-cKO and/or *Mfn2*-cKO) males.

18

### 19 **Antibodies**

20 The details of all commercial antibodies used in this study are presented in  
 21 Supplementary Table S7.

22

### 23 **Histological analysis, immunostaining and imaging**

24 Testes and epididymides from control and cKO mice were collected and fixed  
 25 in Bouin's solution (SIGMA, HT10132) at 4°C overnight and then washed with  
 26 75% alcohol 5 times for 30 minutes each time. Samples were then embedded  
 27 in paraffin, and 5µm sections were cut and stained with periodic acid-Schiff  
 28 (PAS) after being dewaxed and rehydrated. Slides were then mounted with  
 29 Permount (Fisher Chemical<sup>TM</sup>SP15-100) and imaged with a ZEISS

1 microscope. For immunofluorescence staining, testes were fixed in 4% PFA in  
2 PBS overnight at 4°C and embedded in the Tissue-Tek O.C.T. compound  
3 (Sakura Finetek, 4583) on dry ice. A 5µm thick section was cut and  
4 microwaved in 0.01M sodium citrate buffer (pH=6.0) for 5 min to retrieve  
5 antigen. After rinsing with PBS three times, the sections were blocked in  
6 blocking solution (containing 3% normal goat serum and 3% fetal bovine  
7 serum in 1% bovine serum albumin) for 1h at room temperature. Testis  
8 sections then incubated with primary antibodies (Supplementary Table S7)  
9 diluted in blocking solution overnight at 4°C. After washing with PBS, sections  
10 were incubated with Alexa Fluor 488 goat anti-rabbit IgG (1:500; A32731,  
11 Invitrogen) and/or Alexa Fluor 594 goat anti-mouse IgG (1:500, A11032,  
12 Invitrogen) for 1h at room temperature and then stained with DAPI for 5 min,  
13 washed in PBS and mounted using 80% glycerol. Confocal fluorescence  
14 microscopy was conducted using a confocal A1 laser microscope (Nikon,  
15 Japan).

16

## 17 **TUNEL analyses**

18 Testes were fixed in Bouin's solution, embedded in paraffin and sectioned  
19 (5µm). TUNEL staining performed using One Step TUNEL Apoptosis Assay Kit  
20 (Meilunbio Cat. MA0223) according to the manufacturer's instructions. Images  
21 were obtained with a FluoView 1000 microscope (Olympus, Japan).

22

## 23 **Transmission electron microscopy (TEM)**

24 TEM was performed as described previously with some modifications(Wang et  
25 al., 2018). In brief, testes from control and cKO were fixed in 0.1M cacodylate  
26 buffer (pH=7.4) containing 3% paraformaldehyde and 3% glutaraldehyde plus  
27 0.2% picric acid for 2h at 4°C, then for 1h at RT. After three washes with 0.1M  
28 cacodylate buffer, the samples were post-fixed with 1% OsO<sub>4</sub> for 1h at RT.  
29 Then the samples were dehydrated in sequential ethanol solutions and  
30 embedded in an Eponate mixture (Electron Microscopy Sciences, Hatfield, PA,

USA) for polymerization for 24h at 60°C. Ultrathin sections (~70nm) were cut with a diamond knife. The sections were re-stained with uranyl acetate and lead citrate and then photographed using a transmission electron microscope (FEI Tecnai G2 12, Holland). For the calculation of the ERMICC contact index, the formula is the  $LIN/(PerM \times DistER-M)$ . LIN represents the interface length between mitochondria and ER; PerM indicates mitochondria perimeter, and DistER-M is the distance between mitochondria and ER. About 100 mitochondria were considered to calculate for Mito-ER distance, Mito-ER contacts, and ERMICC contact index.

### **Cell culture and transfection**

HEK293T (293T) cells were cultured in DMEM medium with 10% serum. Transfection performed using Lipofectamine 2000 (Invitrogen) according to the manufacturer's instructions. For the transfection of plasmid, 4µg DNA was used in a 45mm diameter plate.

### **Sertoli cell purification**

For Sertoli cell isolation, testes from adult mice were dissected in DHANKS medium and incubated in DMEM/F12 medium containing 1 mg/ml collagenase IV, 0.5 mg/ml Deoxyribonuclease I and 0.5 mg/mL hyaluronidase for 10min at 37 °C. After centrifuge (1000 rpm/min), the precipitates were collected and incubated in the DMEM/F12 medium with 2.5 mg/ml trypsin and 0.5 mg/ml Deoxyribonuclease I for 10min at 37 °C. Then seminiferous tubules were incubated with DMEM/F12 containing 10%FBS for 5 min to inhibit the trypsin digestion. Subsequently, Sertoli cells collected after filtering through 40µm pore-size nylon mesh and stored for the experiments.

### **Protein extracts and Western blots**

Protein extracts were prepared from mouse tissues using RIPA lysis buffer (150 mM sodium chloride, 1.0% NP-40, 0.5% sodium deoxycholate, 0.1% SDS,

and 50mM Tris, pH=8.0). Protein extracts were denatured with 2X loading buffer (4% SDS, 10% 2-mercaptoethanol, 20% glycerol, 0.004% bromophenol blue, 0.125M Tris-HCl, pH=6.8) at 95°C for 10 min and run on a 10% SDS-PAGE, followed by transfer to PVDF membrane. The membrane was probed with primary antibodies (Supplementary Table S7) followed by secondary antibody treatment at 1:10000 dilutions (anti-mouse HRP and anti-rabbit HRP, abbkine). Immun-Star™ HRP (1705040, BIO-RAD) was used for chemiluminescence detection and photographed by ChemiDoc XRS+ system (BIO-RAD).

### Co-immunoprecipitation

For *in vivo* co-immunoprecipitation, mouse testes were homogenized in lysis buffer (20mM HEPES, pH=7.3, 150mM NaCl, 2.5mM MgCl<sub>2</sub>, 0.2 % NP-40, and 1mM DTT) with protease inhibitor cocktail (P1010, Beyotime, China). Relevant antibody and pre-cleaned magnetic protein A/G beads added to the tissue lysate. The lysate was incubated overnight at 4°C with gentle agitation to form the immunocomplex, and the magnetic beads were washed using the lysis buffer for 5 times. The pellet was re-suspended with 30μl lysis buffer and 30μl 2X loading buffer (4% SDS, 10% 2-mercaptoethanol, 20% glycerol, 0.004% bromophenol blue, 0.125 M Tris-HCl, pH=6.8), pipetted up and down several times to mix and elute the protein from the beads, then boiled at 95°C for 10 min and run on a 10% SDS-PAGE. For *in vitro* co-immunoprecipitation, full-length *Mfn2* cDNA was cloned into a modified pcDNA3 vector encoding a 2X FLAG-tag, and full-length *Miwi*, *Ddx4*, *Msy2*, and *Tdrkh* cDNAs were cloned into pCMV vector carrying an MYC-tag. HEK293T cells were transfected with indicated plasmids using Lipofectamine 2000 (Life Technologies). After 48h, immunoprecipitation was performed using anti-MYC rabbit polyclonal antibody (10828-1-AP, Proteintech), followed by a Western blot to identify protein interactions.

1

## 2 **RNA isolation, reverse transcription and RT-qPCR**

3 Total RNA was extracted from mouse tissues using Trizol reagent (Invitrogen,  
4 Cat no.15596-025) following the manufacturer's instructions. For  
5 complementary DNA (cDNA) synthesis, 1µg of RNA was treated with DNase I  
6 (Progema, M6101) to remove the residual genomic DNA and reverse  
7 transcribed with cDNA Synthesis Kit (ThermoFisher, Cat no. 4368814).  
8 RT-qPCR was performed using an SYBR Premix on a StepOne Plus machine  
9 (ABI). Relative gene expression was analyzed using the  $2^{-\Delta\Delta C_t}$  method with  
10 *Arbp* as an internal control. All primers are shown in Supplementary Table S8.

11

## 12 **Purification of spermatogenic cells**

13 STA-PUT method based on sedimentation velocity at unit gravity (Bellve et al.,  
14 1977; Bellve, 1993) was used to purify the pachytene spermatocytes and  
15 round spermatids from adult WT and *Mfn2*-cKO mouse testes. We assessed  
16 cellular morphology using phase contrast microscopy to determine the purity of  
17 the cell population. Pachytene spermatocytes and round spermatids with ≥90%  
18 purity were used for RNA-seq analyses.

19

## 20 **RNA sequencing and bioinformatics analysis**

21 After purification of pachytene spermatocytes and round spermatids from WT  
22 and *Mfn2*-cKO testes, total RNA was isolated using the Trizol reagent following  
23 the manufacturer's protocol and treated with DNase I to digest residual  
24 genomic RNA. The purity, concentration, and integrity were assessed using a  
25 NanoDrop 2000 spectrophotometer (Thermo Scientific), a Qubit RNA Assay  
26 Kit in Qubit 2.0 Fluorometer (Life Technologies), and a Nano 6,000 Assay Kit of  
27 the Bioanalyzer 2,100 system (Agilent Technologies), respectively. Then, a  
28 total amount of 2µg of RNA per sample was used to prepare poly(A+)-enriched  
29 cDNA libraries using the NEBNext Ultra RNA library Prep Kit for Illumina (New

England BioLabs) according to the manufacturer's instructions, and base pairs (raw data) were generated by the Illumina Hi-Seq 2500 platform. Raw reads were processed with cutadapt v1.9.1 to remove adaptors and perform quality trimming. Trimmed reads were mapped to the UCSC mm10 assembly using HiSAT2 (V2.0.1) with default parameters. Differentially expressed genes for all pairwise comparisons were assessed by DESeq2 (v1.10.1) with internal normalization of reads to account for library size and RNA composition bias. Differentially regulated genes in the DESeq2 analysis were defined as two-fold changes with an adjusted *P*-value of <0.05. Alternative splicing (AS) patterns were processed with rMATs software (replicate Multivariate Analysis of Transcript Splicing)(Shen et al., 2014). Splicing events with FDR (false discovery rate) <0.05 and  $|\Delta\psi|>0.05$  were defined as misregulated AS events. Gene Ontology (GO) and Kyoto Encyclopedia of Genes and Genomes (KEGG) analyses were conducted using the database for annotation, visualization, and integrated discovery (DAVID)(Dennis et al., 2003). Rich factor=(number of differentially expressed genes in GO term)/(total number of genes in GO term). The larger rich factor is, the higher enrichment is. The integrative genomics browser tool (IGB)(Freese et al., 2016) was used for efficient and flexible visualization and exploration of spliced sites between WT and *Mfn2*-cKO samples on standard desktop computers.

## **Small RNA-Seq library preparation and sequencing**

For preparing small RNA-seq libraries, two biological testis samples at P25 from WT and *Mfn2*-cKO mice were collected, respectively. Total RNAs extracted using TRIzol reagent (Invitrogen) and subsequently processed to prepare small RNA-Seq library and sequencing as previously described(Dong et al., 2019). For the length distribution of piRNAs analysis, data were normalized by miRNA reads (21–23nt) from small RNA sequencing.

## **Sucrose density gradient fractionation and polysome profiling**

1 Testicular seminiferous tubules were dissected and collected according to  
2 previous literature with minor modifications(Abouhouda et al., 2017;  
3 Karamysheva et al., 2018). Briefly after adding polysome extraction buffer  
4 (20mM Tris-HCl, pH 7.4, 100 mM KCl, 5 mM MgCl<sub>2</sub>, 1 mM DTT, 0.5% NP-40,  
5 1x protease inhibitor cocktail (EDTA-free), 200 µg/ml CHX, 200 units/mL of  
6 RNase inhibitor), the tubules were transferred to a small (0.5-1.0 mL) Dounce  
7 homogenizer to disrupt the tissues with seven to eight strokes of the glass  
8 pestle. The samples were centrifuged at 12,000g in 4°C for 10 min to collect  
9 the supernatant into a new tube. Then, DNase I (final 5 U/ml) was added into  
10 the tube, and the tube was placed on ice for 30 min to allow the DNase I to  
11 degrade any DNA contamination. Equal amounts of cytoplasmic lysates were  
12 carefully loaded on the top of a 10-50% sucrose gradient. All tubes were  
13 equally balanced, and then the gradients were centrifuged for 3h in SW41Ti  
14 swinging bucket rotor at 160,000g at 4 °C using a Beckman ultracentrifuge.  
15 Fractions (300µl/tube) were collected manually and immediately transferred to  
16 an ice bucket. The absorbance was detected at 260nm to display the  
17 polysome profile of the gradients. The proteins were precipitated with 9  
18 volumes of 96% ethanol.

19

## 20 **Statistical analysis**

21 All data are presented as mean ± SEM unless otherwise noted in the figure  
22 legends. Statistical differences between datasets were assessed by one-way  
23 ANOVA or Student's t-test using the SPSS16.0 software. *P*-values are denoted  
24 in figures by \*, *P* < 0.05; \*\*, *P* < 0.01; and \*\*\*, *P* < 0.001.

25

## 26 **Data availability**

27 All data needed to evaluate the conclusions in the paper are present in the  
28 paper and/or the Supplementary Materials. All RNA sequencing data are  
29 deposited in the NCBI SRA (Sequence Read Archive) database with the  
30 accession number of SRP212036. All other supporting data of this study are

available from the corresponding author upon reasonable request.

### **Acknowledgments**

We are grateful for engaging discussions with colleagues from Huazhong University Science and Technology, China, in the very initial phase of the project. This work supported by grants from National Natural Science Foundation of China (31671551 and 81971444 to S.Y.), the Science Technology and Innovation Commission of Shenzhen Municipality (JCYJ20170244 to S.Y.), Natural Science Foundation of Hubei Province (2017CFA069 to S.Y.).

### **Author contributions**

X.W. and S.Y. conceived and designed the research. X.W., Y.W., J.Z., S.G., C.C., S.K., and Z.Z. performed all bench experiments and data analyses. S.Y., X.W., and Z.Z. wrote the manuscript. S.Y. supervised the project. All authors read and approved the manuscript.

### **Conflict of interest**

The authors declare that they have no conflict of interest.

# References

- Aboulhoda, S., Di Santo, R., Therizols, G. and Weinberg, D. (2017) 'Accurate, Streamlined Analysis of mRNA Translation by Sucrose Gradient Fractionation', *Bio Protoc* 7(19).
- Baralle, F. E. and Giudice, J. (2017) 'Alternative splicing as a regulator of development and tissue identity', *Nat Rev Mol Cell Biol* 18(7): 437-451.
- Bellve, A. R. (1993) 'Purification, culture, and fractionation of spermatogenic cells', *Methods Enzymol* 225: 84-113.
- Bellve, A. R., Cavicchia, J. C., Millette, C. F., O'Brien, D. A., Bhatnagar, Y. M. and Dym, M. (1977) 'Spermatogenic cells of the prepuberal mouse. Isolation and morphological characterization', *J Cell Biol* 74(1): 68-85.
- Bouhy, D. and Timmerman, V. (2013) 'Animal models and therapeutic prospects for Charcot-Marie-Tooth disease', *Ann Neurol* 74(3): 391-6.
- Castaneda, J., Genzor, P., van der Heijden, G. W., Sarkeshik, A., Yates, J. R., 3rd, Ingolia, N. T and Bortvin, A. (2014) 'Reduced pachytene piRNAs and translation underlie spermiogenic arrest in Maelstrom mutant mice', *EMBO J* 33(18): 1999-2019.
- Chen, H. and Chan, D. C. (2004) 'Mitochondrial dynamics in mammals', *Curr Top Dev Biol* 59: 119-44.
- Chen, H., Detmer, S. A., Ewald, A. J., Griffin, E. E., Fraser, S. E. and Chan, D. C. (2003) 'Mitofusins Mfn1 and Mfn2 coordinately regulate mitochondrial fusion and are essential for embryonic development', *J Cell Biol* 160(2): 189-200.
- Chen, H., McCaffery, J. M. and Chan, D. C. (2007) 'Mitochondrial fusion protects against neurodegeneration in the cerebellum', *Cell* 130(3): 548-62.
- Chen, H., Vermulst, M., Wang, Y. E., Chomyn, A., Prolla, T. A., McCaffery, J. M. and Chan, D. C. (2010) 'Mitochondrial fusion is required for mtDNA stability in skeletal muscle and tolerance of mtDNA mutations', *Cell* 141(2): 280-9.
- de Brito, O. M. and Scorrano, L. (2008) 'Mitofusin 2 tethers endoplasmic reticulum to mitochondria', *Nature* 456(7222): 605-10.
- De Martino, C., Floridi, A., Marcante, M. L., Malorni, W., Scorza Barcellona, P., Bellocci, M. and Silvestrini, B. (1979) 'Morphological, histochemical and biochemical studies on germ cell mitochondria of normal rats', *Cell Tissue Res* 196(1): 1-22.
- Deng, W. and Lin, H. (2002) 'miwi, a murine homolog of piwi, encodes a cytoplasmic protein essential for spermatogenesis', *Dev Cell* 2(6): 819-30.
- Dennis, G., Jr., Sherman, B. T., Hosack, D. A., Yang, J., Gao, W., Lane, H. C. and Lempicki, R. A. (2003) 'DAVID: Database for Annotation, Visualization, and Integrated Discovery', *Genome Bio* 4(5): P3.
- Dietrich, M. O., Liu, Z. W. and Horvath, T. L. (2013) 'Mitochondrial dynamics controlled by mitofusins regulate AgRP neuronal activity and diet-induced obesity', *Cell* 155(1): 188-99.
- Doiguchi, M., Mori, T., Toshimori, K., Shibata, Y. and Iida, H. (2002) 'Spengen-1 might be an adhesive molecule associated with mitochondria in the middle piece of spermatozoa', *Dev Biol* 252(1): 127-37.
- Dong, J., Wang, X., Cao, C., Wen, Y., Sakashita, A., Chen, S., Zhang, J., Zhang, Y., Zhou, L., Luo, M. et al. (2019) 'UHRF1 suppresses retrotransposons and cooperates with PRMT5 and PIWI proteins in male germ cells', *Nat Commun* 10(1): 4705.
- Estill, M. S., Hauser, R. and Krawetz, S. A. (2019) 'RNA element discovery from germ cell to blastocyst', *Nucleic Acids Res* 47(5): 2263-2275.
- Fanourgakis, G., Lesche, M., Akpinar, M., Dahl, A. and Jessberger, R. (2016) 'Chromatoid Body Protein

- 1 **TDRD6 Supports Long 3' UTR Triggered Nonsense Mediated mRNA Decay', *PLoS Genet*12(5): e1005857.**
- 2 **Freeze, N. H., Norris, D. C. and Loraine, A. E. (2016) 'Integrated genome browser: visual analytics platform**
- 3 **for genomics', *Bioinformatics*32(14): 2089-95.**
- 4 **Grivna, S. T., Pyhtila, B. and Lin, H. (2006) 'MIWI associates with translational machinery and**
- 5 **PIWI-interacting RNAs (piRNAs) in regulating spermatogenesis', *Proc Natl Acad Sci U S A* 103(36):**
- 6 **13415-20.**
- 7 **Gu, W., Tekur, S., Reinbold, R., Eppig, J. J., Choi, Y. C., Zheng, J. Z., Murray, M. T. and Hecht, N. B. (1998)**
- 8 **'Mammalian male and female germ cells express a germ cell-specific Y-Box protein, MSY2', *Biol***
- 9 ***Reprod*59(5): 1266-74.**
- 10 **Hales, K. G. and Fuller, M. T. (1997) 'Developmentally regulated mitochondrial fusion mediated by a**
- 11 **conserved, novel, predicted GTPase', *Cell*90(1): 121-9.**
- 12 **Hall, A. R., Burke, N., Dongworth, R. K., Kalkhoran, S. B., Dyson, A., Vicencio, J. M., Dorn, G. W., II, Yellon, D. M.**
- 13 **and Hausenloy, D. J. (2016) 'Hearts deficient in both Mfn1 and Mfn2 are protected against acute**
- 14 **myocardial infarction', *Cell Death Dis*7: e2238.**
- 15 **Hou, X., Zhu, S., Zhang, H., Li, C., Qiu, D., Ge, J., Guo, X. and Wang, Q. (2019) 'Mitofusin1 in oocyte is essential**
- 16 **for female fertility', *Redox Biol*21: 101110.**
- 17 **Iguchi, N., Tobias, J. W. and Hecht, N. B. (2006) 'Expression profiling reveals meiotic male germ cell**
- 18 **mRNAs that are translationally up- and down-regulated', *Proc Natl Acad Sci U S A*103(20): 7712-7.**
- 19 **Jiang, S., Nandy, P., Wang, W., Ma, X., Hsia, J., Wang, C., Wang, Z., Niu, M., Siedlak, S. L., Torres, S. et al. (2018)**
- 20 **'Mfn2 ablation causes an oxidative stress response and eventual neuronal death in the hippocampus**
- 21 **and cortex', *Mol Neurodegener*13(1): 5.**
- 22 **Johnstone, O. and Lasko, P. (2004) 'Interaction with eIF5B is essential for Vasa function during**
- 23 **development', *Development*131(17): 4167-78.**
- 24 **Karamysheva, Z. N., Tikhonova, E. B., Grozdanov, P. N., Huffman, J. C., Baca, K. R., Karamyshev, A., Denison, R.**
- 25 **B., MacDonald, C. C., Zhang, K. and Karamyshev, A. I. (2018) 'Polysome Profiling in Leishmania, Human**
- 26 **Cells and Mouse Testis', *J Vis Exp*134).**
- 27 **Kotaja, N. and Sassone-Corsi, P. (2007) 'The chromatoid body: a germ-cell-specific RNA-processing**
- 28 **centre', *Nat Rev Mol Cell Bio*8(1): 85-90.**
- 29 **Liu, N., Han, H. and Lasko, P. (2009) 'Vasa promotes Drosophila germline stem cell differentiation by**
- 30 **activating mei-P26 translation by directly interacting with a (U)-rich motif in its 3' UTR', *Genes Dev***
- 31 **23(23): 2742-52.**
- 32 **Ma, L., Buchold, G. M., Greenbaum, M. P., Roy, A., Burns, K. H., Zhu, H., Han, D. Y., Harris, R. A., Coarfa, C.,**
- 33 **Gunaratne, P. H. et al. (2009) 'GASZ is essential for male meiosis and suppression of retrotransposon**
- 34 **expression in the male germline', *PLoS Genet*5(9): e1000635.**
- 35 **Matsuoka, Y., Iguchi, N., Kitamura, K., Nishimura, H., Manabe, H., Miyagawa, Y., Koga, M., Matsumiya, K.,**
- 36 **Okuyama, A., Tanaka, H. et al. (2004) 'Cloning and characterization of a mouse spergen-1 localized in**
- 37 **sperm mitochondria', *Int J Androl*27(3): 152-60.**
- 38 **Mi, Y., Shi, Z. and Li, J. (2015) 'Spata19 is critical for sperm mitochondrial function and male fertility', *Mol***
- 39 ***Reprod Dev*82(11): 907-13.**
- 40 **Misko, A. L., Sasaki, Y., Tuck, E., Milbrandt, J. and Baloh, R. H. (2012) 'Mitofusin2 mutations disrupt axonal**
- 41 **mitochondrial positioning and promote axon degeneration', *J Neurosci*32(12): 4145-55.**
- 42 **Nagamori, I., Cruickshank, V. A. and Sassone-Corsi, P. (2011) 'Regulation of an RNA granule during**
- 43 **spermatogenesis: acetylation of MVH in the chromatoid body of germ cells', *J Cell Sci* 124(Pt 24):**
- 44 **4346-55.**

- 1 **Negrutskii, B. S. and El'skaya, A. V. (1998) 'Eukaryotic translation elongation factor 1 alpha: structure,**
- 2 **expression, functions, and possible role in aminoacyl-tRNA channeling', *Prog Nucleic Acid Res Mol***
- 3 ***Biol*60: 47-78.**
- 4 **Paillusson, S., Stoica, R., Gomez-Suaga, P., Lau, D. H. W., Mueller, S., Miller, T. and Miller, C. C. J. (2016)**
- 5 **'There's Something Wrong with my MAM: the ER-Mitochondria Axis and Neurodegenerative Diseases',**
- 6 ***Trends Neurosci*39(3): 146-157.**
- 7 **Palmer, C. S., Osellame, L. D., Stojanovski, D. and Ryan, M. T. (2011) 'The regulation of mitochondrial**
- 8 **morphology: intricate mechanisms and dynamic machinery', *Cell Signal*23(10): 1534-45.**
- 9 **Ramalho-Santos, J., Varum, S., Amaral, S., Mota, P. C., Sousa, A. P. and Amaral, A. (2009) 'Mitochondrial**
- 10 **functionality in reproduction: from gonads and gametes to embryos and embryonic stem cells', *Hum***
- 11 ***Reprod Update*15(5): 553-72.**
- 12 **Ramskold, D., Wang, E. T., Burge, C. B. and Sandberg, R. (2009) 'An abundance of ubiquitously expressed**
- 13 **genes revealed by tissue transcriptome sequence data', *PLoS Comput Biol*5(12): e1000598.**
- 14 **Ren, M., Xu, Y., Erdjument-Bromage, H., Donelian, A., Phoon, C. K. L., Terada, N., Strathdee, D., Neubert, T. A.**
- 15 **and Schlame, M. (2019) 'Extramitochondrial cardiolipin suggests a novel function of mitochondria in**
- 16 **spermatogenesis', *J Cell Biol*.**
- 17 **Rouzier, C., Bannwarth, S., Chaussonot, A., Chevrollet, A., Verschueren, A., Bonello-Palot, N., Fragaki, K.,**
- 18 **Cano, A., Pouget, J., Pellissier, J. F. et al. (2012) 'The MFN2 gene is responsible for mitochondrial DNA**
- 19 **instability and optic atrophy 'plus' phenotype', *Brain*135(Pt 1): 23-34.**
- 20 **Sadate-Ngatchou, P. I., Payne, C. J., Dearth, A. T. and Braun, R. E. (2008) 'Cre recombinase activity specific**
- 21 **to postnatal, premeiotic male germ cells in transgenic mice', *Genesis*46(12): 738-42.**
- 22 **Santel, A. and Fuller, M. T. (2001) 'Control of mitochondrial morphology by a human mitofusin', *J Cell Sci***
- 23 **114(Pt 5): 867-74.**
- 24 **Sasikumar, A. N., Perez, W. B. and Kinzy, T. G. (2012) 'The many roles of the eukaryotic elongation factor 1**
- 25 **complex', *Wiley Interdiscip Rev RNA*3(4): 543-55.**
- 26 **Sassone-Corsi, P. (2002) 'Unique chromatin remodeling and transcriptional regulation in**
- 27 **spermatogenesis', *Science*296(5576): 2176-8.**
- 28 **Saxe, J. P., Chen, M., Zhao, H. and Lin, H. (2013) 'Tdrkh is essential for spermatogenesis and participates**
- 29 **in primary piRNA biogenesis in the germline', *EMBO J*32(13): 1869-85.**
- 30 **Schneeberger, M., Dietrich, M. O., Sebastian, D., Imbernon, M., Castano, C., Garcia, A., Esteban, Y.,**
- 31 **Gonzalez-Franquesa, A., Rodriguez, I. C., Bortolozzi, A. et al. (2013) 'Mitofusin 2 in POMC neurons**
- 32 **connects ER stress with leptin resistance and energy imbalance', *Cell*155(1): 172-87.**
- 33 **Shen, S., Park, J. W., Lu, Z. X., Lin, L., Henry, M. D., Wu, Y. N., Zhou, Q. and Xing, Y. (2014) 'rMATS: robust and**
- 34 **flexible detection of differential alternative splicing from replicate RNA-Seq data', *Proc Natl Acad Sci U***
- 35 ***SA*111(51): E5593-601.**
- 36 **Soper, S. E., van der Heijden, G. W., Hardiman, T. C., Goodheart, M., Martin, S. L., de Boer, P. and Bortvin, A.**
- 37 **(2008) 'Mouse maelstrom, a component of nuage, is essential for spermatogenesis and transposon**
- 38 **repression in meiosis', *Dev Cell*15(2): 285-97.**
- 39 **Soumillon, M., Necsulea, A., Weier, M., Brawand, D., Zhang, X., Gu, H., Barthes, P., Kokkinaki, M., Nef, S.,**
- 40 **Gnirke, A. et al. (2013) 'Cellular source and mechanisms of high transcriptome complexity in the**
- 41 **mammalian testis', *Cell Rep*3(6): 2179-90.**
- 42 **Takebe, M., Onohara, Y. and Yokota, S. (2013) 'Expression of MAEL in nuage and non-nuage**
- 43 **compartments of rat spermatogenic cells and colocalization with DDX4, DDX25 and MIWI', *Histochem***
- 44 ***Cell Biol*140(2): 169-81.**

- 1 Tournier, C., Dong, C., Turner, T. K., Jones, S. N., Flavell, R. A. and Davis, R. J. (2001) 'MKK7 is an essential
- 2 component of the JNK signal transduction pathway activated by proinflammatory cytokines', *Genes*
- 3 *Dev*15(11): 1419-26.
- 4 Toyooka, Y., Tsunekawa, N., Takahashi, Y., Matsui, Y., Satoh, M. and Noce, T. (2000) 'Expression and
- 5 intracellular localization of mouse Vasa-homologue protein during germ cell development', *Mech Dev*
- 6 93(1-2): 139-49.
- 7 Varuzhanyan, G., Rojansky, R., Sweredoski, M. J., Graham, R. L., Hess, S., Ladinsky, M. S. and Chan, D. C.
- 8 (2019) 'Mitochondrial fusion is required for spermatogonial differentiation and meiosis', *Elife*8.
- 9 Vasileva, A., Tiedau, D., Firooznia, A., Muller-Reichert, T. and Jessberger, R. (2009) 'Tdrd6 is required for
- 10 spermiogenesis, chromatoid body architecture, and regulation of miRNA expression', *Curr Biol*19(8):
- 11 630-9.
- 12 Wang, X., Lv, C., Guo, Y. and Yuan, S. (2020) 'Mitochondria Associated Germinal Structures in
- 13 Spermatogenesis: piRNA Pathway Regulation and Beyond', *Cells*9(2).
- 14 Wang, X., Wen, Y., Dong, J., Cao, C. and Yuan, S. (2018) 'Systematic In-Depth Proteomic Analysis of
- 15 Mitochondria-Associated Endoplasmic Reticulum Membranes in Mouse and Human Testes',
- 16 *Proteomics*18(14): e1700478.
- 17 Westermann, B. (2010) 'Mitochondrial fusion and fission in cell life and death', *Nat Rev Mol Cell Biol*
- 18 11(12): 872-84.
- 19 Wrobel, L., Topf, U., Bragoszewski, P., Wiese, S., Sztolsztener, M. E., Oeljeklaus, S., Varabyova, A., Lirski, M.,
- 20 Chroscicki, P., Mroczek, S. et al. (2015) 'Mistargeted mitochondrial proteins activate a proteostatic
- 21 response in the cytosol', *Nature*524(7566): 485-8.
- 22 Yang, J., Medvedev, S., Reddi, P. P., Schultz, R. M. and Hecht, N. B. (2005a) 'The DNA/RNA-binding protein
- 23 MSY2 marks specific transcripts for cytoplasmic storage in mouse male germ cells', *Proc Natl Acad*
- 24 *Sci USA*102(5): 1513-8.
- 25 Yang, J., Medvedev, S., Yu, J., Tang, L. C., Agno, J. E., Matzuk, M. M., Schultz, R. M. and Hecht, N. B. (2005b)
- 26 'Absence of the DNA-/RNA-binding protein MSY2 results in male and female infertility', *Proc Natl Acad*
- 27 *Sci USA*102(16): 5755-60.
- 28 Yao, Z., Diener, K., Wang, X. S., Zukowski, M., Matsumoto, G., Zhou, G., Mo, R., Sasaki, T., Nishina, H., Hui, C. C.
- 29 et al. (1997) 'Activation of stress-activated protein kinases/c-Jun N-terminal protein kinases
- 30 (SAPKs/JNKs) by a novel mitogen-activated protein kinase kinase', *J Biol Chem*272(51): 32378-83.
- 31 Zhang, J., Wang, Q., Wang, M., Jiang, M., Wang, Y., Sun, Y., Wang, J., Xie, T., Tang, C., Tang, N. et al. (2016) 'GASZ
- 32 and mitofusin-mediated mitochondrial functions are crucial for spermatogenesis', *EMBO Rep* 17(2):
- 33 220-34.
- 34 Zuchner, S., Mersyanova, I. V., Muglia, M., Bissar-Tadmouri, N., Rochelle, J., Dadali, E. L., Zappia, M., Nelis, E.,
- 35 Patitucci, A., Senderek, J. et al. (2004) 'Mutations in the mitochondrial GTPase mitofusin 2 cause
- 36 Charcot-Marie-Tooth neuropathy type 2A', *Nat Genet*36(5): 449-51.

1

## 2 **Figure legends**

### 3 **Figure. 1. MFN2 displays a dynamic cytoplasm expression profile during**

4 **spermatogenesis. (A)** Double immunostaining with MFN2 and  $\gamma$ -H2A.X on

5 WT (wild-type) adult testis sections in different stages of seminiferous tubules

6 are shown. Nuclei were stained with DAPI. Scale bar=10 $\mu$ m. Spg,

7 Spermatogonia; PL, Preleptotene spermatocytes; L, Leptotene spermatocytes;

8 Z, Zygotene spermatocytes; PS, Pachytene spermatocytes; RS, round

9 spermatids. **(B)** Double immunostaining with MFN2 and  $\gamma$ -H2A.X on different

10 types of spermatogenic cells showing a dynamic expression through the whole

11 process of spermatogenesis. Nuclei were stained with DAPI. Scale bar=10 $\mu$ m.

12 **(C)** Co-immunostaining of MFN2 and ATP5A (an outer mitochondria

13 membrane marker) in stage VII-VIII seminiferous tubule from WT testes.

14 Nuclei were stained with DAPI. Scale bar=10 $\mu$ m.

15

### 16 **Figure. 2. Conditional ablation of MFN2 in postnatal male germ cells**

17 **results in age-dependent spermatogenic defects and male infertility. (A)**

18 RT-qPCR analysis showing the dramatic decrease in the mRNA level of *Mfn2*

19 in adult *Mfn2*-cKO testes. Data are presented as mean  $\pm$  SEM, n = 5. \*\**P*<0.01.

20 **(B)** Western blots of MFN2 expression in control and *Mfn2*-cKO testes.

21 GAPDH serves as a loading control. **(C)** Histogram showing the quantification

22 of MFN2 protein levels in (b). **(D)** Double immunostaining with MFN2 and

23  $\gamma$ -H2A.X showing MFN2 was undetectable in *Mfn2*-cKO testis sections. Nuclei

24 were stained with DAPI. Scale bar=10 $\mu$ m. **(E)** Gross morphology of the testis

25 and the epididymis from WT, heterozygote (Cre/+, *Mfn2*<sup>+/flox</sup>), and *Mfn2*-cKO

26 (Cre/+, *Mfn2*<sup>flox/flox</sup>) mice at postnatal day 56 (P56). **(F)** Testes growth curve

27 shows that the *Mfn2*-cKO testis weight was significantly decreased from P35.

28 Data are presented as mean  $\pm$  SEM, n = 5. \**P*<0.05. **(G)** Periodic acid-Schiff

29 (PAS) staining showing the histology of testis sections from control and

1 *Mfn2*-cKO mice at P42, P60, P90 and P120. Asterisk (\*) represents the  
2 vacuolated seminiferous tubules. Scale bar=50µm. (H) PAS staining showing  
3 the histology of epididymis sections from control and *Mfn2*-cKO mice at P60.  
4 Scale bar=50µm. (I) Histograms showing the number of retrieved sperm from  
5 the control and *Mfn2*-cKO cauda epididymides. (J) Deformed sperm are  
6 shown in *Mfn2*-cKO male mice. Scale bar=10µm. (K) Pie charts showing the  
7 proportional distribution of normal and malformed sperm in control and  
8 *Mfn2*-KO male mice. (L) PAS staining showing the histology of testis sections  
9 from control and *Mfn1/2*-cDKO (*Mfn1* and *Mfn2* double conditional knockout)  
10 mice at P25 and P56. Scale bar=100µm. (M) Co-immunostaining of DDX4 (a  
11 germ cell marker) and ATP5A (a mitochondria marker) in testis sections from  
12 control and *Mfn1/2*-cDKO mice at P25. Nuclei were stained with DAPI. Scale  
13 bar=10µm.

14

15 **Figure. 3. Loss of MFN2 in postnatal germ cells causes mitochondria, ER**  
16 **and MAM defects in testes. (A)** TEM showing the fragmented and swelling  
17 mitochondria (M) in pachytene spermatocytes from *Mfn2*-cKO mouse testes at  
18 P60. Right panels represent the zoomed-in mitochondria from the square  
19 areas in the left panels. Arrows indicate inter-mitochondrial cement (IMC). (B)  
20 TEM showing the condensed swelling mitochondria without obvious cristae,  
21 ER fragmentation, and enlarged mitochondria-ER distance in round spermatid  
22 from *Mfn2*-cKO mouse testes at P60. Right panels represent the zoomed-in  
23 from the square areas in the left panels. Yellow rectangles indicate MAM  
24 structures. M, Mitochondria; ER, Endoplasmic reticulum; MAM, Mitochondria  
25 associated ER membranes. (C) Scatter plot showing the aspect ratio (AR) in  
26 round spermatids from control and *Mfn2*-cKO mouse testes at P60. AR  
27 represents the ratio of the major axis to the minor axis of mitochondria. (D) The  
28 distribution of AR in (C) showing an increased percentage of short  
29 mitochondria in *Mfn2*-cKO round spermatids. \*\* $P<0.01$ . (E) Histograms  
30 showing the distance between mitochondria and ER in round spermatids from

1 control and *Mfn2*-cKO mouse testes at P60. \*\* $P < 0.01$ . (F) Histograms showing  
2 the decreased contact area between mitochondria and ER in *Mfn2*-cKO round  
3 spermatids. \*\* $P < 0.01$ . (G) Histograms showing the ERMICC values in round  
4 spermatids from control and *Mfn2*-cKO mouse testes at P60. ERMICC =  
5 mitochondrial-ER interface length / (mitochondrial perimeter x  
6 mitochondrial-ER distance). \*\* $P < 0.01$ . (H) Co-immunostaining of Calreticulin  
7 (an ER and MAM marker) and  $\gamma$ -H2A.X in testis sections from control and  
8 *Mfn2*-cKO mice at P18. Nuclei were stained with DAPI. Scale bar=10 $\mu$ m. (I)  
9 Co-immunostaining of Calreticulin and  $\gamma$ -H2A.X in testis sections from control  
10 and *Mfn2*-cKO mice at P60. Nuclei were stained with DAPI. Scale bar=20 $\mu$ m.  
11 (J) qPCR analyses showing the mtDNA copy numbers in control, *Mfn1*-cKO,  
12 and *Mfn2*-cKO mouse testes at P60. ND1 and 16S are the two genes encoded  
13 by mtDNA. \* $P < 0.05$ . (K) Respiratory enzymes COX (encoded by  
14 mitochondrial DNA) and SDH (encoded by nuclear DNA) staining of testis  
15 sections from adult control, *Mfn1*-cKO, and *Mfn2*-cKO mice. Scale bar=50 $\mu$ m.

16  
17 **Figure. 4. MFN2 interacts with nuage-associated proteins and regulates**  
18 **their expressions in spermatogenic cells. (A)** Co-immunoprecipitation of  
19 MFN2 followed by western blot detection of MIWI, DDX4, GASZ, TDRKH, and  
20 MSY2 in adult mouse testes. (B-E) Reciprocal immunoprecipitation showing  
21 that MFN2 detected in the immunoprecipitants from MIWI (b), TDRKH (c),  
22 DDX4 (d), and GASZ (e) in the adult mouse testes, respectively. (F) MFN2  
23 interacts with MIWI and TDRKH *in vitro*. HEK293T cells were transfected with  
24 indicated plasmids. After 48h of transfection, immunoprecipitation was  
25 performed using anti-MYC antibodies and detected by anti-MYC and  
26 anti-FLAG antibodies, respectively. (G) MFN2 interacts with DDX4 and MSY2  
27 *in vitro*. HEK293T cells were transfected with indicated plasmids.  
28 Immunoprecipitation was performed using anti-MYC antibody and detected by  
29 anti-MYC and anti-FLAG antibodies, respectively. (H) Co-immunostaining of  
30 ATP5A with MIWI, DDX4, GASZ, and TDRKH in pachytene spermatocyte and

1 round spermatid from control and *Mfn2*-cKO mice at P60, respectively. Scale  
2 bar=10  $\mu$ m.

3

4 **Figure. 5. Global gene expression altered in *Mfn2*-cKO spermatogenic**  
5 **cells. (A-B)** Heatmap is showing the differential expression genes in purified  
6 pachytene spermatocytes (A) and round spermatids (B) from adult WT and  
7 *Mfn2*-cKO testes, respectively. The upper left images are showing the purity  
8 and morphology of isolated pachytene spermatocytes (PS) and round  
9 spermatids (RS), respectively. Significantly regulated genes have a *P*-value of  
10 <0.05 and a fold change of > 2.0. Two biological replicates indicated in the  
11 heat-map. **(C-D)** Gene ontology (GO) term analyses showing the top 20 GO  
12 terms for the up-regulated (C) and down-regulated (D) genes in *Mfn2*-cKO  
13 pachytene spermatocytes. Rich factor= (number of differentially expressed  
14 genes in GO term)/(total number of genes in GO term). A larger rich factor  
15 indicates higher enrichment. Top 5 GO terms by rich factor highlighted in red.  
16 **(E-F)** Gene ontology (GO) term analyses showing the top 20 GO terms for the  
17 up-regulated (E) and down-regulated (F) genes in *Mfn2*-cKO round spermatids.  
18 Top 5 GO terms by rich factor highlighted in red. **(G-H)** Validation of the up-  
19 and down-regulated genes selected from RNA-seq data in purified pachytene  
20 spermatocytes (G) and round spermatids (H) by RT-qPCR analyses.

21

22 **Figure. 6. Ablation of MFN2 in postnatal germ cells leads to misregulated**  
23 **alternative splicing (AS) in spermatogenic cells. (A-B)** Pie charts showing  
24 the percentages of misregulated splicing events identified from RNA-seq data  
25 in pachytene spermatocytes (A) and round spermatids (B) from WT and  
26 *Mfn2*-cKO mice (fold change> 2; *P* < 0.05). **(C)** Different types of alternative  
27 splicing are shown. In these graphics, boxes represent exons and lines  
28 represent introns. Exon regions included in the message by alternative splicing  
29 are colored with pink and yellow, while constitutive exons are shown in blue. **(D)**  
30 Stacked bar plot showing the ratio of AS status including up- (upper panel) and

1 down-regulated (lower panel) events in pachytene spermatocytes (PS) and  
 2 round spermatids (RS). Numbers on the bars are the amount of corresponding  
 3 misregulated splicing events. **(E-F)** Gene ontology (GO) term analyses  
 4 showing the top 20 GO terms for the genes with altered splicing events in  
 5 pachytene spermatocytes (E) and round spermatids (F). Top 5 GO terms by  
 6 rich factor selection highlighted in red. **(G-H)** Pie charts showing the  
 7 percentages of mRNA expression level alterations in 1001 genes with  
 8 misregulated alternative splicing in pachytene spermatocytes (G), and 684  
 9 genes with misregulated alternative splicing in round spermatids (H). **(I)**  
 10 Screenshot from the IGB (Integrated Genome Browser) software showing high  
 11 inclusion levels for an intron in the *Map2k7* gene in *Mfn2*-cKO pachytene  
 12 spermatocytes (the left panel), and RT-PCR validation of the misregulated  
 13 alternative splicing in WT and *Mfn2*-cKO pachytene spermatocytes (right  
 14 panel). *Arbp* served as an internal control.

15

16 **Figure. 7. MFN2 associates with mRNA translation processes and**  
 17 **regulates gamete-specific mRNA fates.** **(A)** Untreated (EDTA-) and  
 18 EDTA-treated (EDTA+) post-nuclear testicular extract from adult WT mice  
 19 were fractionated on linear 10–50% sucrose density gradients and analyzed  
 20 by UV spectrometry. The distribution of MFN2 protein is detected by Western  
 21 blotting. RPS6 protein serves as a positive control. **(B)** Cytoplasmic polysome  
 22 profiling of control (blue line) and *Mfn2*-cKO (red line) testes at P35. **(C)**  
 23 Quantifications of the ratio of polysomes to monosomes (80S) in control (Ctrl)  
 24 and *Mfn2*-cKO testes are shown. **(D)** Immunoprecipitation showing MFN2 was  
 25 detected in the immunoprecipitants from MSY2 in the adult mouse testes. **(E)**  
 26 Co-immunostainings of MSY2 and  $\gamma$ -H2A.X in stage IV-VI and VII-VIII  
 27 seminiferous tubules from adult control and *Mfn2*-cKO testes. Nuclei were  
 28 stained with DAPI. RS, round spermatids; PS, pachytene spermatocytes.  
 29 Scale bar=10 $\mu$ m. **(F)** Heat-map is showing the differential expression levels of  
 30 12 MSY2-bound male gamete-specific mRNAs in both pachytene

1 spermatocytes (PS) and round spermatids (RS) from RNA-Seq data in WT and  
2 *Mfn2*-cKO mice. (G) Western blots analysis of the protein levels of *Spata19* in  
3 control and *Mfn2*-cKO testes at P25 and P44, respectively. (H)  
4 Co-immunostaining of SPATA19 and  $\gamma$ -H2A.X in P25 testes from control and  
5 *Mfn2*-cKO mice. Nuclei were stained with DAPI. Scale bar=10 $\mu$ m. (I)  
6 Reciprocal immunoprecipitation showing eEF1A2 and eEF1A1 were detected  
7 in the immunoprecipitants from MFN2 in the adult mouse testes. (J-K)  
8 Reciprocal immunoprecipitation showing MFN2 was detected in the  
9 immunoprecipitants from eEF1A1 (J) and eEF1A2 (K) in the adult mouse  
10 testes, respectively. (L) Co-immunostainings of eEF1A1 and ATP5A (left  
11 panel), eEF1A2 and ATP5A (right panel) in P25 testes from control and  
12 *Mfn2*-cKO mice. Nuclei were stained with DAPI. Scale bar=10 $\mu$ m.

13

14 **Figure. 8. The working model illustrates the function of MFN2 in male**  
15 **germ cell development.** (A) In WT spermatocytes, MFN2 cooperates with  
16 Nuage associated proteins in pachytene spermatocytes and round spermatids,  
17 including MIWI, DDX4, TDRKH, GASZ, and MSY2 to form interaction  
18 complexes for maintaining normal morphology of mitochondria, MAM and ER,  
19 and mRNA translation via interaction with the eukaryotic elongation factor  
20 eEF1A1 and eEF1A2. (B) In MFN2 deficient pachytene spermatocytes and  
21 round spermatids, Nuage-associated proteins are ectopically expressed,  
22 including a decrease of MIWI, DDX4, and GASZ expression, and an increase  
23 of MSY2 expression. Meanwhile, in the cytoplasm, the disassociated  
24 MFN2-Nuage protein complexes caused some proteins are misregulated in  
25 mRNA and/or protein level, especially gamete-specific genes, such as  
26 SPATA19 is early translated, which leads to disrupted male germ cell  
27 development and male fertility.

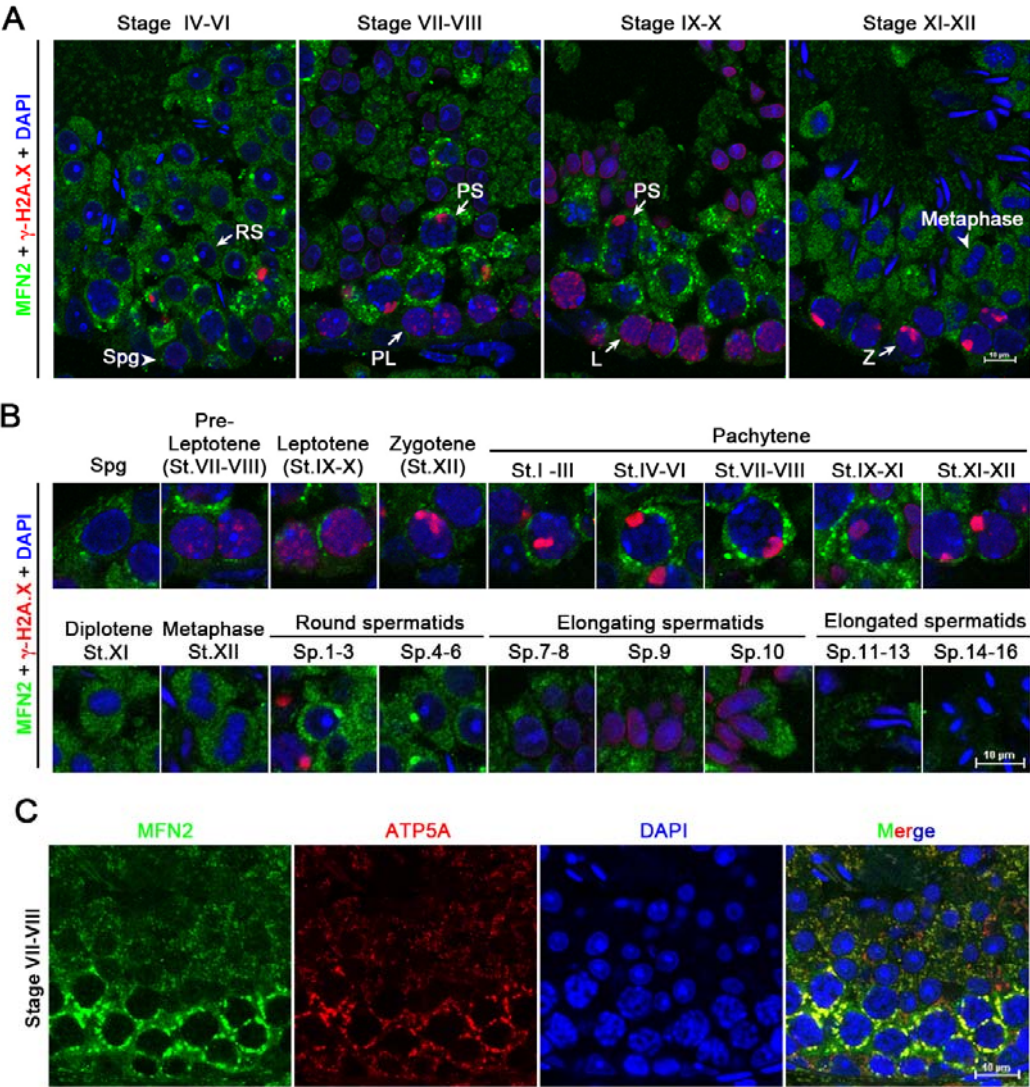
28

29

30

1

2 **Figure 1**



3

4

5

6

7

8

9

10

11

## Figure 2

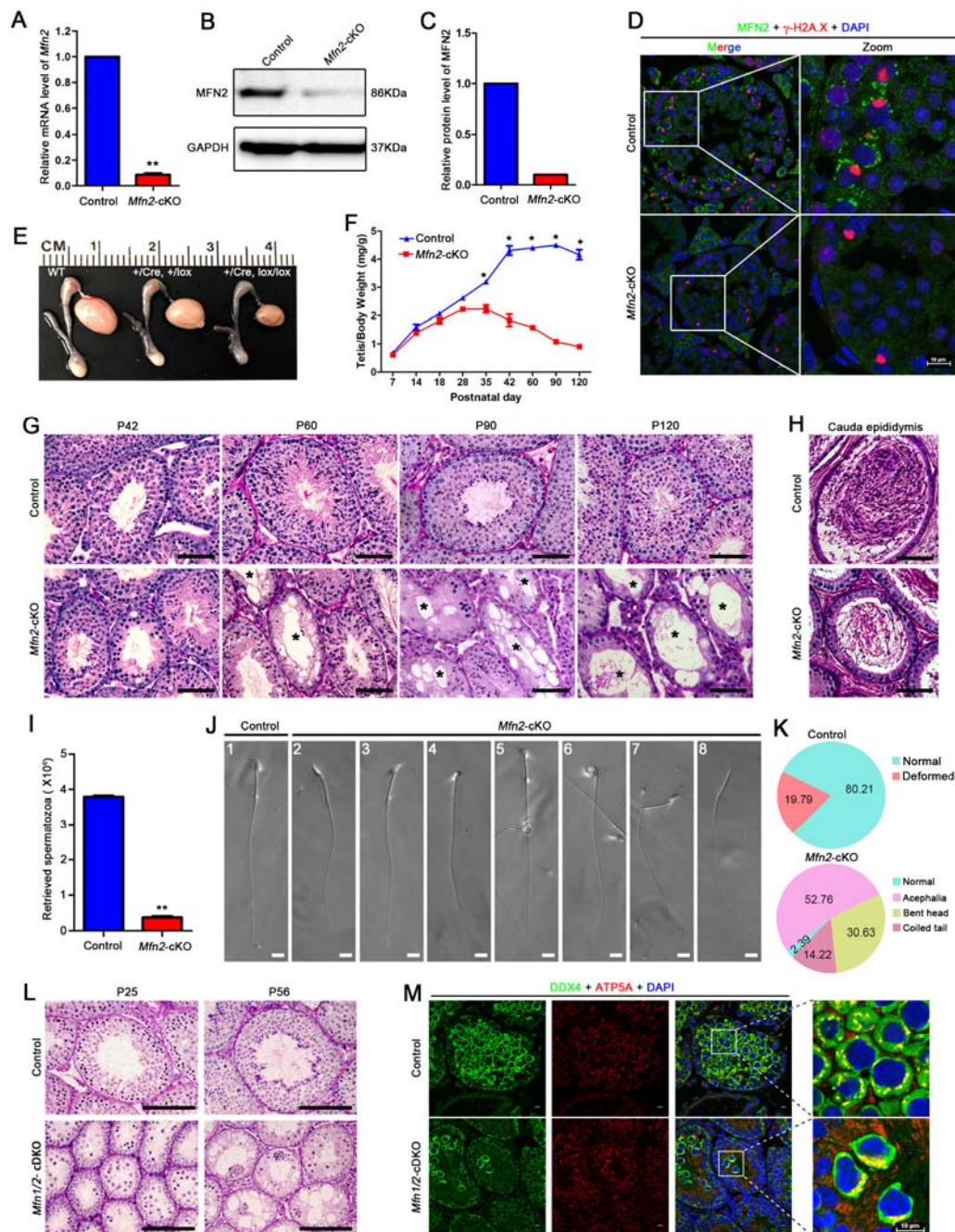


**Figure 3**

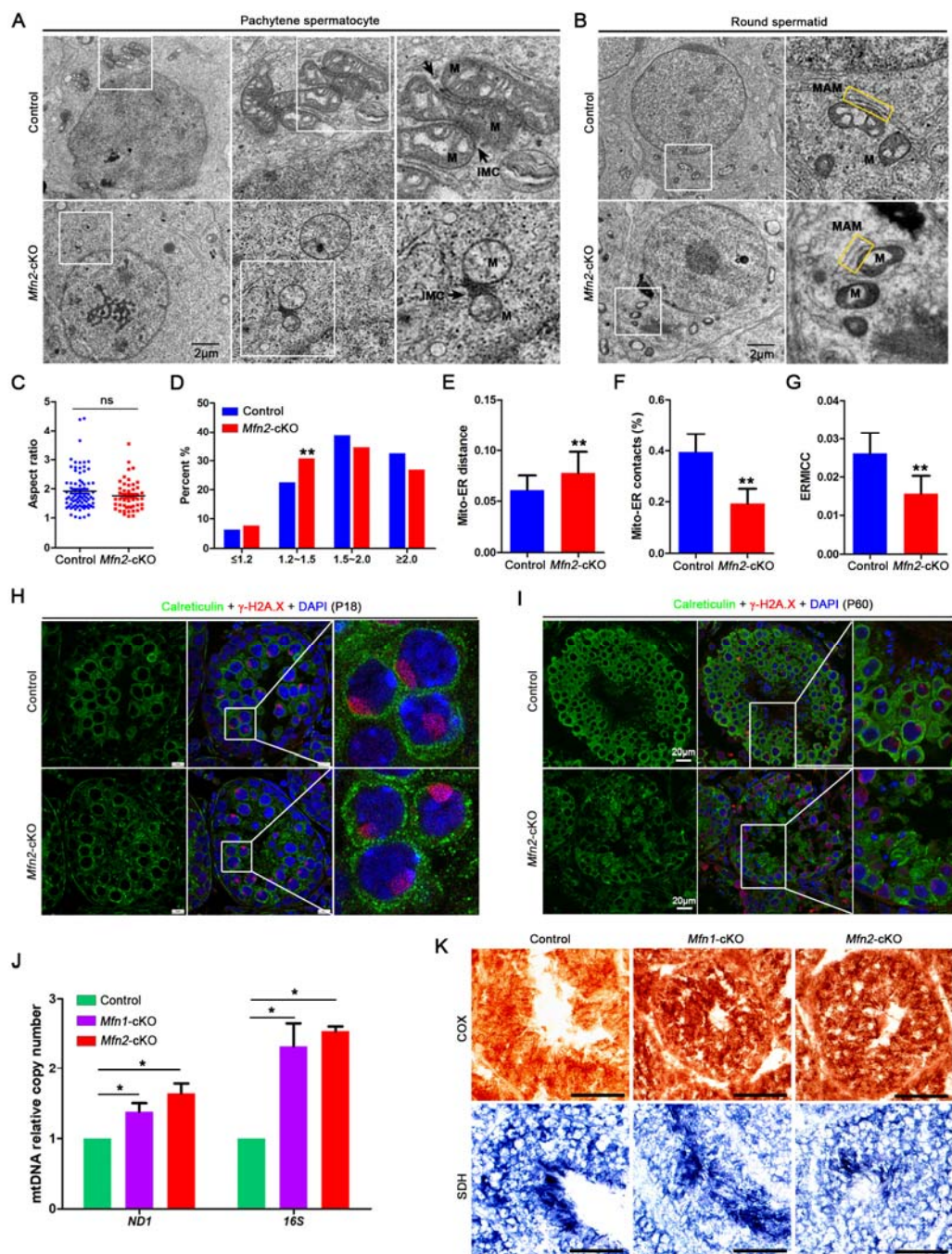


**Figure 4**

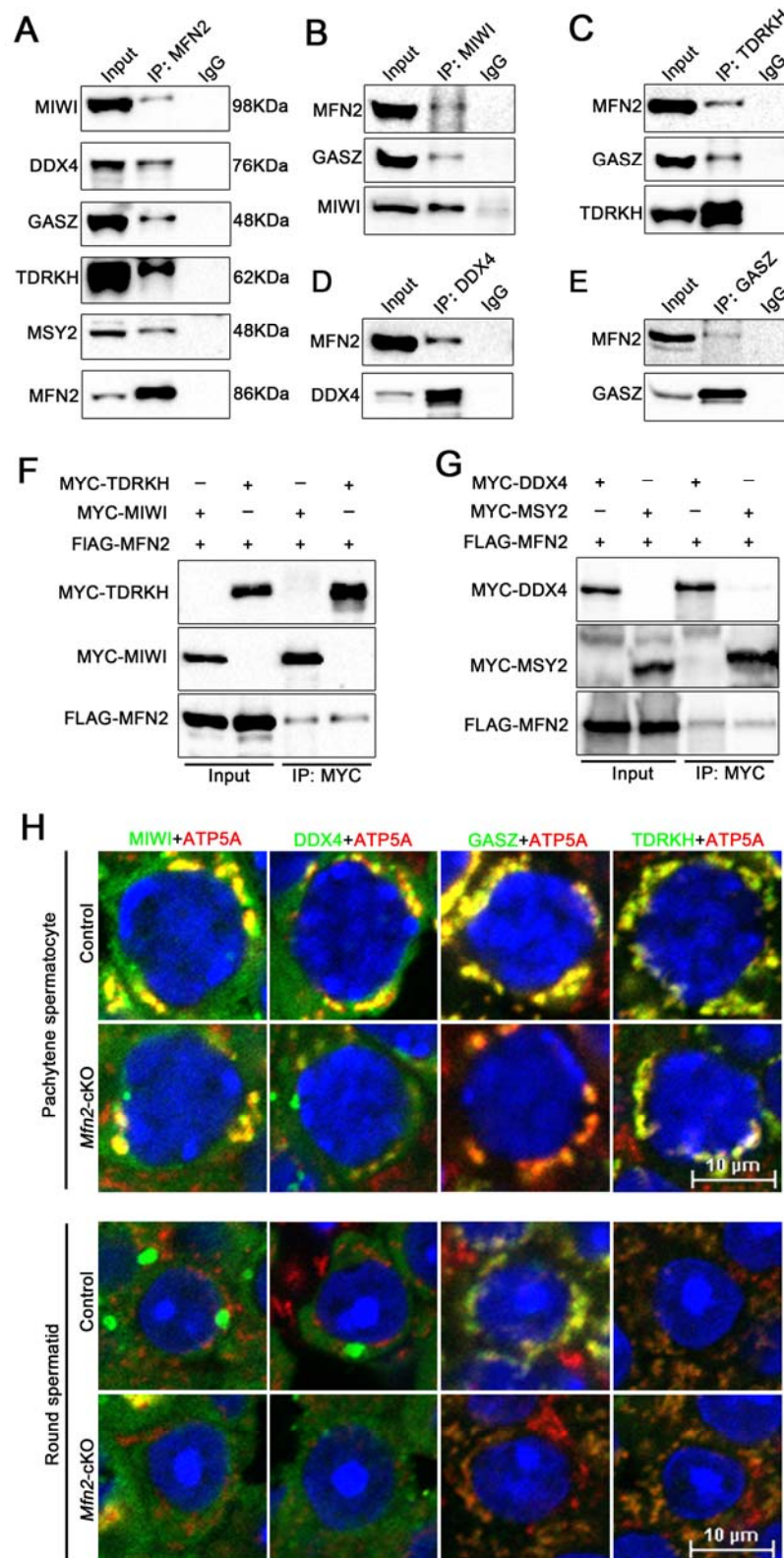


**Figure 5**

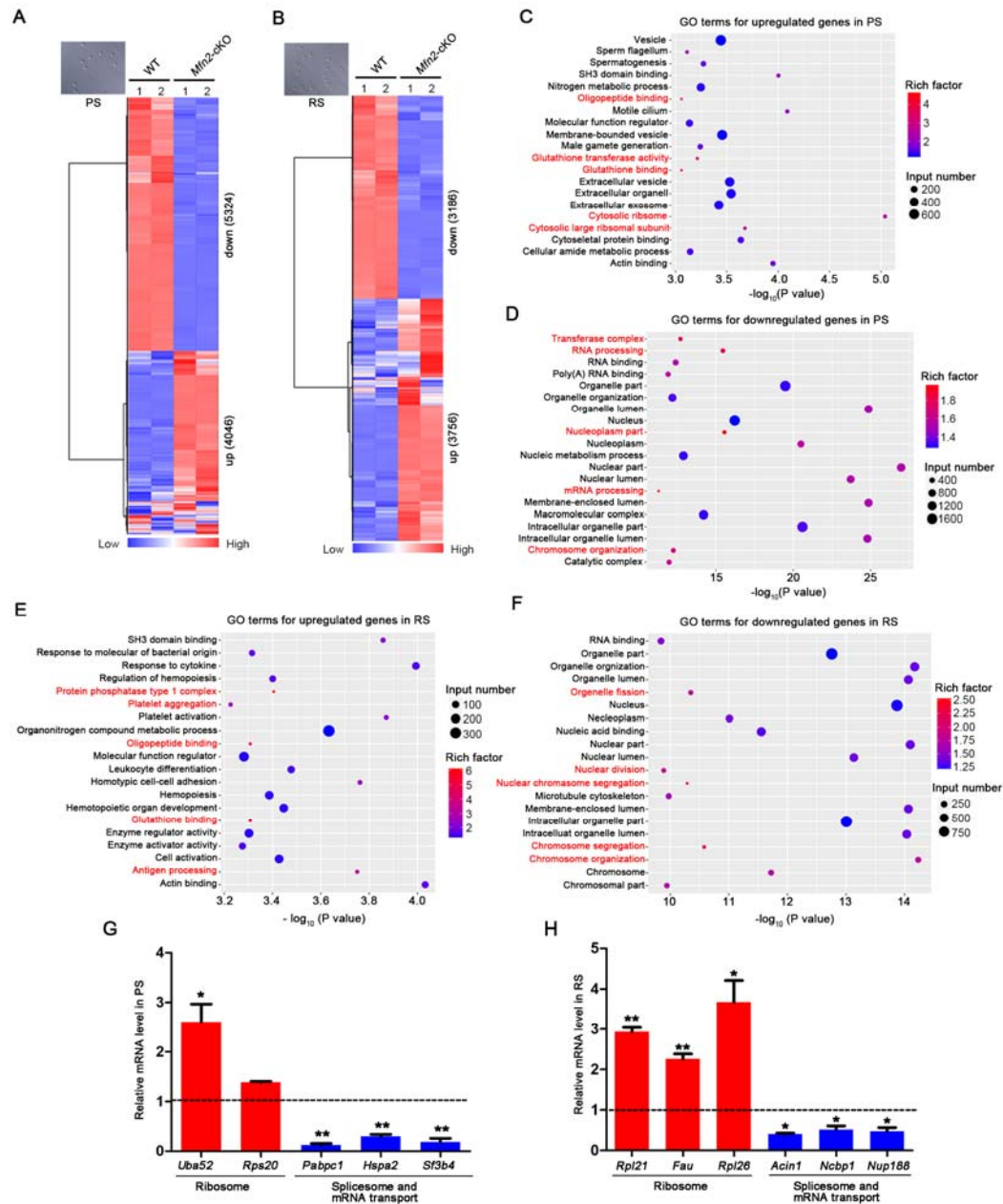


**Figure 6**

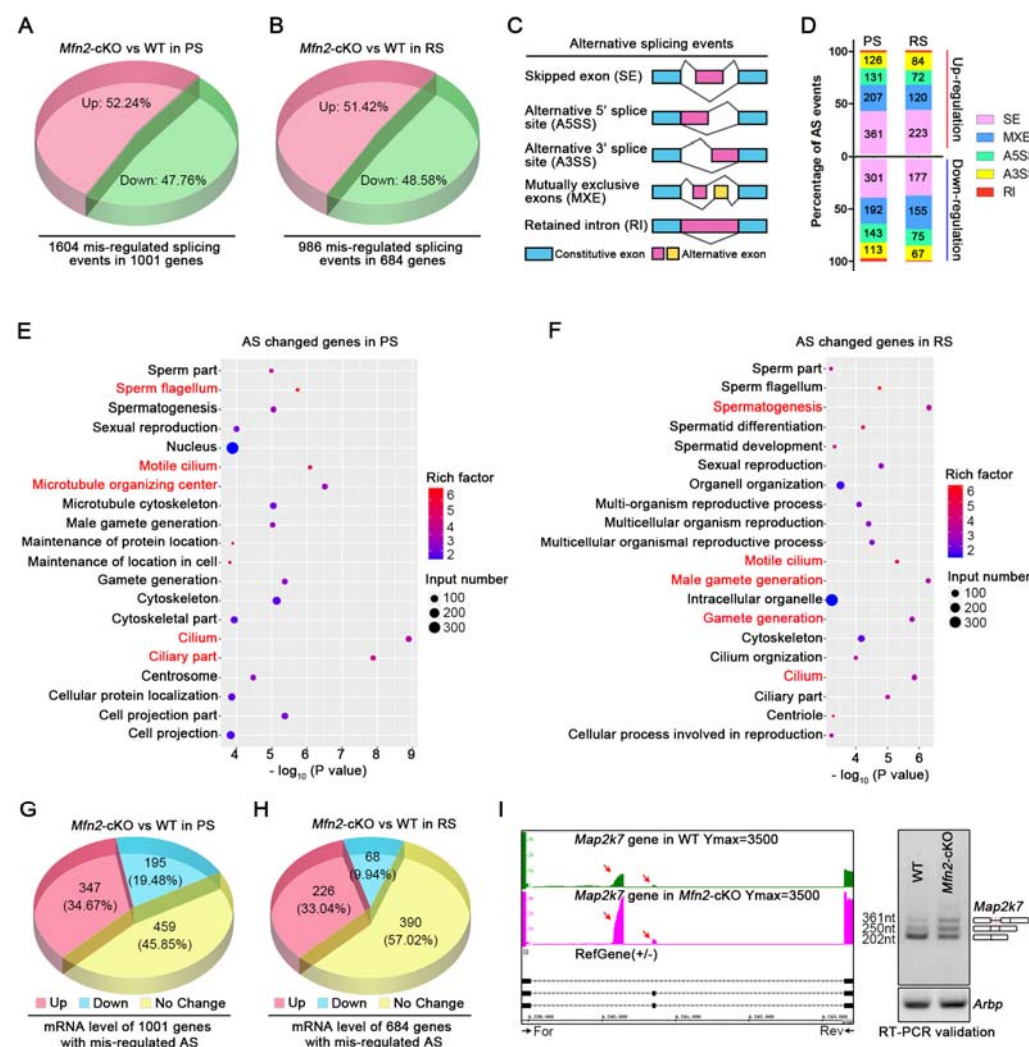
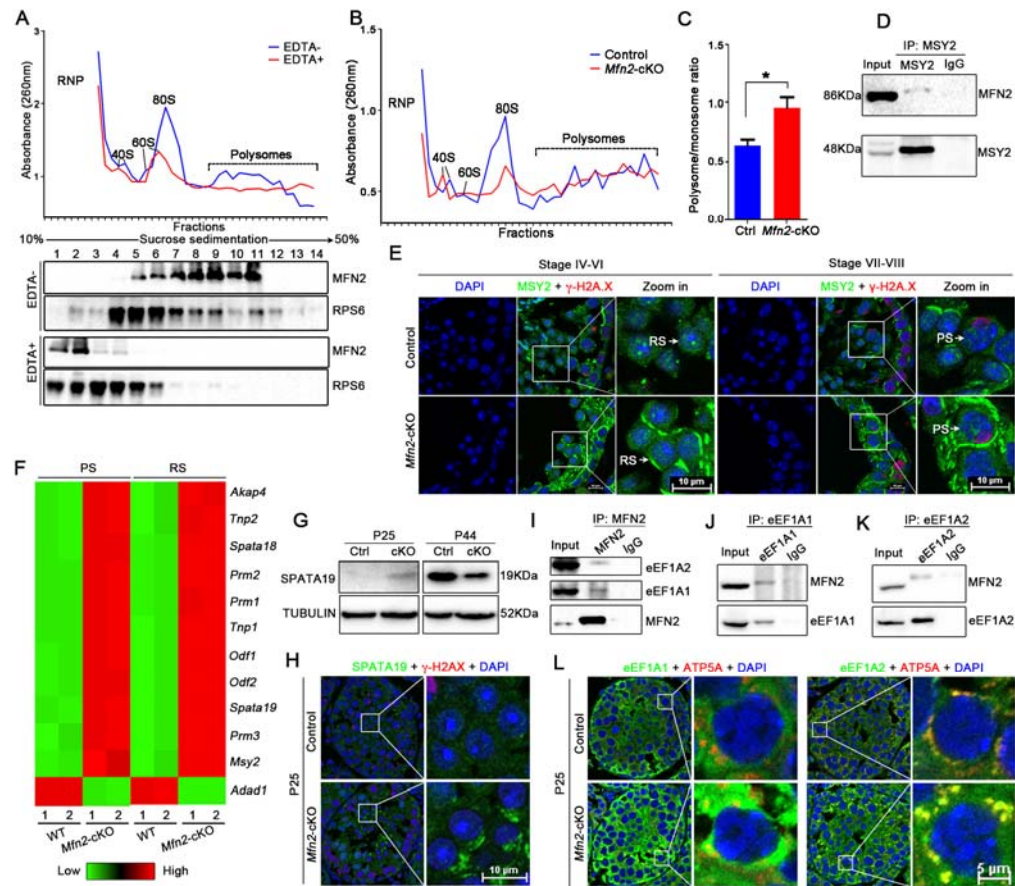
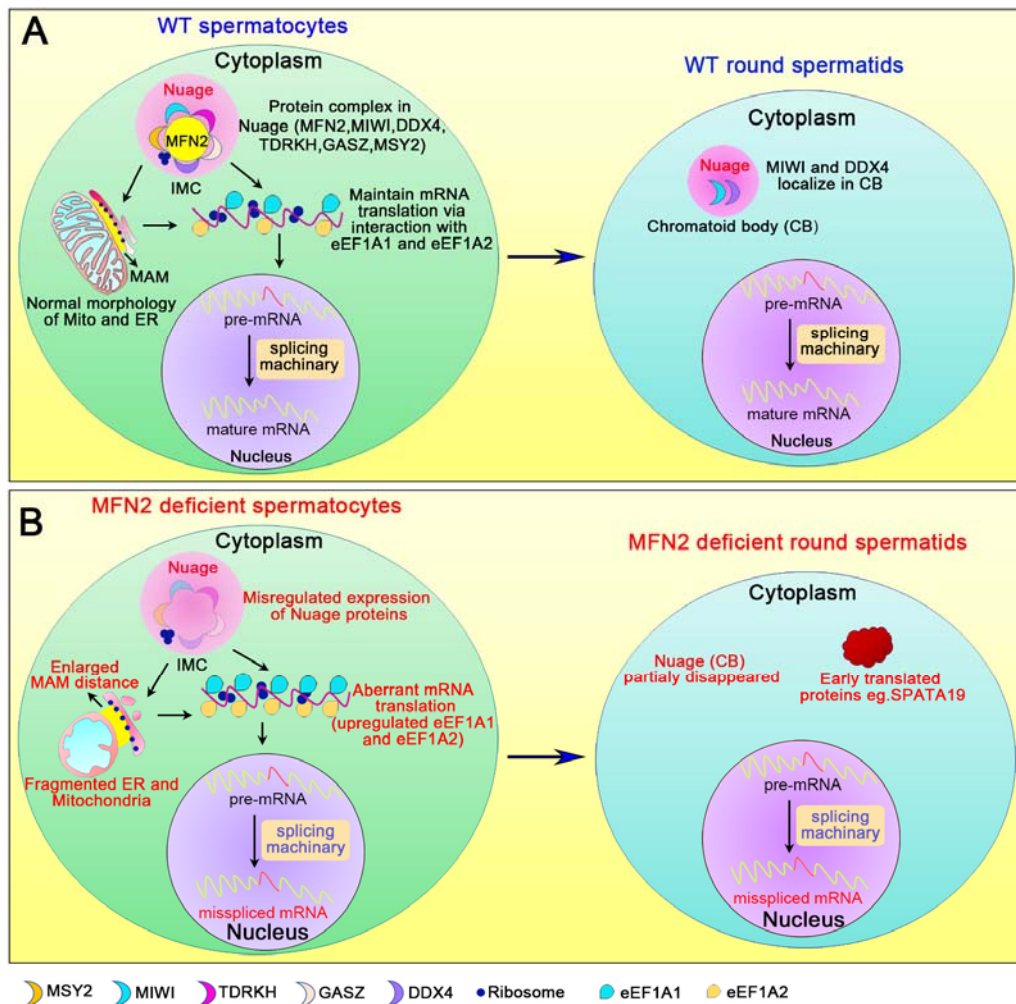


## Figure 7

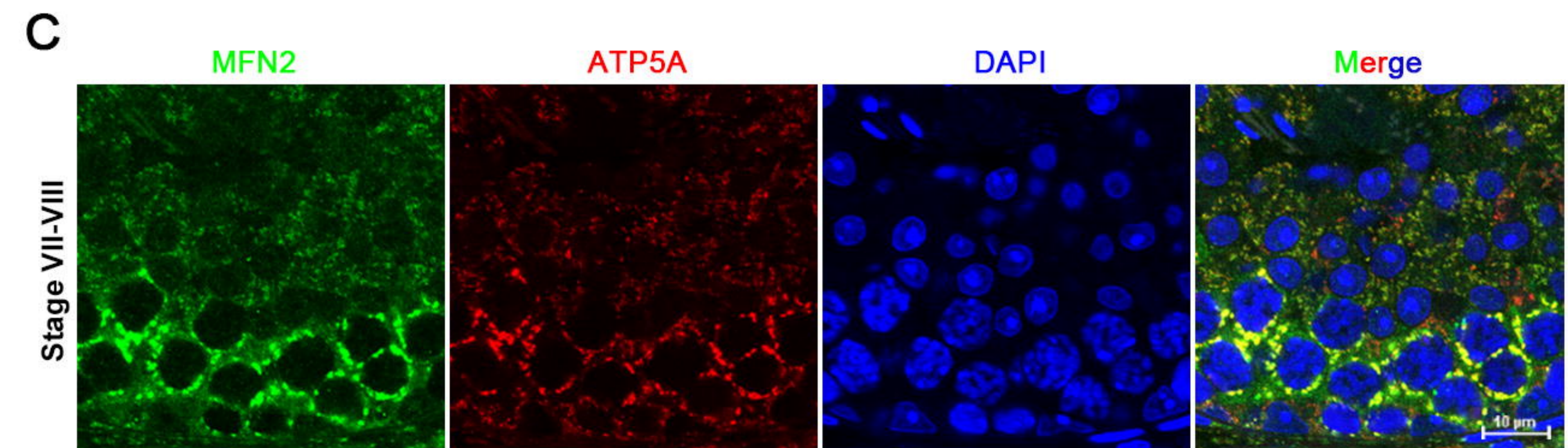
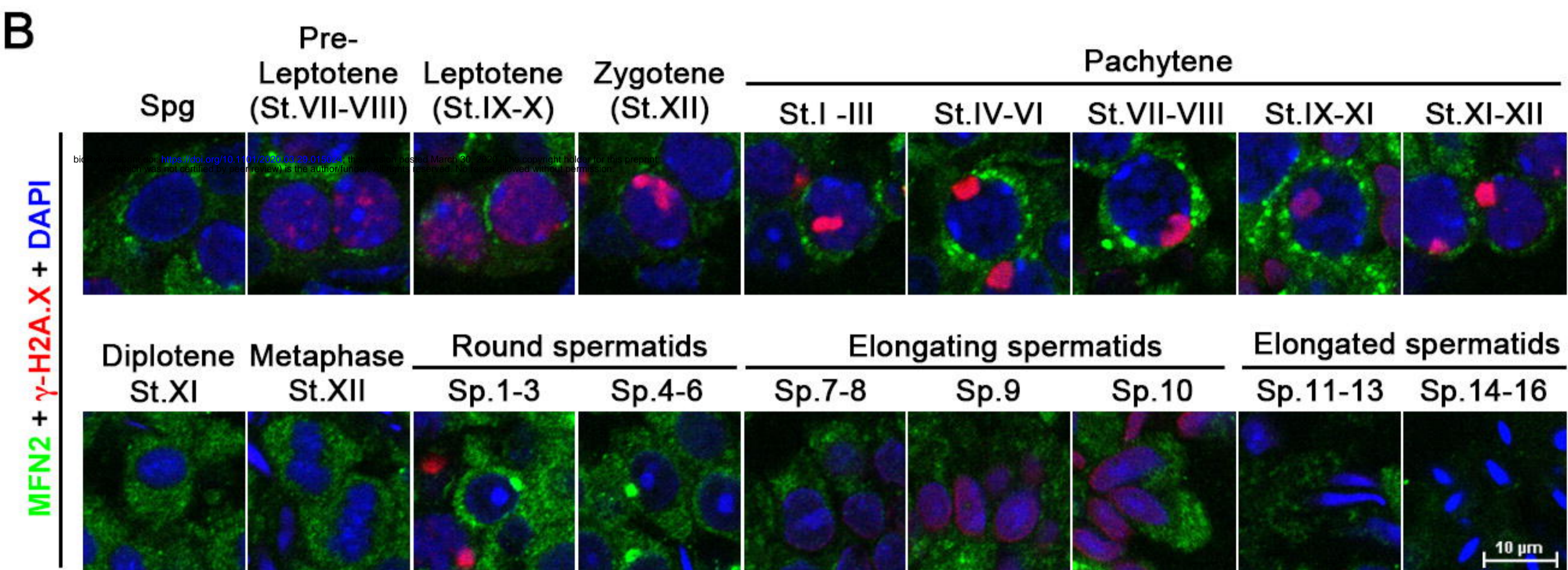
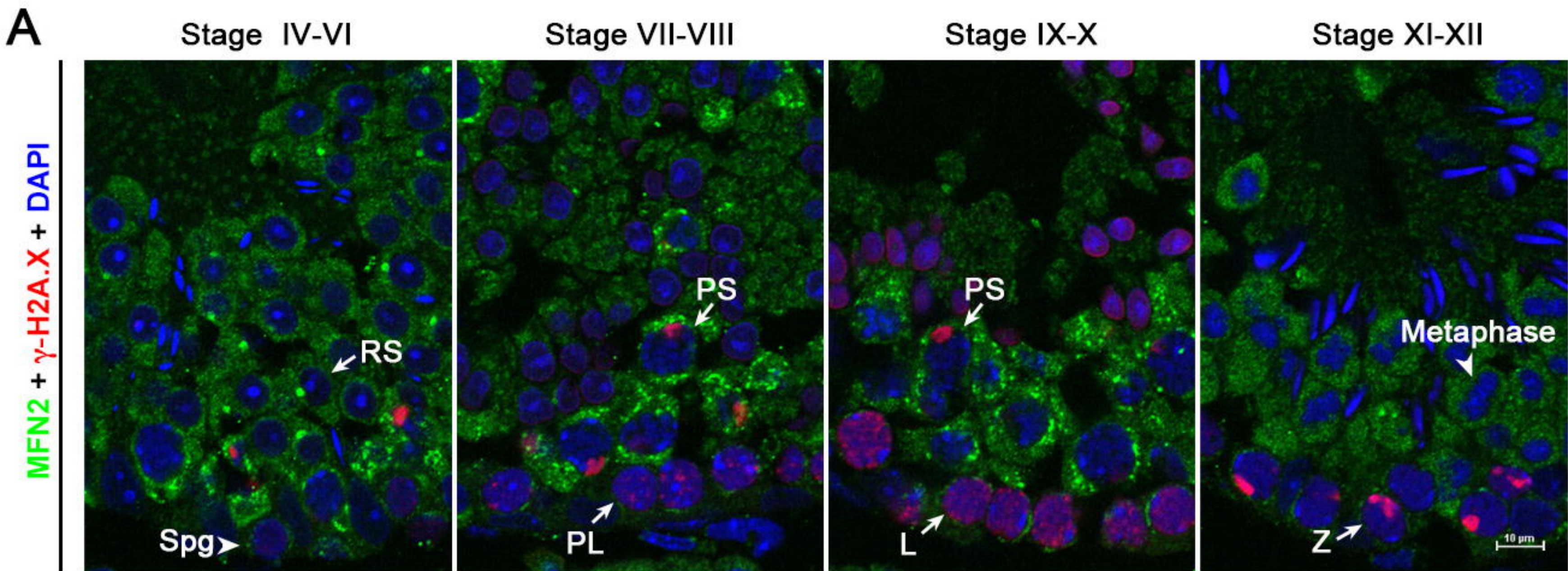


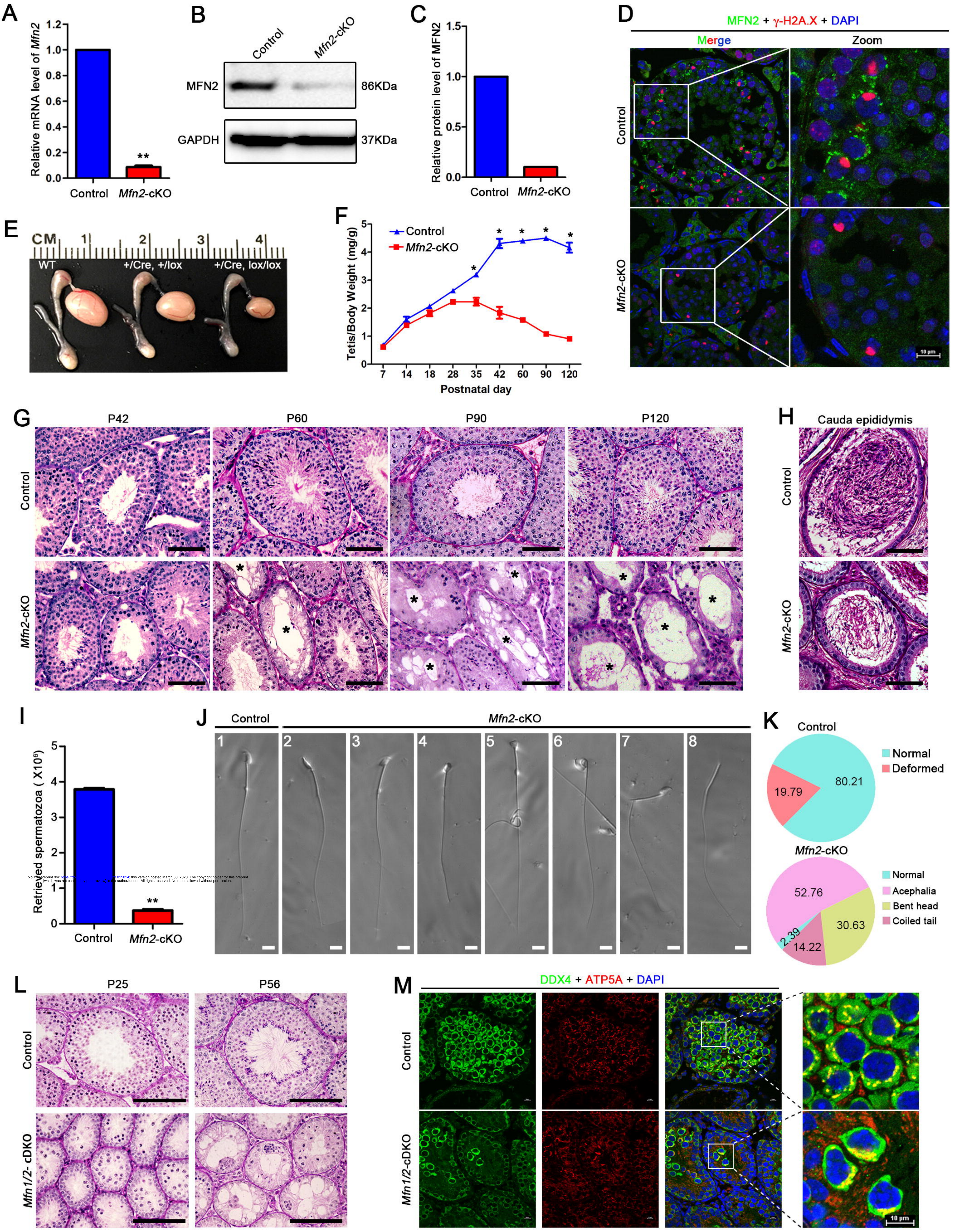
1

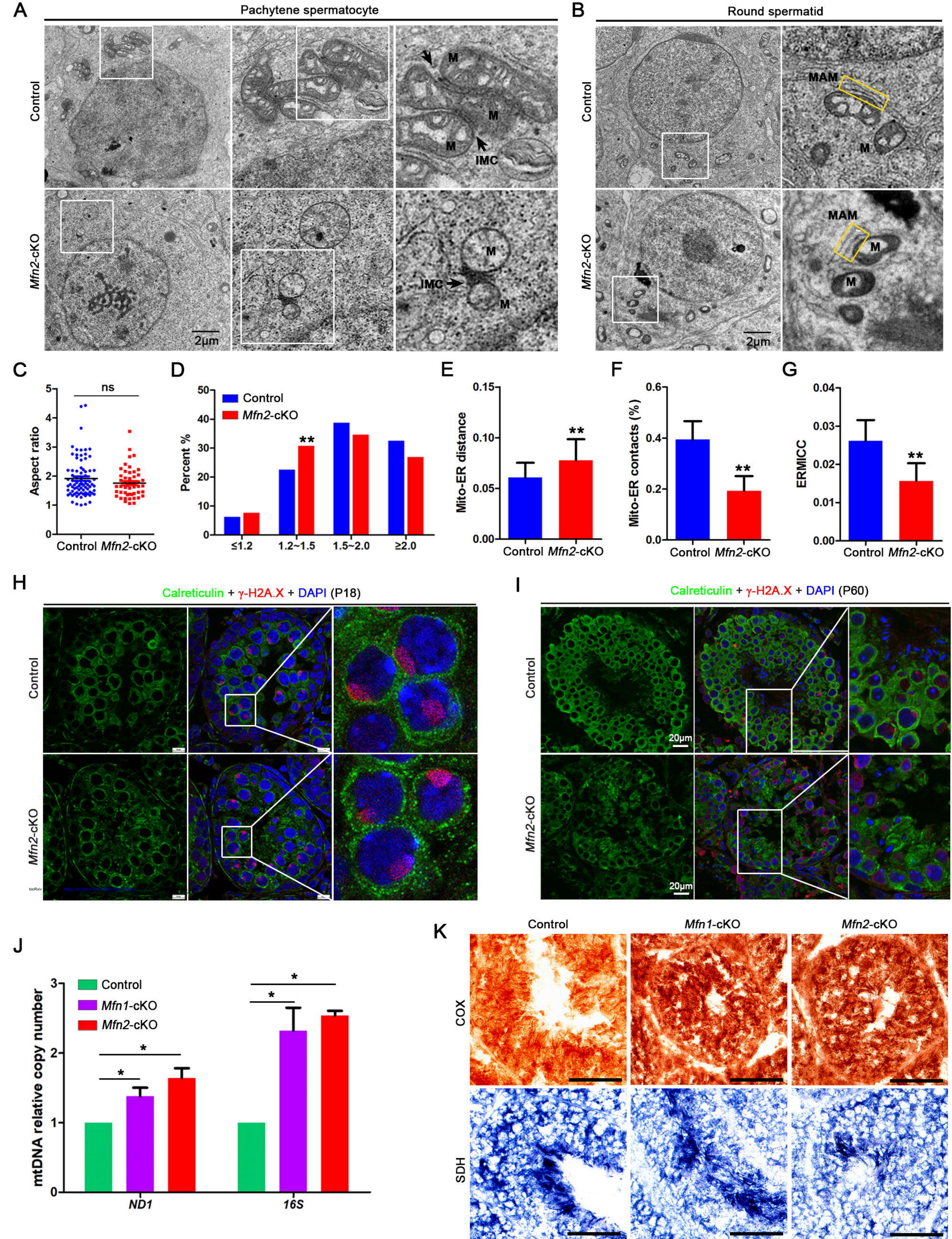
2 **Figure 8**

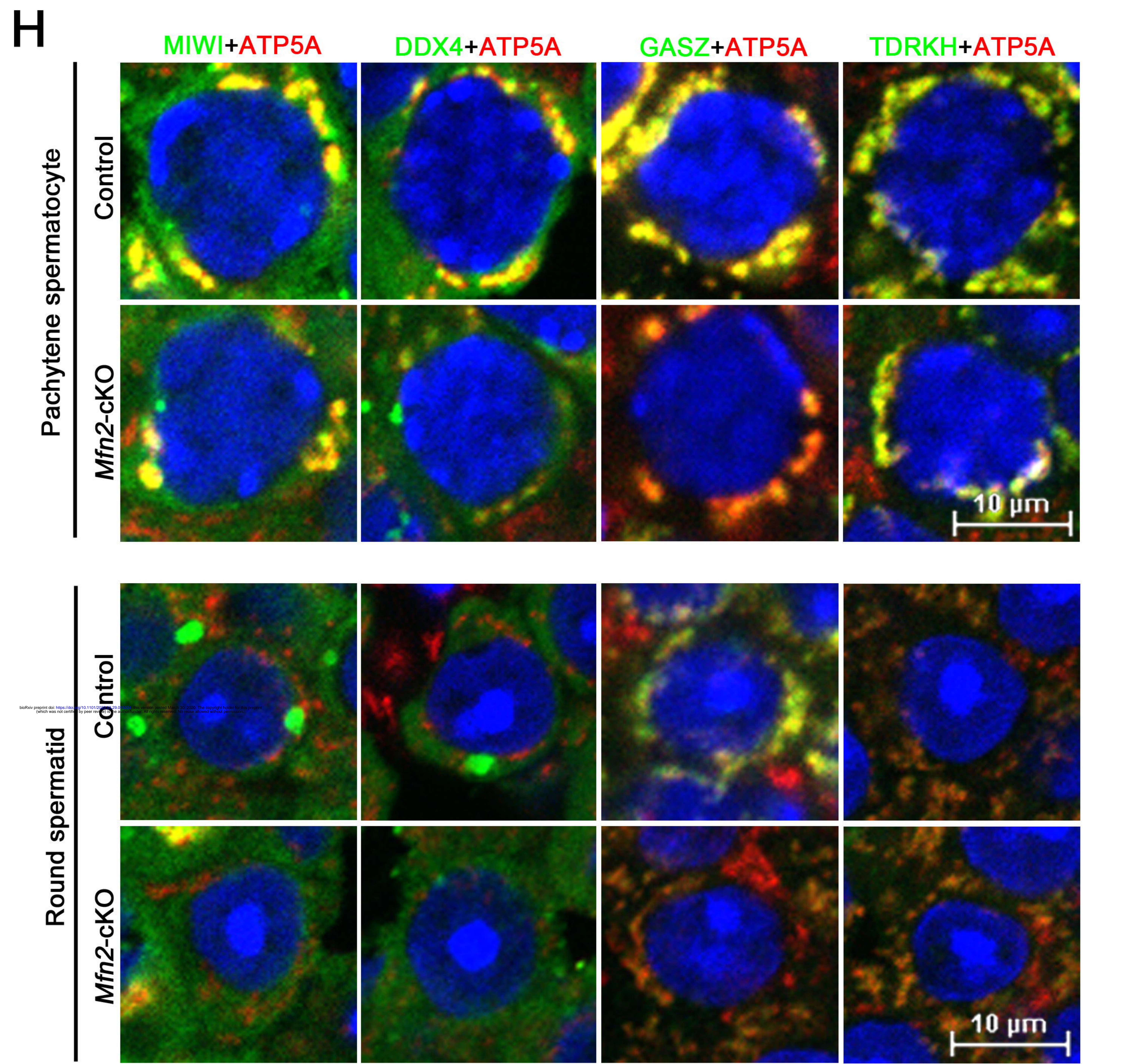
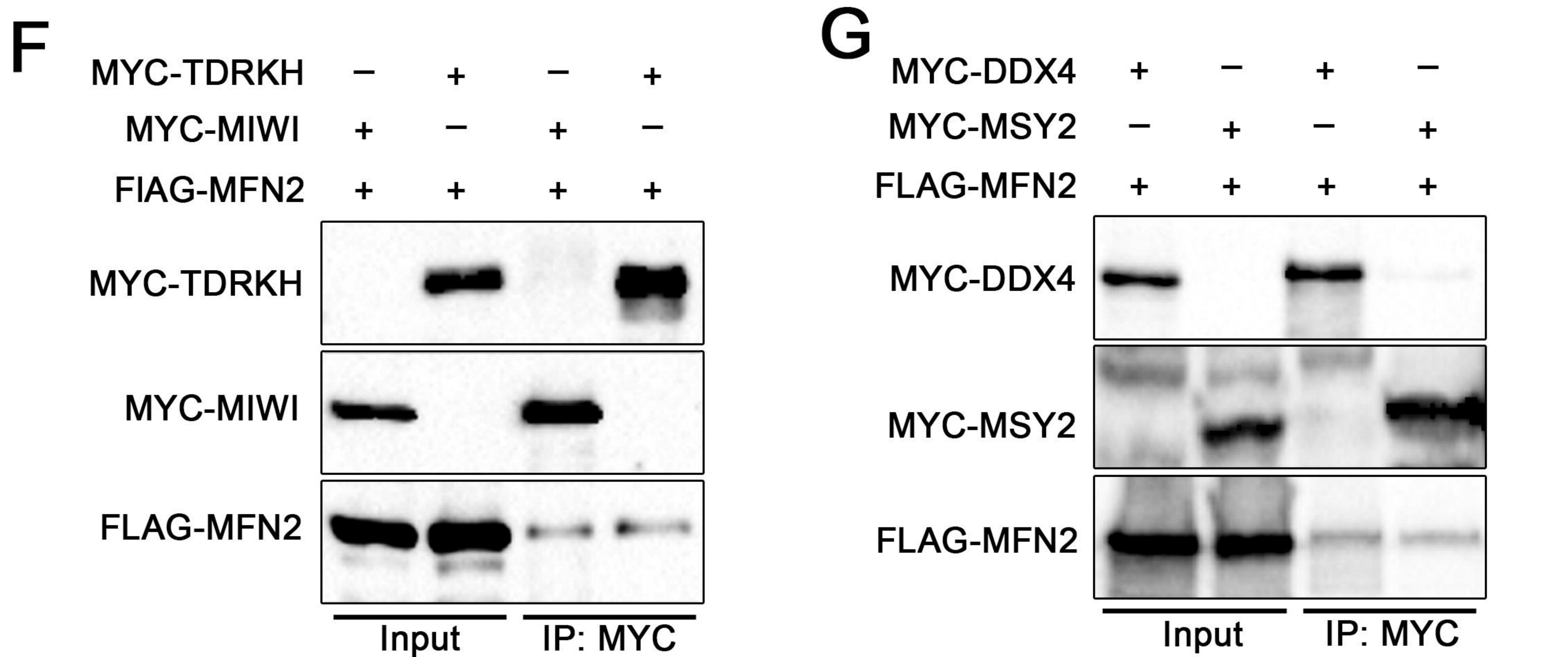
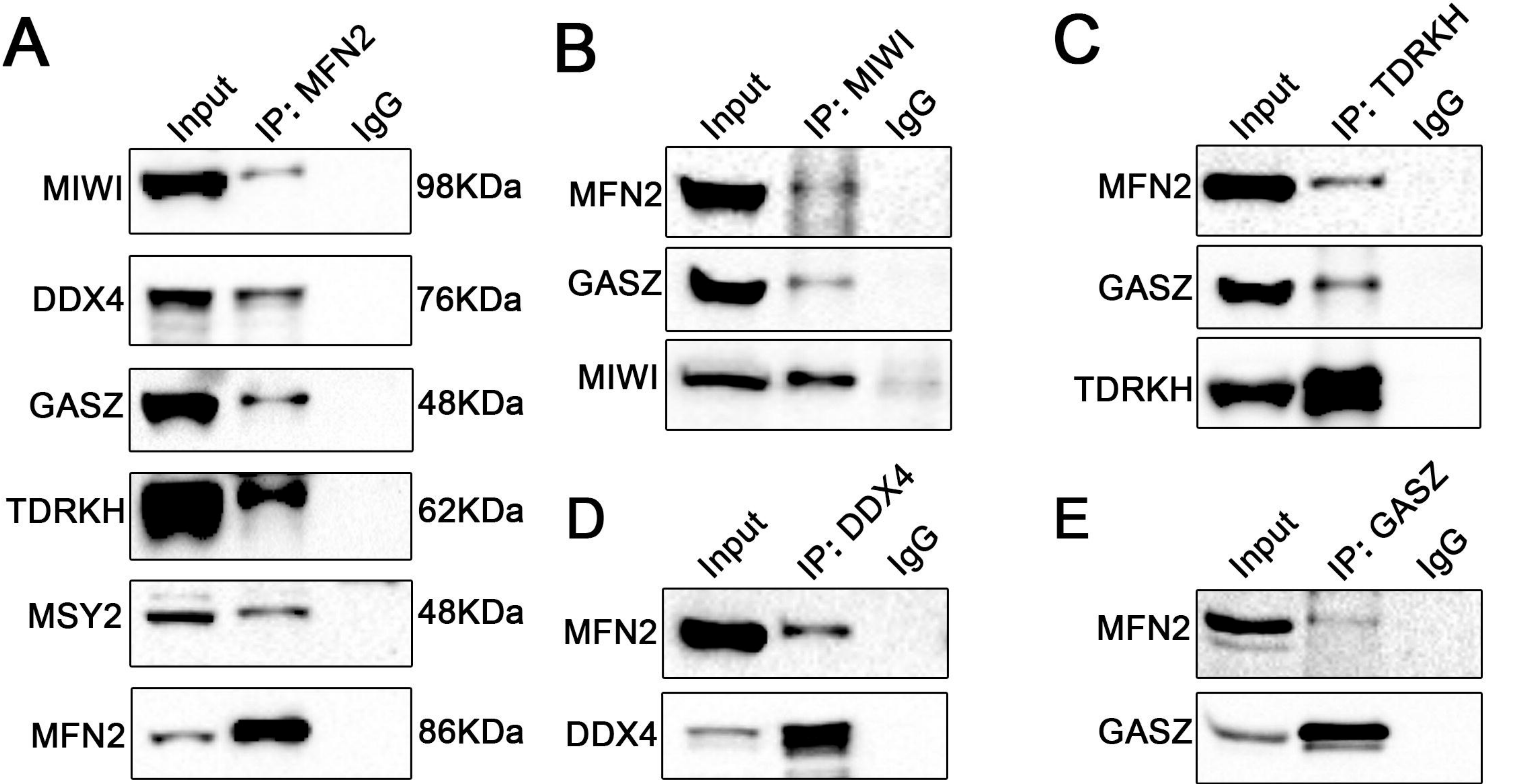


3

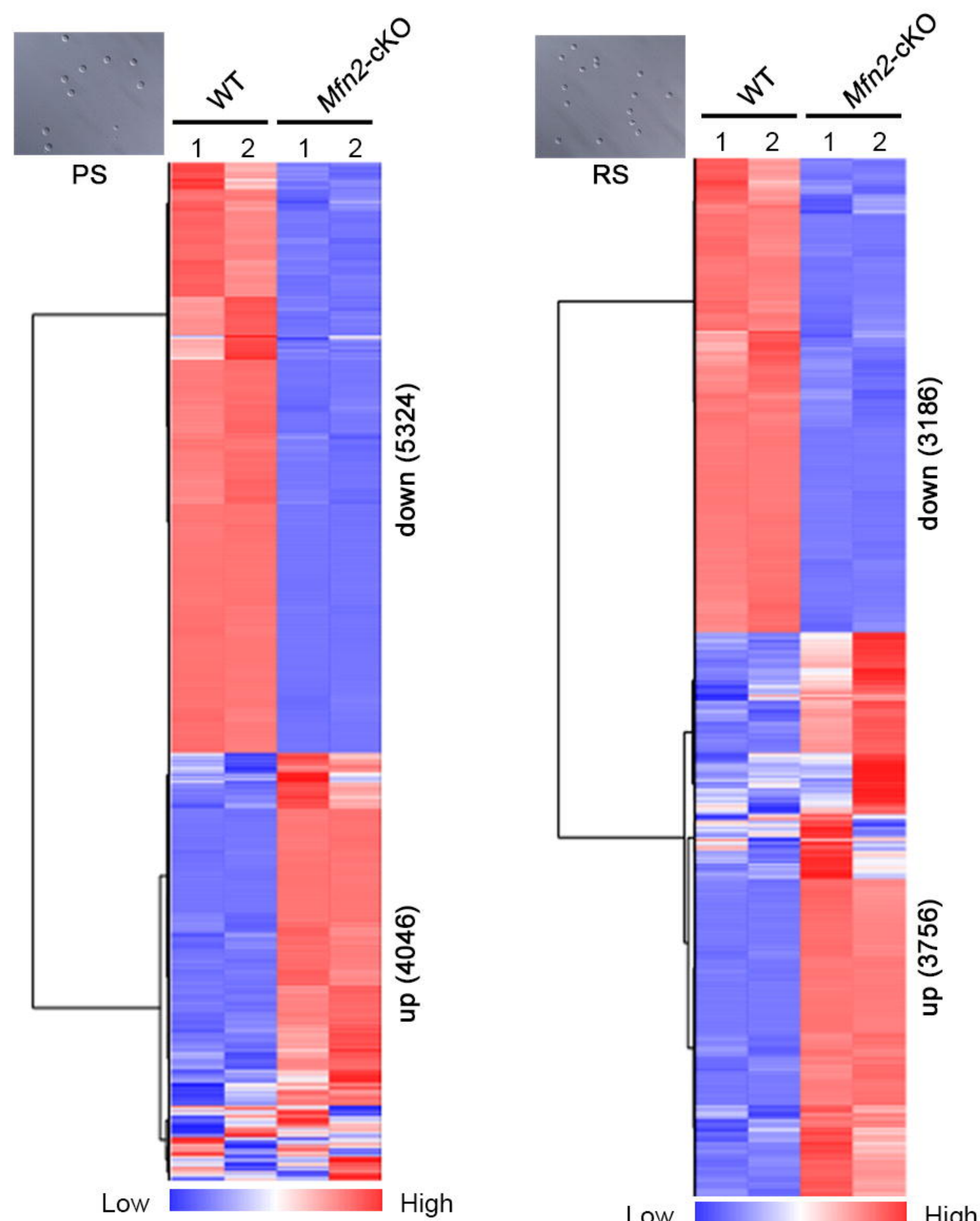




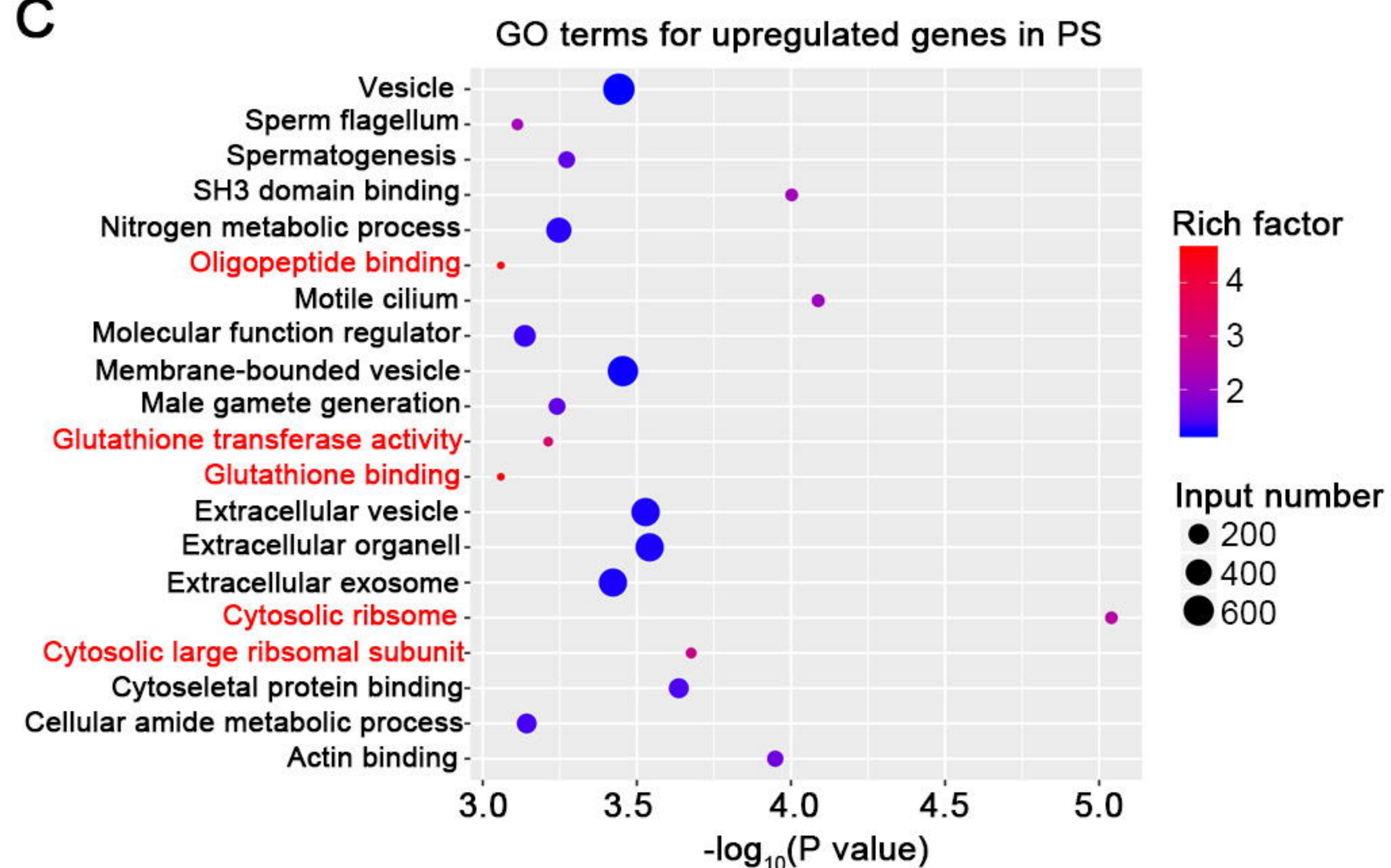




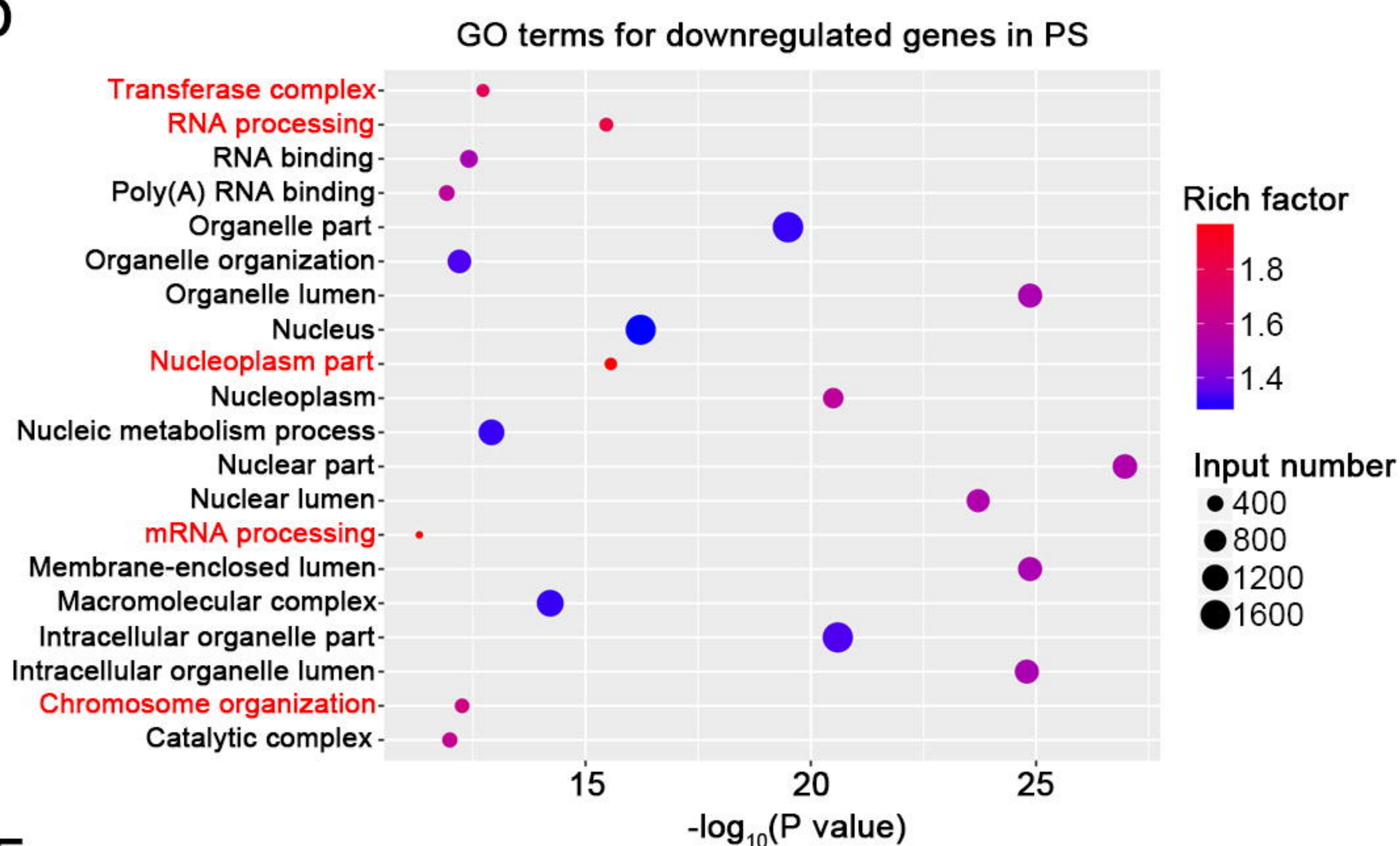
A



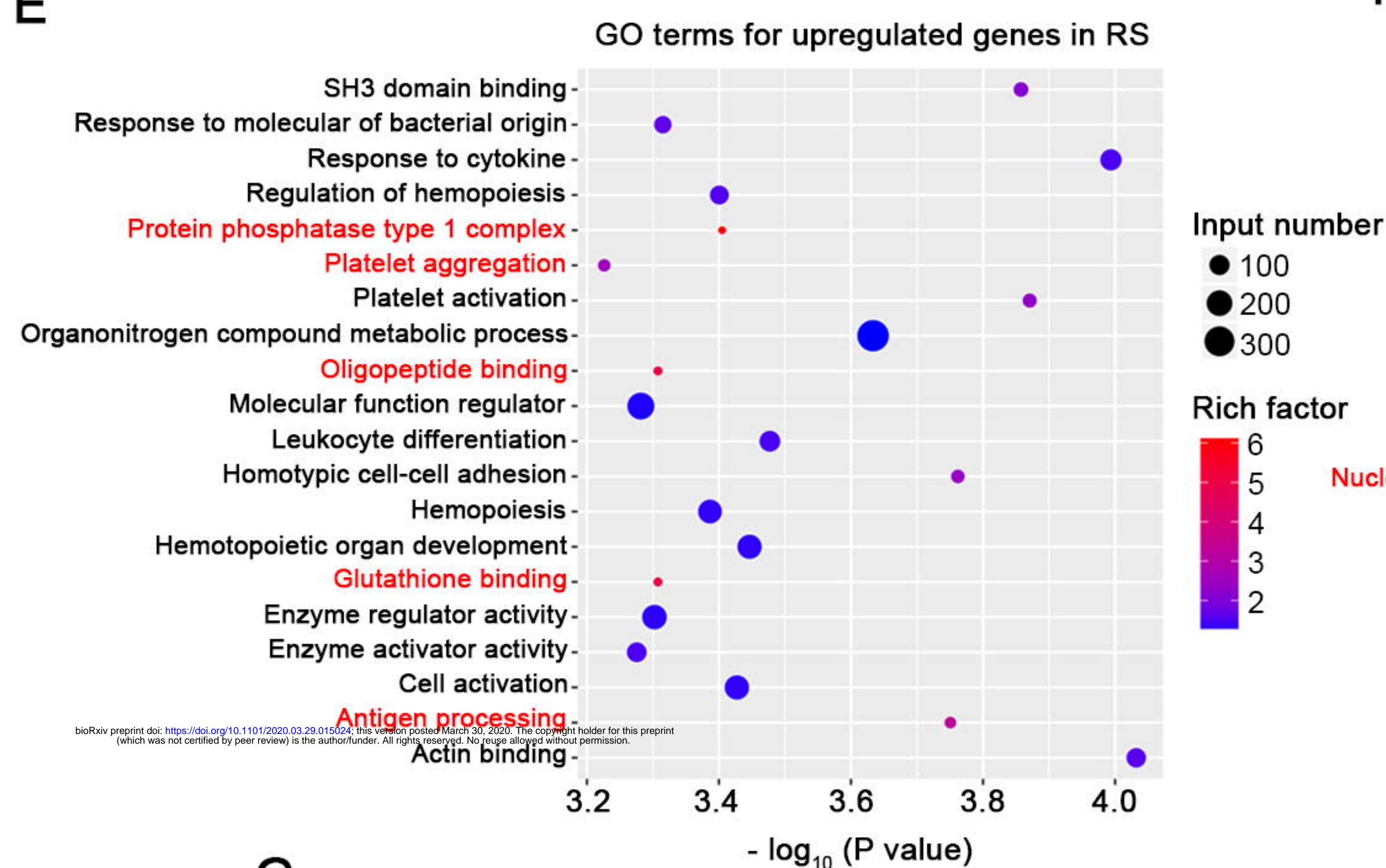
C



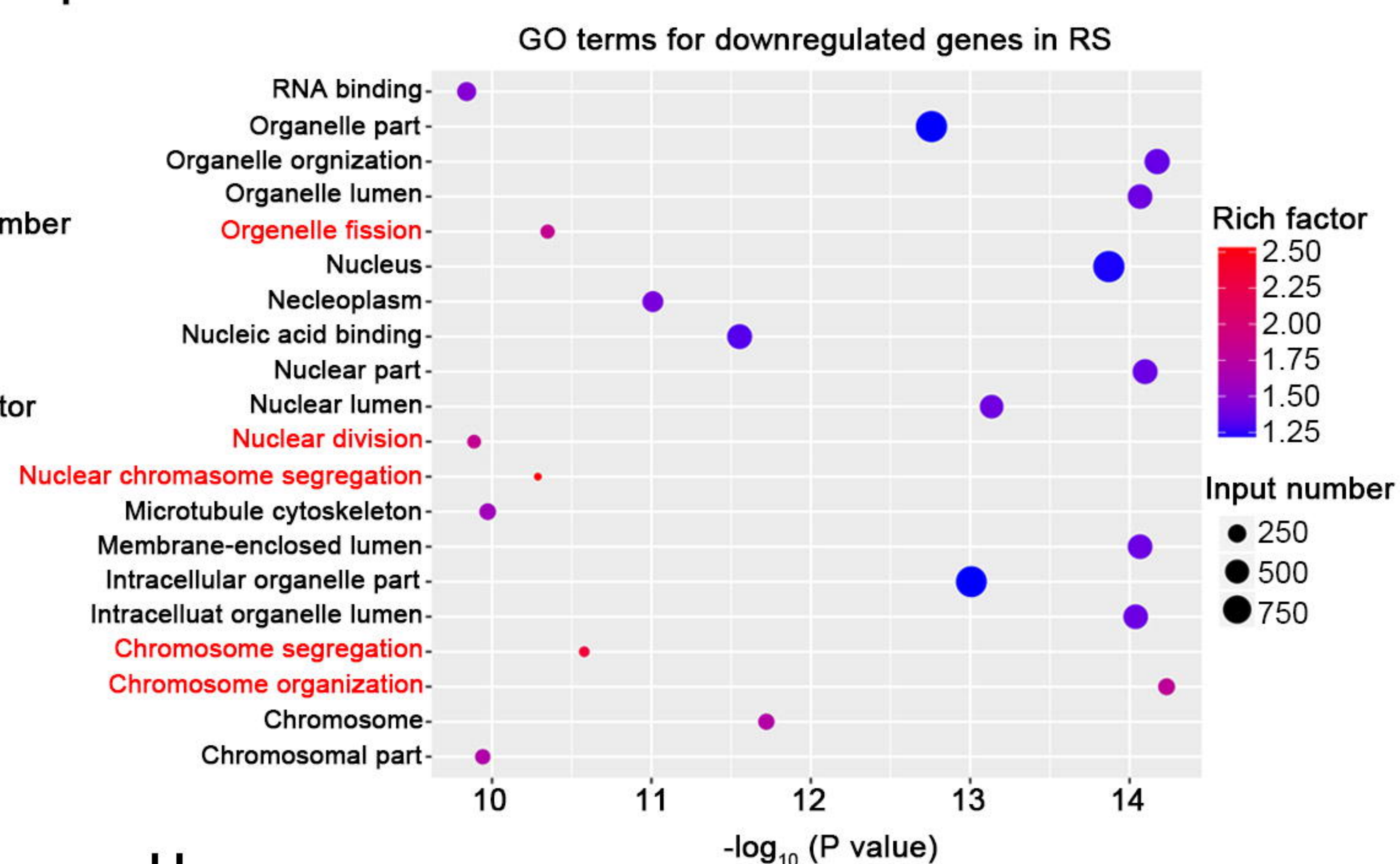
D



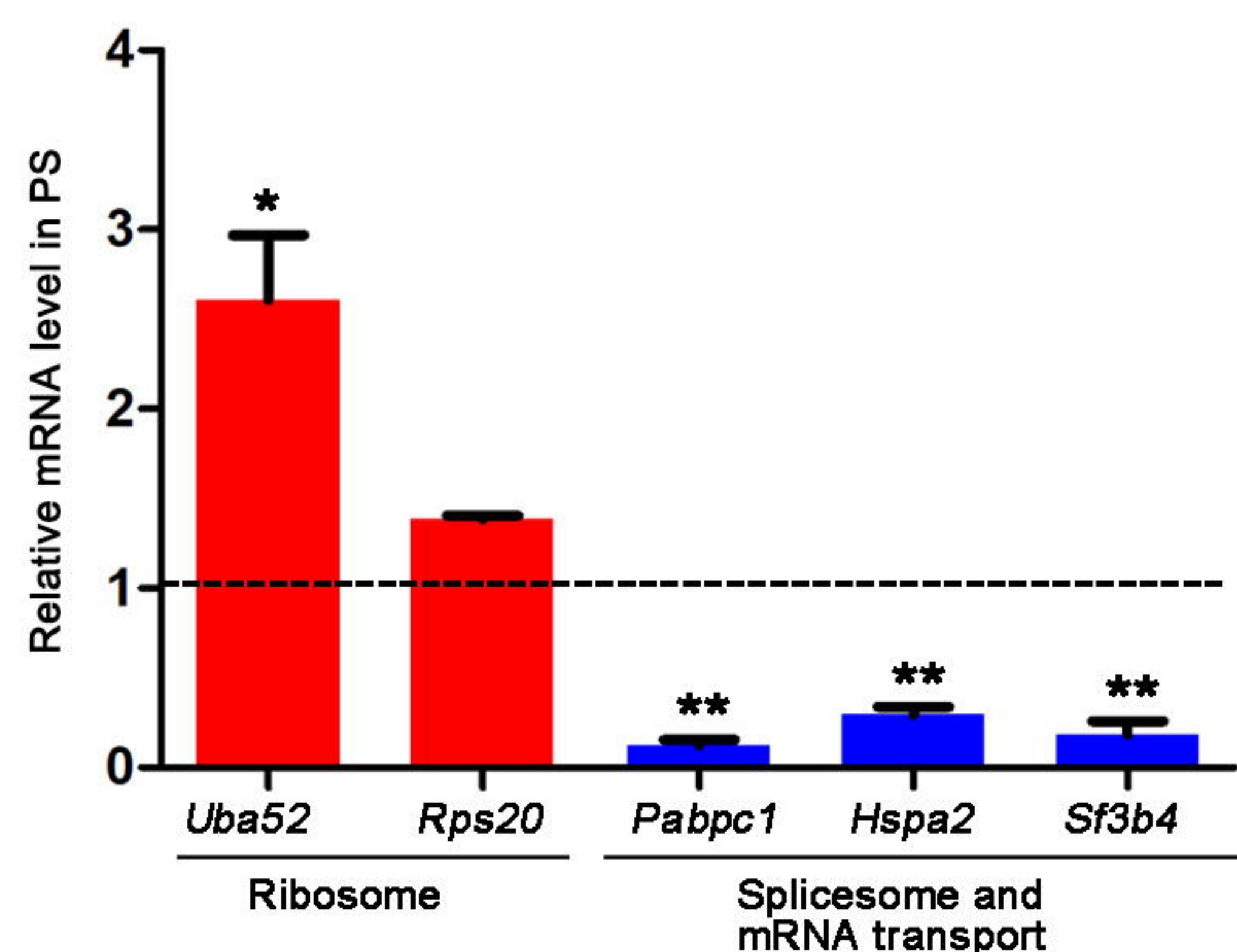
E



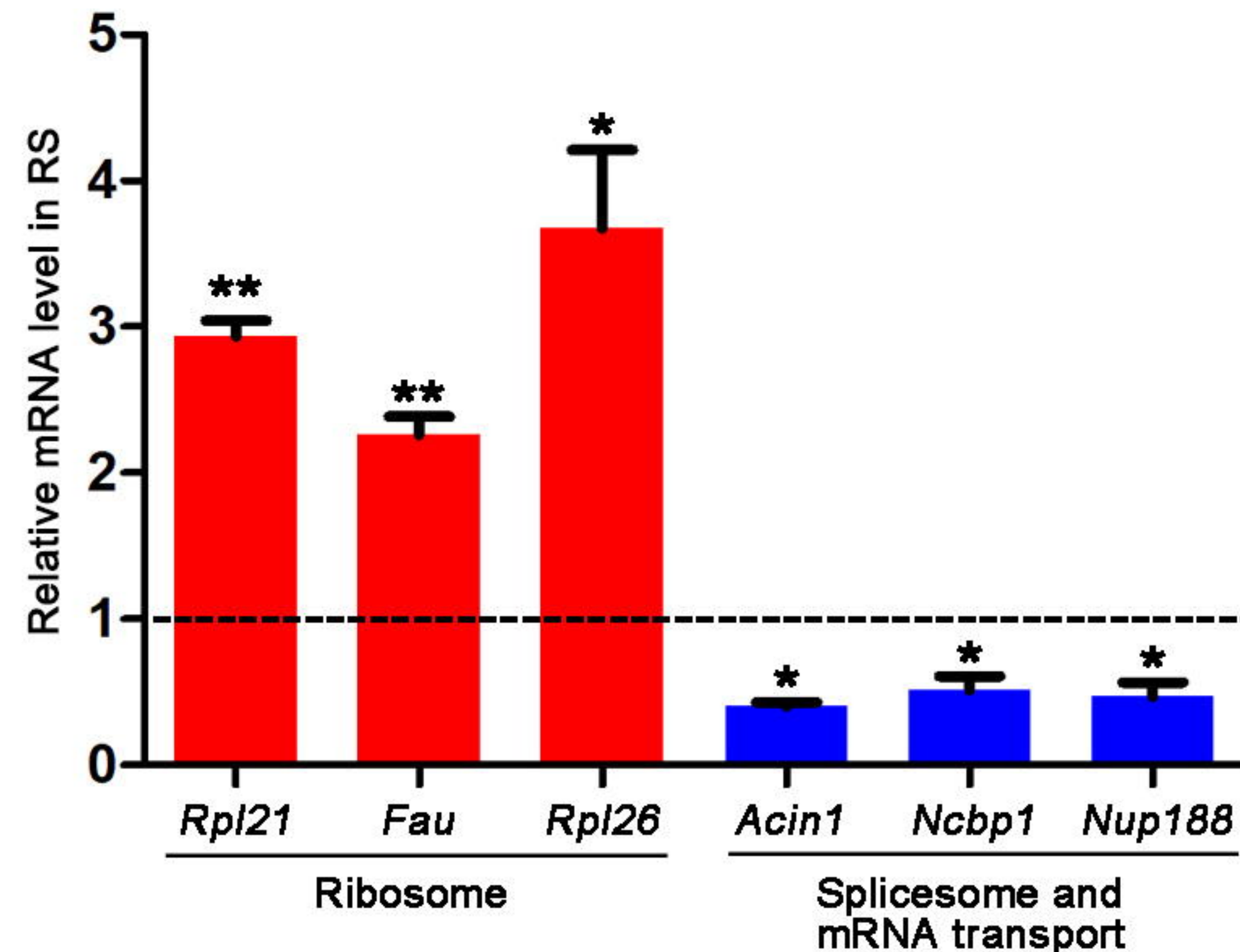
F



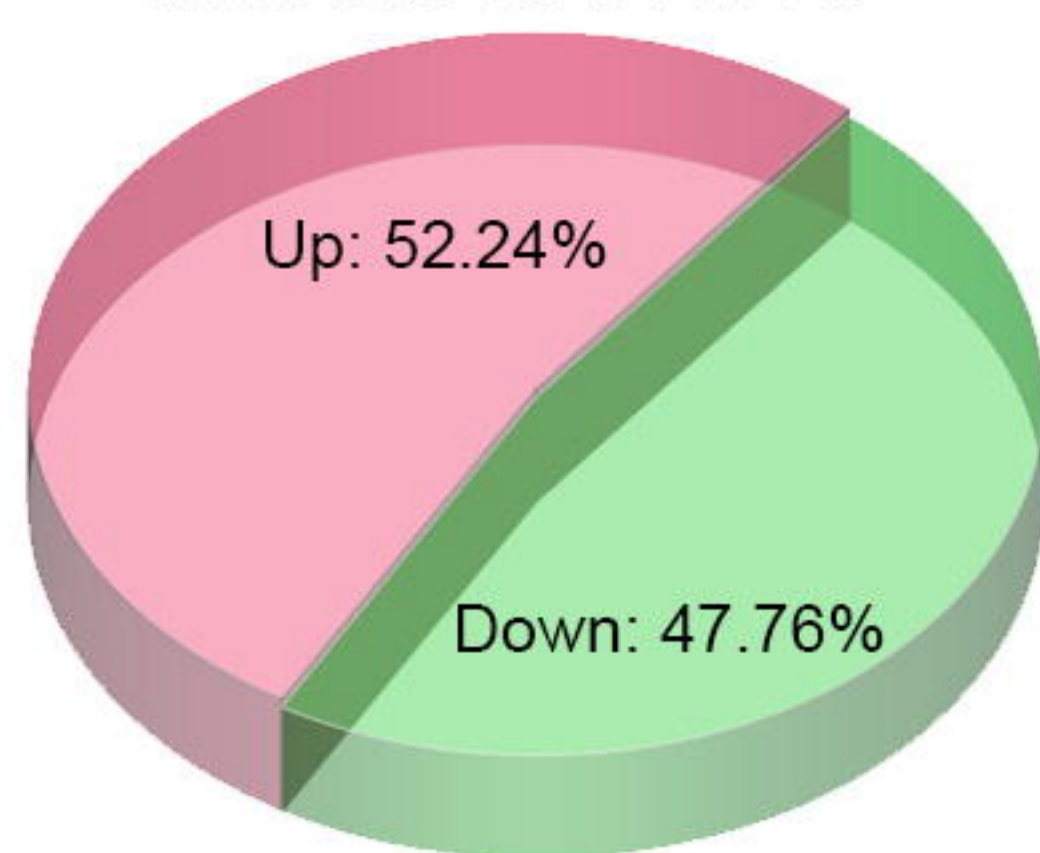
G



H

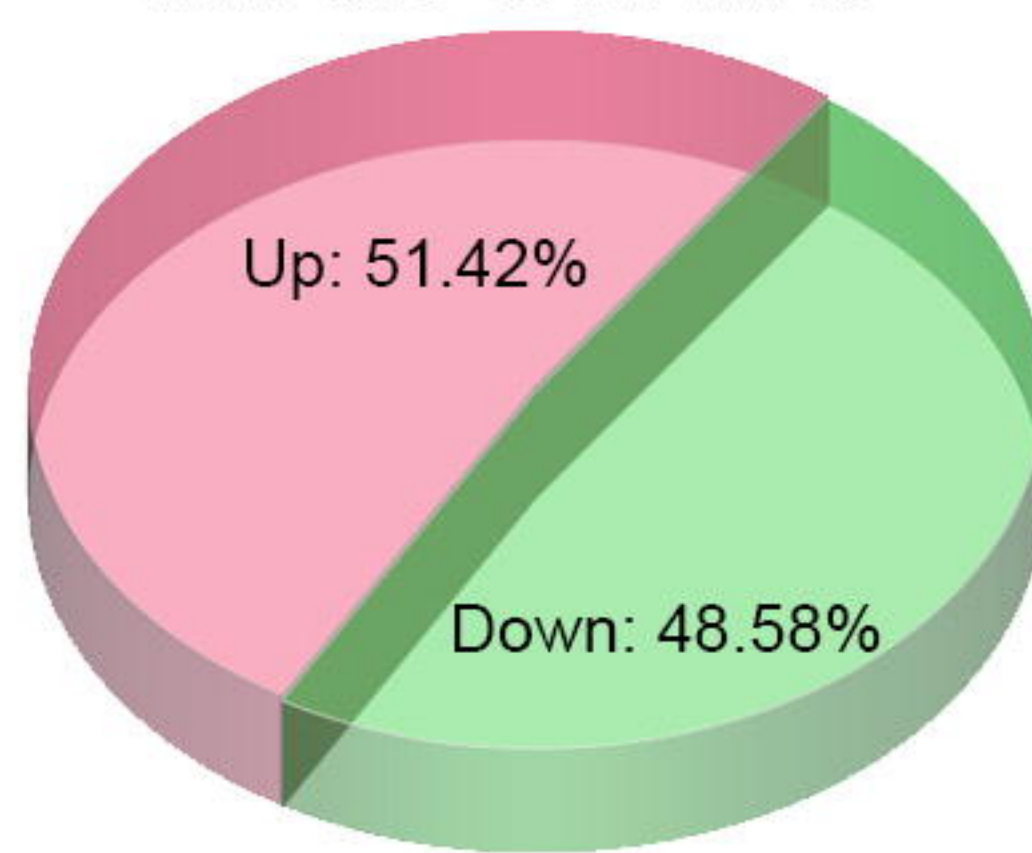


A

*Mfn2*-cKO vs WT in PS

1604 mis-regulated splicing events in 1001 genes

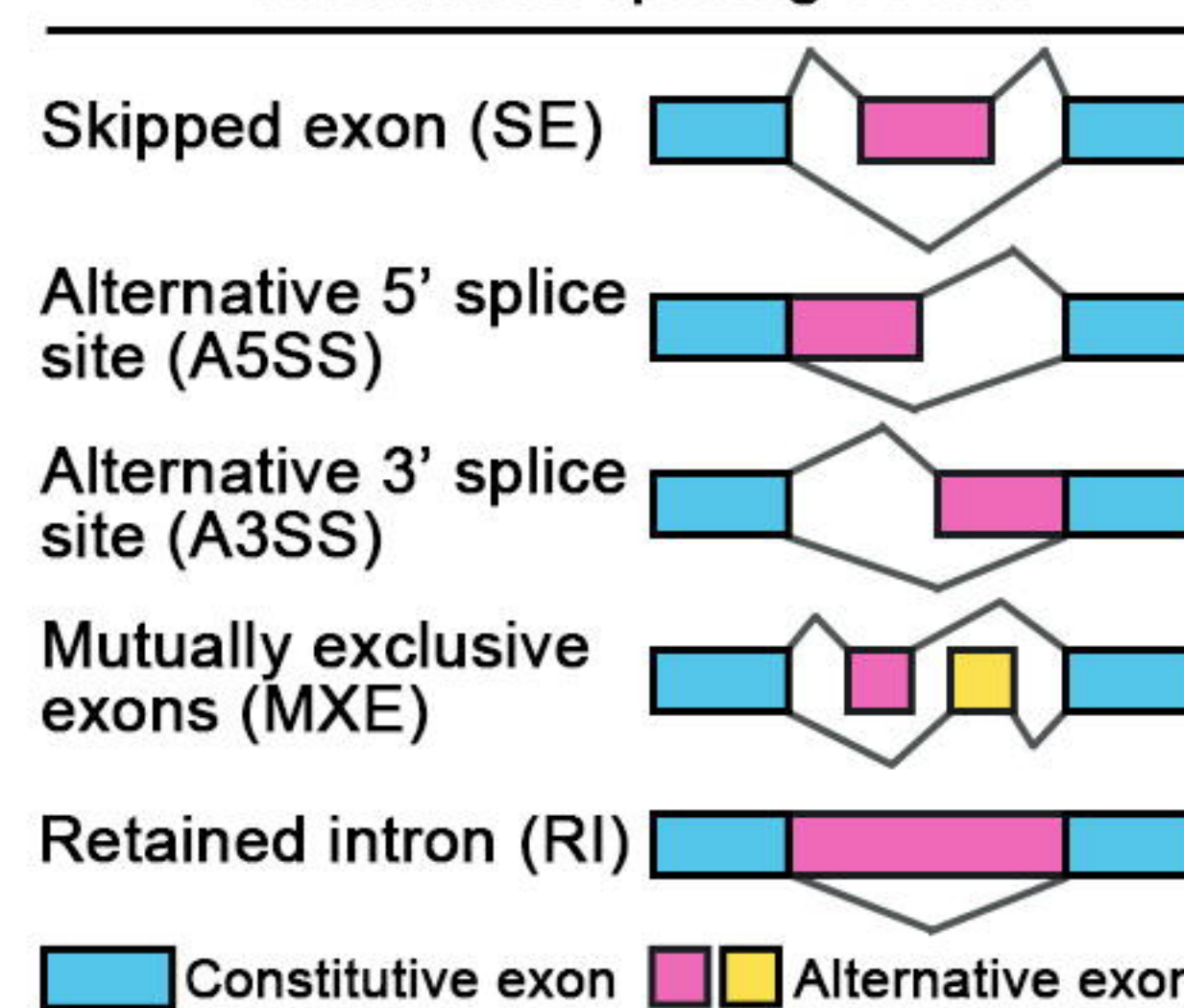
B

*Mfn2*-cKO vs WT in RS

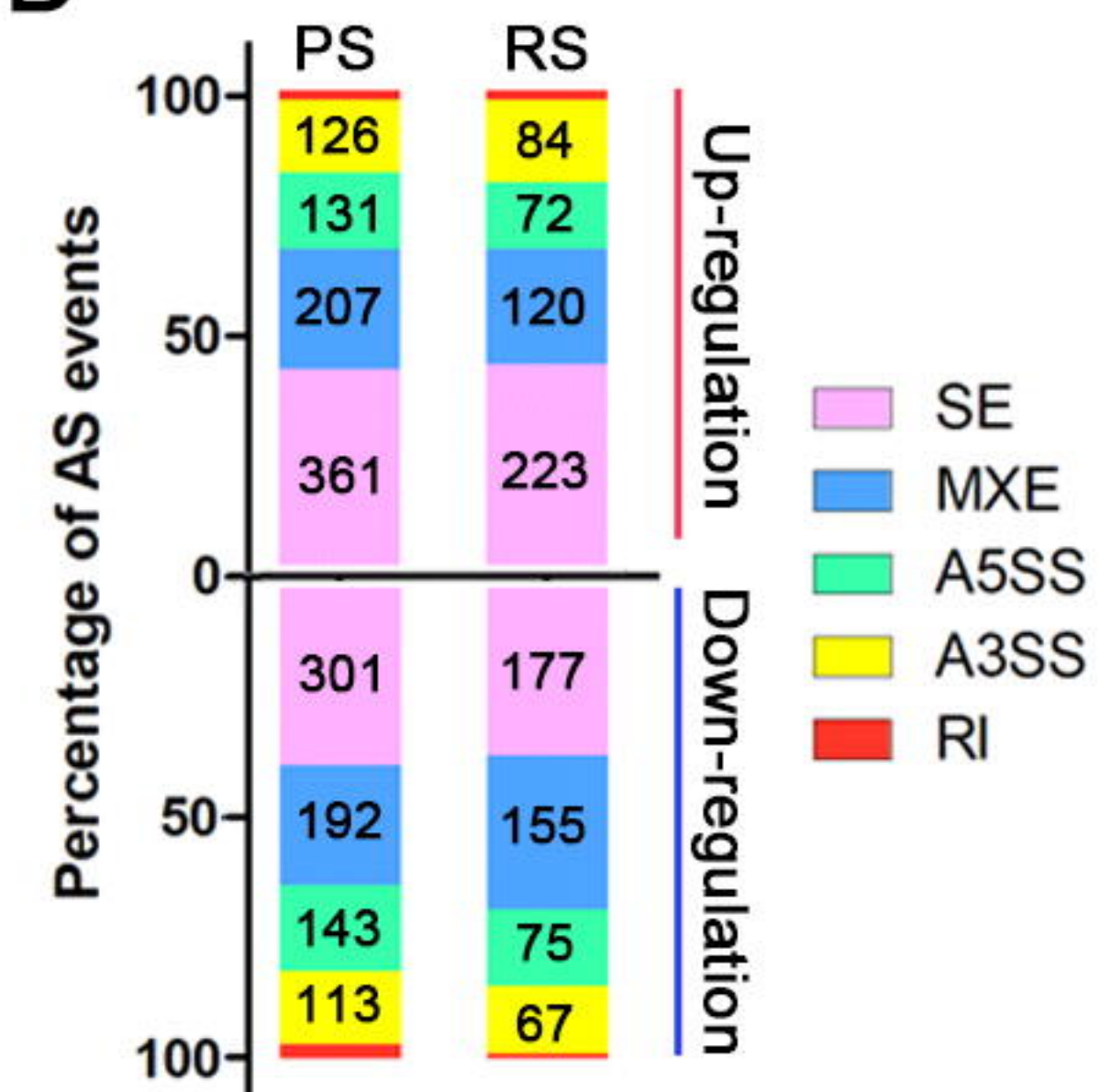
986 mis-regulated splicing events in 684 genes

C

Alternative splicing events

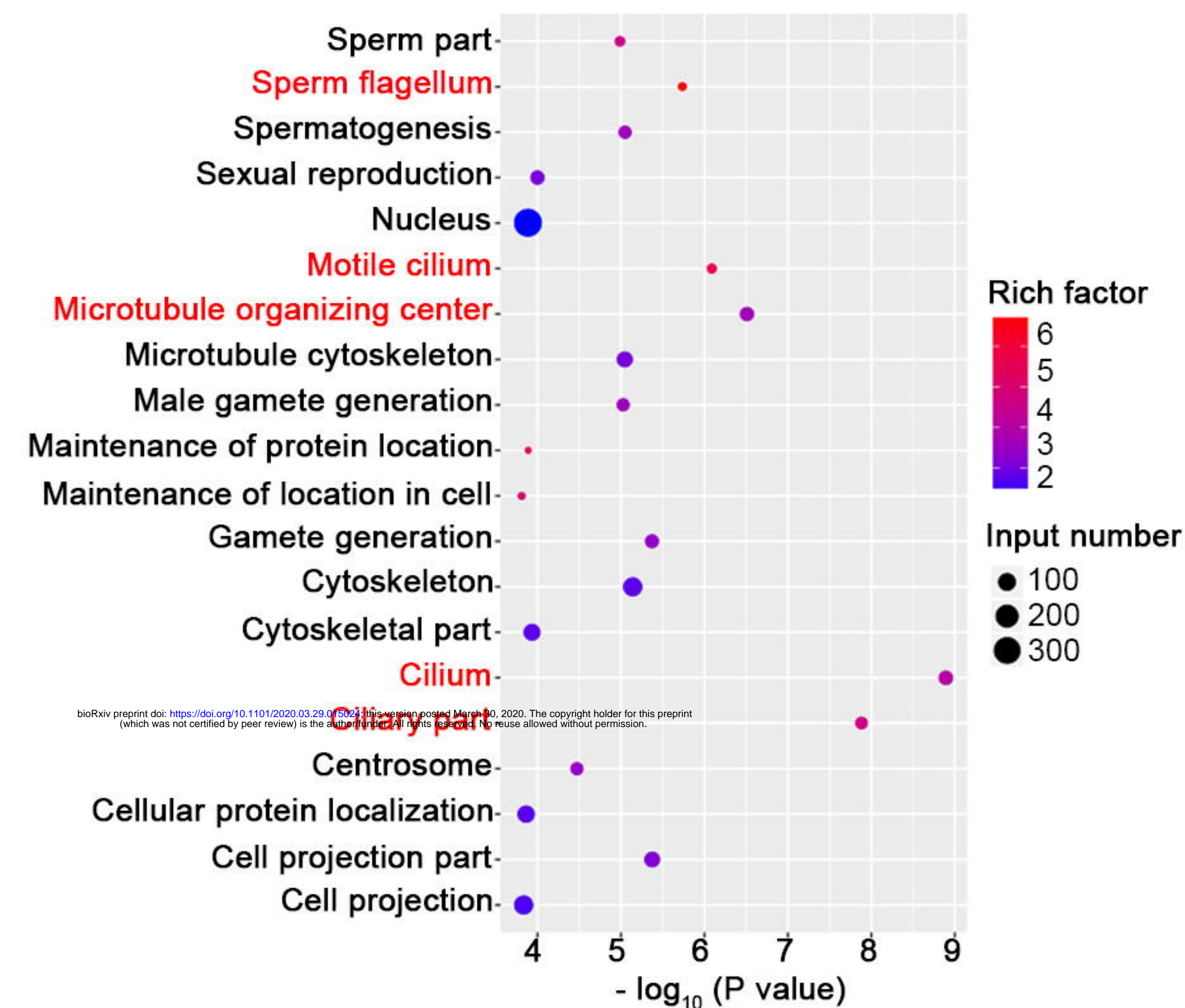


D



E

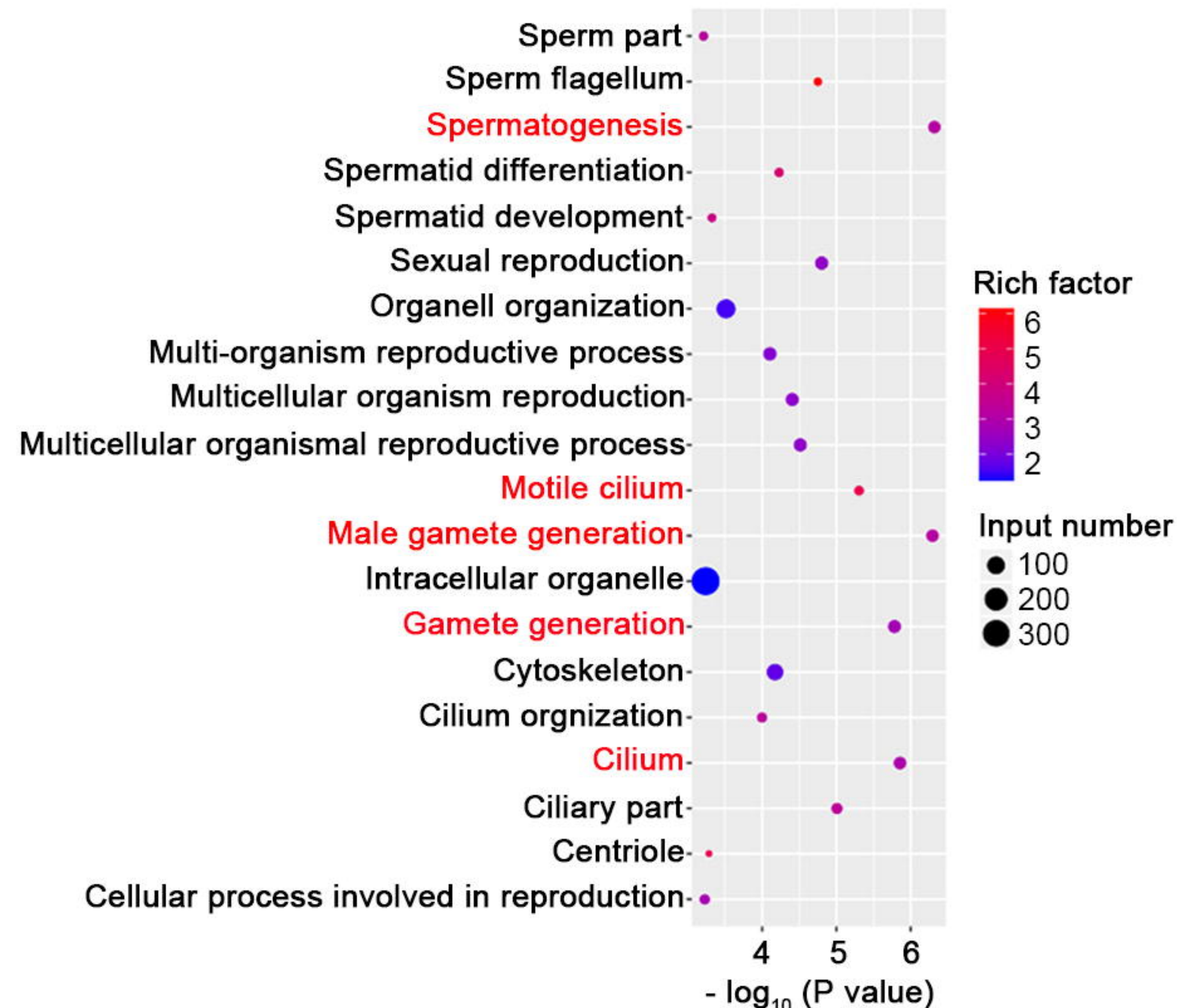
AS changed genes in PS



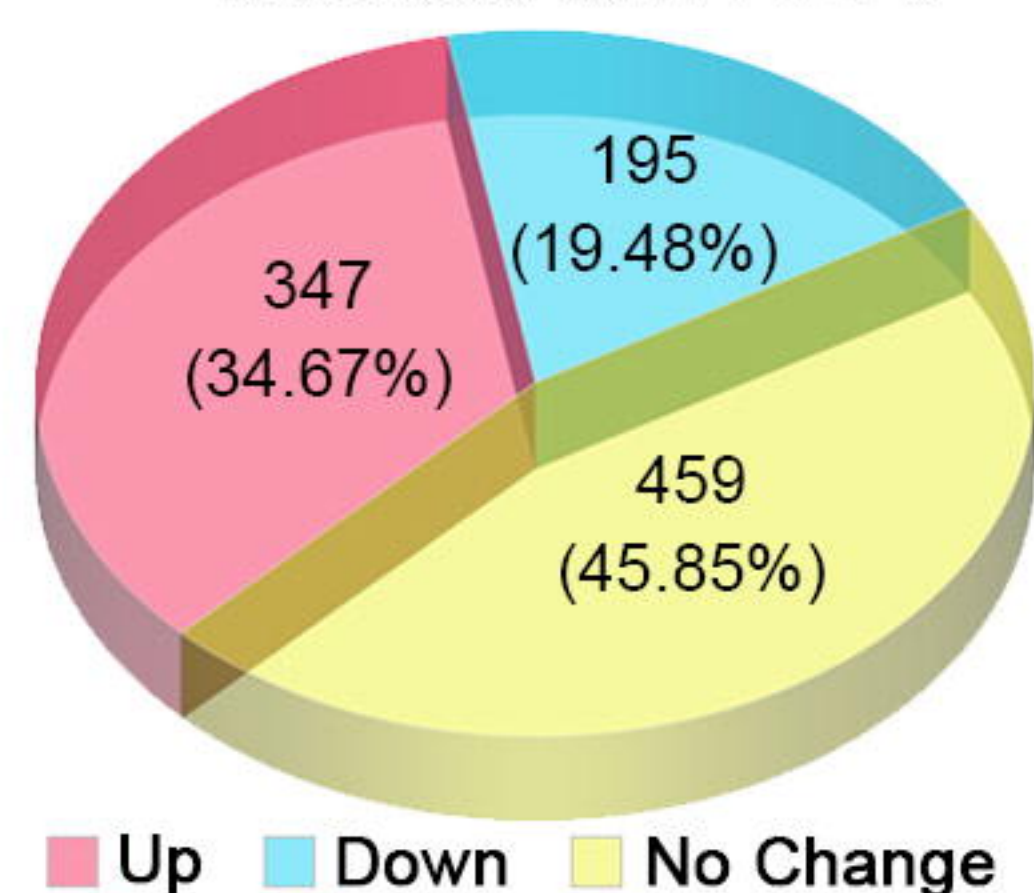
bioRxiv preprint doi: <https://doi.org/10.1101/2020.03.29.015021>; this version posted March 30, 2020. The copyright holder for this preprint (which was not certified by peer review) is the author/funder. All rights reserved. No reuse allowed without permission.

F

AS changed genes in RS

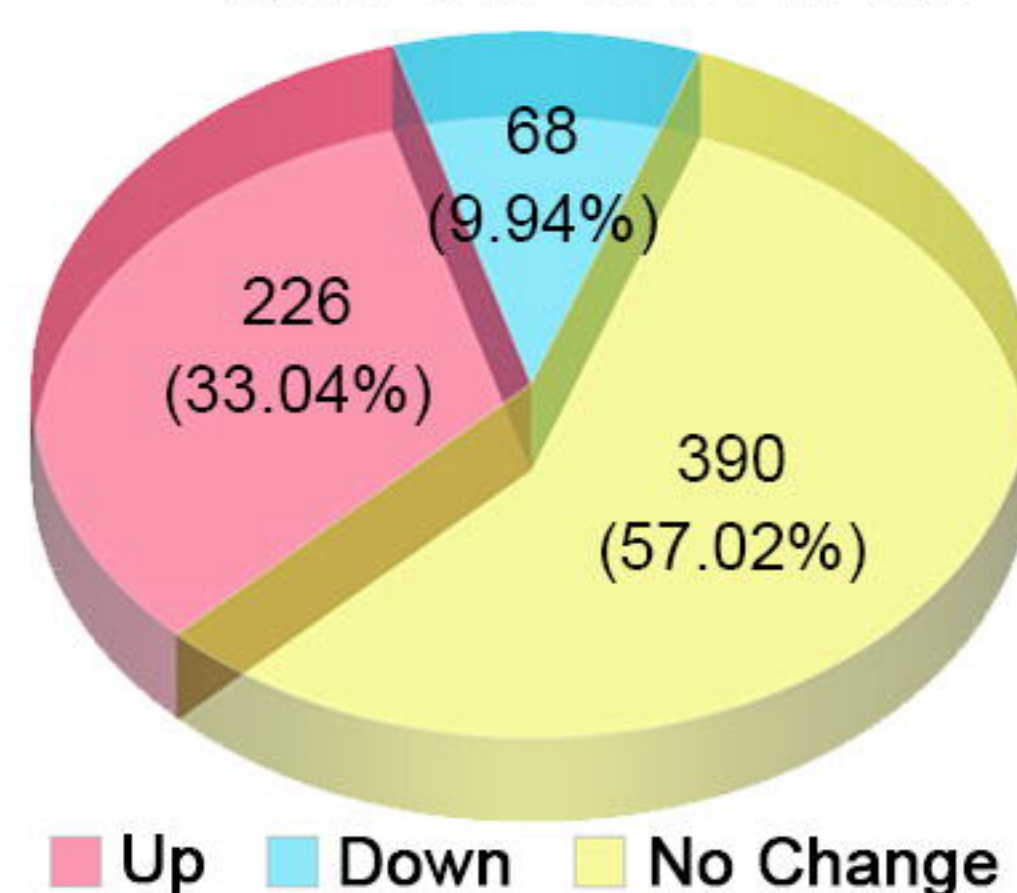


G

*Mfn2*-cKO vs WT in PS

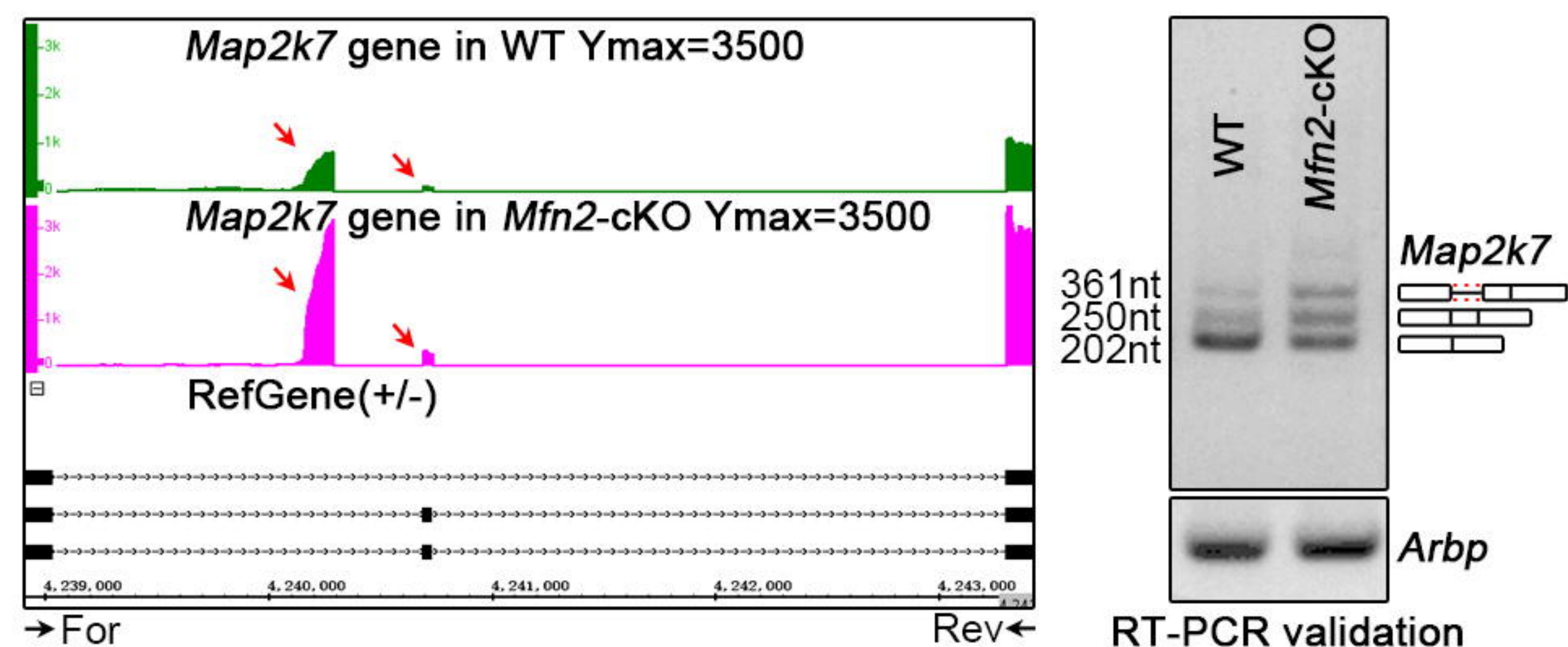
mRNA level of 1001 genes with mis-regulated AS

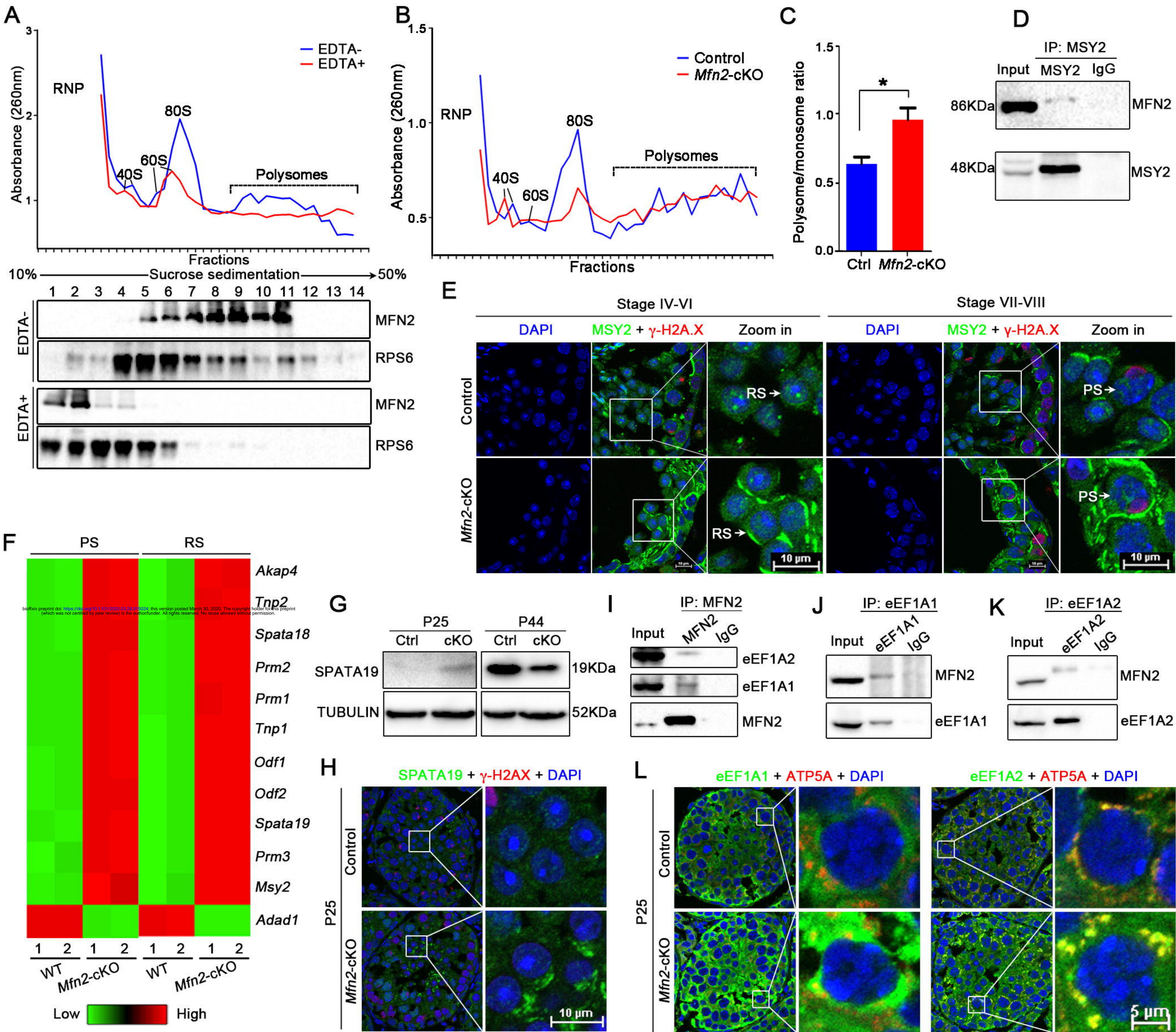
H

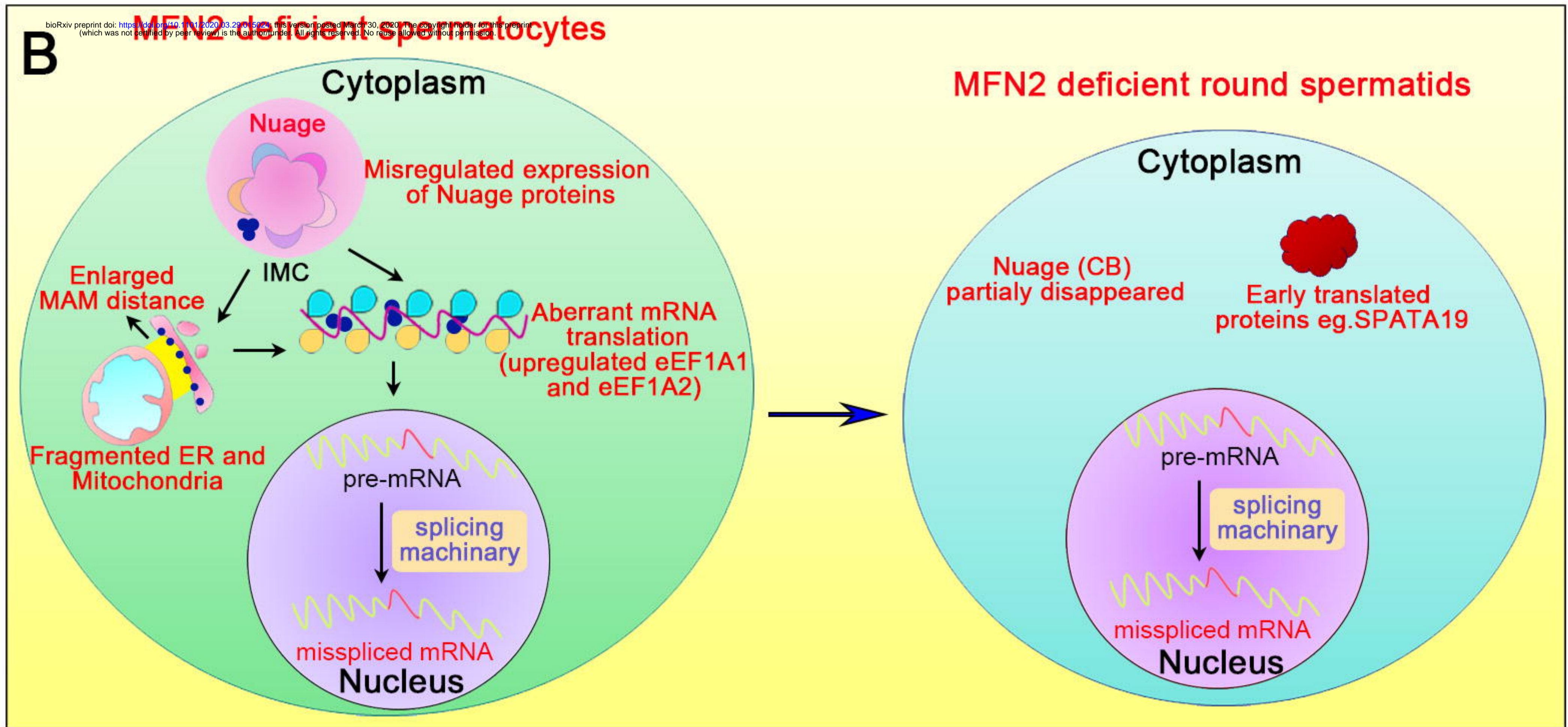
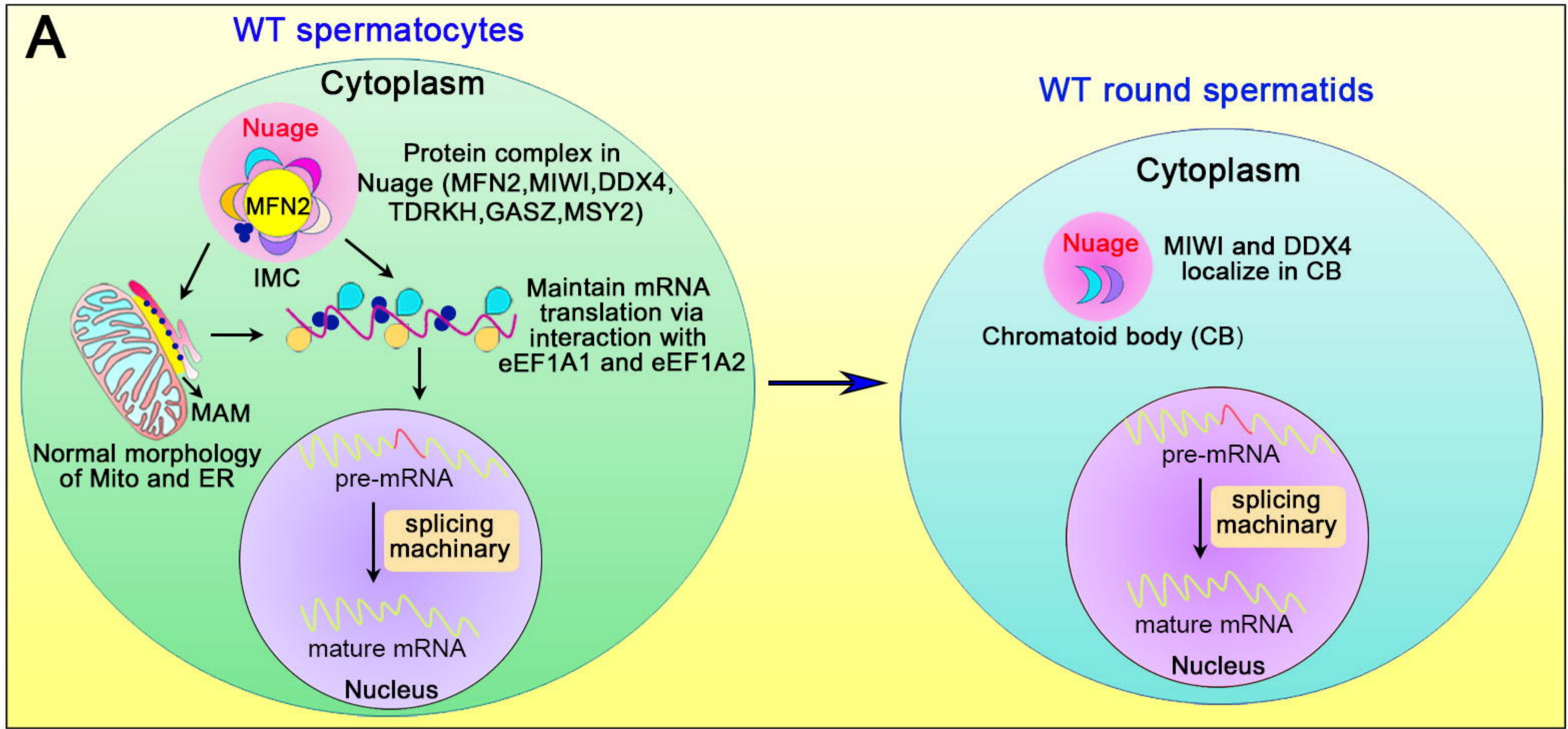
*Mfn2*-cKO vs WT in RS

mRNA level of 684 genes with mis-regulated AS

I







MSY2 MIWI TDRKH GASZ DDX4 Ribosome eEF1A1 eEF1A2